

**Real-time In Situ Measurements of Trace Gases  
from Agriculturally Cultivated Soils by Means of  
Laser Spectroscopic Techniques**

**Dissertation zur Erlangung des Doktorgrades  
der Naturwissenschaften (Dr. rer. nat.)**

**Fakultät Naturwissenschaften  
Universität Hohenheim**

Institut für Physik und Meteorologie

vorgelegt von  
Malte Hillebrand

aus Essen  
2008

Dekan:	Prof. Dr. Heinz Breer
1. berichtende Person:	Prof. Dr. Ulrich Haas
2. berichtende Person:	Prof. Dr. Andreas Fangmeier
Eingereicht am:	23.05.2008
Mündliche Prüfung am:	25.07.2008

Die vorliegende Arbeit wurde am 14.07.2008 von der Fakultät Naturwissenschaften der Universität Hohenheim als "Dissertation zur Erlangung des Doktorgrades der Naturwissenschaften" angenommen.

# Table of Contents

<b>1</b>	<b>AIM AND SCOPE.....</b>	<b>1</b>
<b>2</b>	<b>INTRODUCTION.....</b>	<b>3</b>
2.1	NORTH CHINA PLAIN .....	3
2.1.1	<i>Problems of the North China Plain.....</i>	<i>5</i>
2.1.2	<i>Agricultural History of China .....</i>	<i>6</i>
2.2	INTERNATIONAL RESEARCH TRAINING GROUP .....	7
2.3	SUBPROJECT 1.4 .....	8
<b>3</b>	<b>STATE-OF-THE-ART .....</b>	<b>9</b>
3.1	GREENHOUSE EFFECT .....	9
3.1.1	<i>Methane.....</i>	<i>12</i>
3.1.2	<i>Ammonia.....</i>	<i>16</i>
3.2	OPTICAL SPECTROSCOPY.....	19
3.3	PHOTOACOUSTIC SPECTROSCOPY.....	20
3.3.1	<i>Photoacoustic Spectroscopy of Gases.....</i>	<i>21</i>
3.3.2	<i>Resonant and Nonresonant Photoacoustic Spectroscopy.....</i>	<i>22</i>
3.3.3	<i>Q-factor .....</i>	<i>25</i>
3.4	TRACE GAS MEASURING DEVICES .....	27
3.5	SEMICONDUCTOR LASER.....	31
<b>4</b>	<b>MATERIAL AND METHODS.....</b>	<b>33</b>
4.1	EXPERIMENTAL FIELD STATION DONGBEIWANG.....	34
4.2	TUNABLE DIODE LASER PHOTOACOUSTIC MEASURING DEVICE .....	36
4.2.1	<i>Photoacoustic Detection Unit .....</i>	<i>36</i>
4.2.2	<i>Temperature Control Unit.....</i>	<i>40</i>
4.2.3	<i>Electronic Unit.....</i>	<i>40</i>
4.2.4	<i>External Laser Diode Driver.....</i>	<i>41</i>
4.2.5	<i>Data Capture Unit.....</i>	<i>41</i>
4.2.6	<i>Gas Flow Accessories .....</i>	<i>43</i>
4.3	SELECTION OF ABSORPTION LINES.....	44
4.4	LASER DIODES .....	46
4.4.1	<i>Laser Diodes for Methane Detection .....</i>	<i>46</i>
4.4.2	<i>Laser Diodes for Ammonia Detection.....</i>	<i>46</i>

4.5	CALIBRATION OF THE TUNABLE DIODE LASER PHOTOACOUSTIC SYSTEM .....	47
4.5.1	<i>Problems During Ammonia Calibration</i> .....	50
4.6	CLOSED CHAMBER TECHNIQUE.....	51
4.6.1	<i>Advantages and Disadvantages of Closed Chambers</i> .....	52
4.6.2	<i>Self-developed Closed Dynamic Chambers</i> .....	52
4.6.3	<i>Tightness Test</i> .....	56
4.6.4	<i>Cooling of the Closed Chambers</i> .....	57
<b>5</b>	<b>RESULTS AND DISCUSSION.....</b>	<b>61</b>
5.1	SOIL-ATMOSPHERE EXCHANGE OF METHANE.....	61
5.1.1	<i>Closed Chamber Measurements in Dongbeiwang</i> .....	61
5.1.2	<i>Flux Calculation</i> .....	62
5.2	SOIL-ATMOSPHERE EXCHANGE OF METHANE DURING WINTER WHEAT GROWING SEASON .....	64
5.3	SOIL-ATMOSPHERE EXCHANGE OF METHANE DURING SUMMER MAIZE GROWING SEASON .....	68
5.3.1	<i>24 Hour Measurement</i> .....	69
5.4	ATMOSPHERIC BOUNDARY LAYER.....	72
5.5	AMBIENT AIR METHANE MEASUREMENTS.....	73
5.5.1	<i>Measurements of Methane at Dongbeiwang</i> .....	73
5.5.2	<i>Measurements of Methane at the Campus of the China Agricultural University</i> ...	77
5.5.3	<i>Measurements of Methane at the Liulitun Landfill</i> .....	81
5.5.4	<i>Measurements of Methane at the Campus of the Beijing University</i> .....	85
5.5.5	<i>Measurements of Methane at the Shang Zhuang Experimental Field Station</i> .....	87
5.6	METHANE EMISSIONS FROM CARS .....	89
5.6.1	<i>Measurements of Methane by the Tunable Diode Laser Photoacoustic Device</i> .....	91
5.7	AMMONIA EMISSION MEASUREMENTS.....	93
<b>6</b>	<b>SUMMARY AND OUTLOOK .....</b>	<b>95</b>
<b>7</b>	<b>ZUSAMMENFASSUNG UND AUSBLICK.....</b>	<b>99</b>
<b>8</b>	<b>REFERENCES .....</b>	<b>105</b>
<b>9</b>	<b>APPENDIX .....</b>	<b>115</b>
9.1	LIST OF TABLES.....	115
9.2	LIST OF FIGURES .....	116

---

## Abbreviations and Acronyms

A/D	analog-digital
CAU	China Agricultural University
CNG	compressed natural gas
DBW	Dongbeiwang (experimental field)
DFB	distributed feedback (laser diode)
DIN	Deutsche Industrie-Norm (German Institute for Standardization)
FWHM	full width at half maximum
GC	gas chromatograph
GWP	Global Warming Potential
HITRAN	high resolution transmission molecular absorption database
IPCC	Intergovernmental Panel on Climate Change
IR	infrared (spectral range)
IRTG	International Research Training Group
MIR	middle-infrared (spectral range)
MSW	municipal solid waste
NCP	North China Plain
NIR	near-infrared (spectral range)
OS	optical spectroscopy
P.R. China	People's Republic of China
PA	photoacoustic
PAS	photoacoustic spectroscopy
ppb	parts per billion; $10^{-9}$
ppm	parts per million; $10^{-6}$
RF	radiative forcing
SNR	signal to noise ratio
TDL-PA	tunable diode laser photoacoustic
TDL-PAS	tunable diode laser photoacoustic spectroscopy
UV	ultraviolet (spectral range)
VIS	visible (spectral range)

---

## Symbols

$b$	slope of the regression line
$c_0$	speed of sound
$C_0$	concentration at the time of closure
$F$	gas flux rate
$h$	chamber height
$J_m$	Bessel function
$k, m, n$	eigenvalues defining the longitudinal, azimuthal and radial modes
$L$	length of a cylinder
$M$	molecular weight of methane
$p_j$	normal vibration mode
$P_j$	normalization coefficient
$Q$	quality factor
$R$	radius of a cylinder
$s_0$	standard deviation
$t$	time
$T$	ambient air temperature
$\nu_0$	resonance frequency
$V_c$	chamber volume
$V_m$	volume occupied by 1 mol of methane at standard pressure
$z, r, \phi$	standard cylindrical coordinates
$\alpha$	degradation rate constant
$\chi_{DL}$	detection limit
$\omega_j$	frequency of the $j$ th mode

## 1 Aim and Scope

The present thesis was conducted within the first phase of the International Research Training Group (IRTG) “Modeling Material Flows and Production Systems for Sustainable Resource Use in Intensified Crop Production in the North China Plain” implemented in 2004. It is a cooperation between the University of Hohenheim and the China Agricultural University (CAU) in Beijing, China, financed by the German Research Foundation as well as by the Chinese Ministry of Education, respectively. Different disciplines are conducting research within eleven subprojects. This thesis was implemented within subproject 1.4 incorporated at the Institute of Physics and Meteorology at the University of Hohenheim.

In the working group “Spectroscopy” of the Institute two laser spectroscopic devices for methane and ammonia detection were developed [Reinhardt 2002; Sauter 2004]. They are based on Tunable Diode Laser Photoacoustic Spectroscopy (TDL-PAS) using near-infrared (NIR) diode lasers emitting at 1651 nm for methane and 1532 nm for ammonia detection, respectively.

One aim of this work was to construct a new Tunable Diode Laser Photoacoustic (TDL-PA) measuring device for soil-atmosphere methane exchange measurements and adapting it to the harsh climatologic conditions in China, e.g. high variation in temperature, high humidity and particulate matter emissions. Moreover it was necessary to modify the system so that unattended operations over a period of several days were possible. For that purpose all components had to be tested in the laboratory in Germany before the field campaign at the experimental field Dongbeiwang (DBW) of the CAU was started.

The already existing TDL-PA system for ammonia detection had to be installed in a thermally stabilized housing to guarantee a long-term stability of the applied diode laser. Furthermore a new diode laser emitting at 1512 nm, another absorption peak of ammonia, was tested and replaced the laser diode used before.

Another aim was to design mobile closed chambers for the trace gas exchange measurements between arable soils and the atmosphere. They consisted of a frame as basis made from stainless steel that was installed permanently in the soil of DBW and a hood made from Plexiglas which was placed on the frame whenever a measurement was made and was

removed afterwards again. Seven of the frames were constructed in China while three hoods of different heights (250, 500 and 1000 mm) were built in Germany and transported to the CAU. A further innovation of this new design was the possibility to insert up to eight cooling packs that cooled down the enclosed air in the chambers by mixing it via two fans.

The trace gas exchange data obtained by applying the TDL-PA device and the new chambers should then be compared with data obtained by gas chromatograph (GC) measurement techniques using already existing chambers in DBW. By this means the accuracy of the measurements should be verified.

## 2 Introduction

### 2.1 North China Plain

The North China Plain (NCP) is based on the deposits of the Huang He (Yellow River) and is the largest alluvial plain of eastern Asia. It extends from 32° to 41° northern latitude and 113° to 120° eastern longitude, with an elevation up to 100 m above sea level. Seven provinces and municipalities participate in the NCP. These are: Anhui, Beijing, Hebei, Henan, Jiangsu, Shandong and Tianjin. The covered area by the NCP is about 328,000 km<sup>2</sup>, which is 3.3% of Chinas total area. Figure 2.1 provides a map of China showing the location of the NCP. A detailed map of the NCP can be found in Figure 2.2.

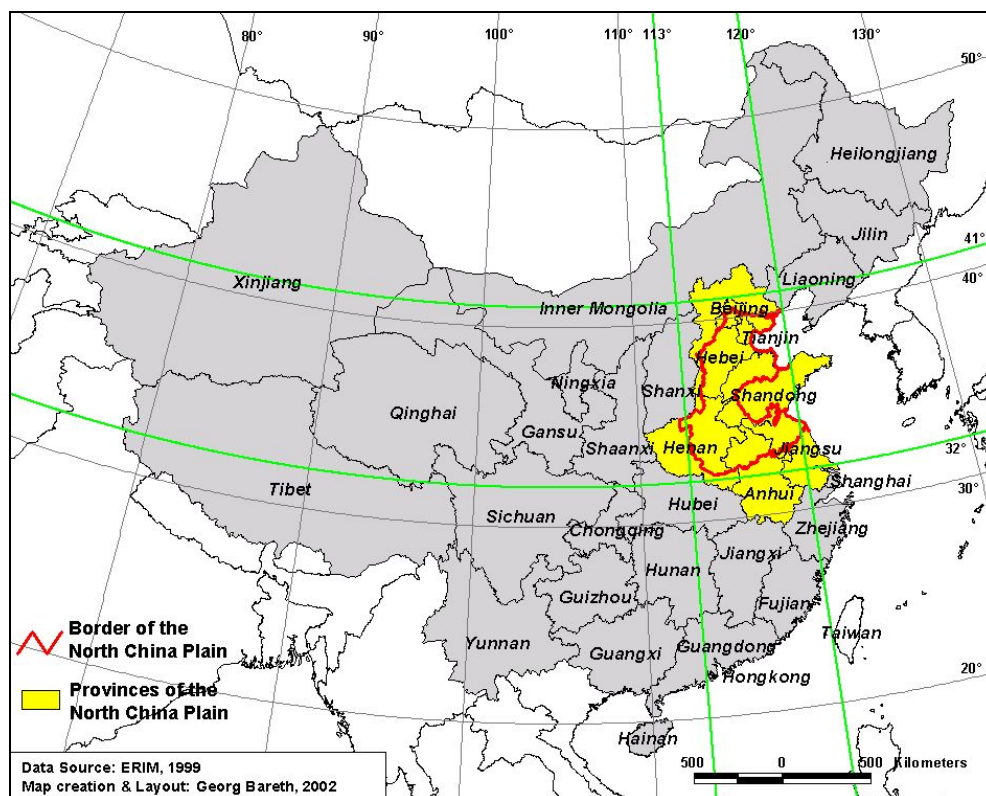


**Figure 2.1:** Geographical location and administrative units of the NCP. Map provided by G. Bareth.

The NCP is one of the most important agricultural regions in China. With 800 million inhabitants it is also one of the most densely populated regions in China. Some areas of the NCP even contain 600 – 1000 inhabitants km<sup>-2</sup> [Länderbericht-China 2007].

The mean annual temperature (1951 – 1988) is about 13°C and the temperature sum is ranging from 4500 to 5000 (> 0°C). The vegetation period is 180 – 200 days [Böning-Zilkens 2004]. Annual precipitation ranges between 500 – 600 mm in the northern part and 600 – 900 mm in the southern part. The summer humid monsoon climate, with about 70% of

the precipitation is in summer, makes irrigation necessary for winter crops. The major soil types are cinnamon soils on calcic alluvial deposits, i.e. Calcaric Fluvisols after FAO classification [FAO 1998]. Average soil parameters are a silt soil texture, pH ranging from 7.5 to 8.5 and the content of organic matter from 0.5 to 1% [Hseung 1986].



Figure 2.2: Detailed map of the NCP. Map provided by C. Rumbaur.

Farmland in the NCP represents 16.9 million ha, covering 18% of China's whole agricultural land area. The dominating crops are wheat (34% of the crop land), maize (20%) and soybeans (8%). Usually three harvests in two years are yielded resulting in a cropping-index of 1.5. The limiting factors are uneven distributed soil quality as well as the unpredictable summer precipitation [Länderbericht-China 2007]. Despite this the NCP is called the “Granary of China” due to its highest agricultural productivity of all China. The grain production quadrupled in the last four decades. It contributes about 41% of wheat and 25% of maize yields to the total grain yield in China.

### **2.1.1 Problems of the North China Plain**

In July 2007 there were currently 1.32 billion people living in China, representing 21.5% of the world population. Until 2030 the Chinese population will reach 1.6 billion people. Some problems arise due to this fact particularly because most people are living in the East and South of China. Like mentioned above, 800 million people are nowadays living in the NCP. On the one hand they need accommodations while on the other hand they must be fed. This leads to urbanization and infrastructure developing at the expense of arable land shrinkage. On these residual areas the yield must be increased as much as possible. This was done during the last two decades by different measures.

An increase in irrigated acreage occurred by transformation of rainfed acreage into irrigated acreage. Today 56.7% of the arable land in the NCP is irrigated [Länderbericht-China 2007]. Moreover the fertilizer input grew more than 50 times from 1962 (0.63 million tons) to 1995 (33.18 million tons), with 80% being nitrogenous fertilizer. Nowadays the average amount of nitrogen applied in the NCP is 400 kg ha<sup>-1</sup> and is still increasing while the yield growth rate stagnates and the nitrogen use efficiency decreases. Most farmers apply nitrogen beyond the crop demand, resulting in a nitrogen surplus. The environmental effects of this unsustainable agriculture are as follows:

- Nitrogen leaching, runoff and volatilization
- Groundwater contamination
- Enhanced greenhouse gas emissions
- Decrease of soil fertility causing a yield reduction
- Decline of groundwater table in both shallow and deep aquifers
- Degradation
- Salinization

The reason for this unsustainable agriculture can be found in the agricultural history of China below-mentioned.

### **2.1.2 Agricultural History of China**

After the foundation of the P.R. China in 1949 a land reform was conducted and large land owners were disseized. Until 1952 about 50 million ha arable land (43% of the total arable land) were given to 120 million small scale farmers. From 1953 – 1957 the annual rise in agronomic production was 4.5%. During the “Great Leap Forward” followed by the “Three Bitter Years” from 1958 – 1961 the rural population had to produce steel instead of crops. The fields were neglected and crop failure accumulated, enhanced by natural disasters, nearly 30 million people died of starvation. From 1962 – 1965 the tension eased a little and agriculture was stepwise mechanized and de-collectivized. By the outbreak of the “Cultural Revolution” from 1966 – 1969 this development was interrupted and nothing was done to improve the agriculture. After the “Cultural Revolution” the further improvement and de-collectivization of the agricultural sector was again put into focus in the years 1969 – 1976. Private lots cropped by families were allowed from 1978 and the agricultural production was decentralized leading to a better supply and rising of the farmers incomes by the adoption of the “Household Production Responsibility System” [Länderbericht-China 2007]. During that time the intensification in crop production started continuing until today. Moreover with all these disasters in mind the farmers are trying to increase their yield by applying too much fertilizers, water and pesticides.

## **2.2 International Research Training Group**

Due to the rapid development of China's agriculture in the last years, production practices and systems which are environmentally sound and economically and socially viable, had not been an important issue so far. Thus, serious environmental problems like water availability and pollution, air pollution, soil contamination and erosion were raised. At present, there is a significant research deficit in clearly identifying, measuring and modeling the related material flow effects. In addition, their interactions have to be explained by suitable integrated multi level modeling approaches. Strategies to reduce or avoid negative effects have to be developed, analyzed and assessed on field, farm and regional level in order to derive suitable agro-environmental policy measures.

To put the focus on sustainability cropping systems and management practices the IRTG "Modeling Material Flows and Production Systems for Sustainable Resource Use in Intensified Crop Production in the North China Plain" was established in 2004. It is financed by the German Research Foundation and by the Chinese Ministry of Education and is a cooperation between the University of Hohenheim and the CAU.

The major hypothesis of the IRTG is that adjustments in cropping systems and management practices provide potential for sustainable resource protection on a high yield level. To verify this hypothesis research is conducted within eleven subprojects from various disciplines, e.g. soil science, plant nutrition, plant ecology, physics, biogeophysics, plant production, plant breeding, farm management, agricultural informatics and rural development policy, which are divided into the following three subgroups:

Material Flows / Pollution Analysis, Cropping Systems and Farm Level, Regional and Sectoral Assessments

The present thesis was conducted within subproject 1.4.

### **2.3 Subproject 1.4**

The subproject 1.4 was incorporated into the Material Flows / Pollution Analysis subgroup. With the title reading “Real-time In situ Measurements of Trace Gases from Agriculturally Cultivated Soils by Means of Laser Spectroscopic Techniques” it was concerned with developing, constructing and establishing a new trace gas measuring technique in China.

To monitor and to collect real-time data of the trace gas exchange at various locations of an agricultural area an appropriate measurement device must be mobile, inexpensive and robust. Additionally, it must be sensitive enough to detect trace gas concentrations in the parts per million (ppm) to parts per billion (ppb) range with a time resolution better than some few minutes. These are prerequisites to evaluate the exchange of climate relevant trace gases (e.g. methane and ammonia) with agriculturally cultivated soils.

An approved spectroscopic method that meets these conditions is the photoacoustic spectroscopy (PAS), which is a well known technique for the very sensitive detection of weak absorptions and is particularly appropriate for measurements at atmospheric pressure. Better results are usually achieved with resonant PAS where the photoacoustic (PA) cell works as a resonator in which standing waves (modes) can be formed. A major task of this subproject was to establish such a detection system using NIR diode lasers as spectroscopic light sources. The time resolution of this portable and temperature stabilized PA spectrometer is better than one minute. Furthermore, this detection system is coupled with a new designed mobile and height adjustable accumulation box. This box can be easily transported to different agricultural areas and adapted to the various heights of the vegetation up to 100 cm. The complete device must be carefully calibrated and quality assurance must be guaranteed by comparative measurements to obtain accurate and reliable data of trace gas emissions in the course of the field campaigns during the vegetation periods.

## 3 State-of-the-art

### 3.1 Greenhouse Effect

The Earth's surface is warmed by the radiation energy from the Sun, predominantly in the visible (VIS) and ultraviolet (UV) part of the spectrum. A surface of one square meter in area outside the atmosphere and directly facing the Sun receives about 1370 W of solar radiation. Due to the fact that only few parts of the Earth's surface are facing the Sun directly, the average energy falling on one square meter of a level surface outside the atmosphere is only one-quarter of this or about 343 W. While passing the atmosphere about six percent of this radiation is scattered back to space by atmospheric molecules and ten percent is reflected from the land and ocean surface. The remaining energy, about  $288 \text{ W m}^{-2}$ , is absorbed by the surface and the atmosphere of the Earth. The same amount of energy must be radiated back to space by the Earth to balance the absorbed energy. This happens by emitting outgoing thermal radiation, primarily in the infrared (IR) part of the spectrum with the wavelength maximum at about  $10 \mu\text{m}$ . Without climate relevant trace gases present in the atmosphere the temperature of the Earth would be at about 255 K. In fact the surface temperature of the Earth is about 288 K. The reason for this temperature difference is the presence of climate relevant trace gases and clouds, respectively. This is known as the natural greenhouse effect. Mainly following trace gases contribute to the natural greenhouse effect: Water vapor with 20.6 K, carbon dioxide (7.2 K), ozone (2.4 K), nitrous oxide (1.4 K) and methane (0.8 K) [Houghton 2004].

The most important greenhouse gas is water vapor the concentration of which in the atmosphere depends mostly on the temperature of the surface of the oceans. Water vapor originates through evaporation from the ocean surface and is not influenced directly by human activity. Anthropogenic emissions of the other mentioned trace gases have led to an additional anthropogenic greenhouse effect. Besides carbon dioxide, methane, nitrous oxide and halocarbons are contributing most to the anthropogenic greenhouse effect, causing further global warming. Additionally the concentration of water vapor in the atmosphere rises due to higher temperatures, which may enhance the greenhouse effect. This in turn causes more warming which leads to a self-reinforcing cycle [Le Treut et al. 2007].

Other direct and indirect influences on the greenhouse effect originate from tropospheric and stratospheric ozone, aerosols and land use change, respectively, leading to either increase or decrease of the mean global temperature. The newest assessment report of the

Intergovernmental Panel on Climate Change (IPCC) calculated a temperature increase ranging between 1.8 K and 4.0 K depending on the used emission scenario [IPCC 2007].

To compare the relative greenhouse effects of different atmospheric constituents the term radiative forcing (RF) was introduced by the IPCC. It is defined as the change in average net radiation at the top of the troposphere which occurs because of a change in the concentration of a greenhouse gas or because of some other changes in the overall climate system [Houghton 2004]. RF for an atmospheric constituent is reported as the difference in RF between the present-day (2005) and the beginning of the industrial era (approximately 1750) and is given in the unit  $W m^{-2}$  [IPCC 2007]. Figure 3.1 shows the global average RF subdivided into anthropogenic and natural sources. Positive values mean a temperature increase of the Earth's surface while negative values mean a decrease. The total RF of the anthropogenic emitted greenhouse gases carbon dioxide, methane, nitrous oxide and halocarbons from the years 1750 to 2005 is  $2.46 W m^{-2}$ . Of these gases carbon dioxide has the highest fraction with  $1.66 W m^{-2}$  followed by methane ( $0.48 W m^{-2}$ ), halocarbons ( $0.34 W m^{-2}$ ) and nitrous oxide ( $0.16 W m^{-2}$ ) [IPCC 2007].

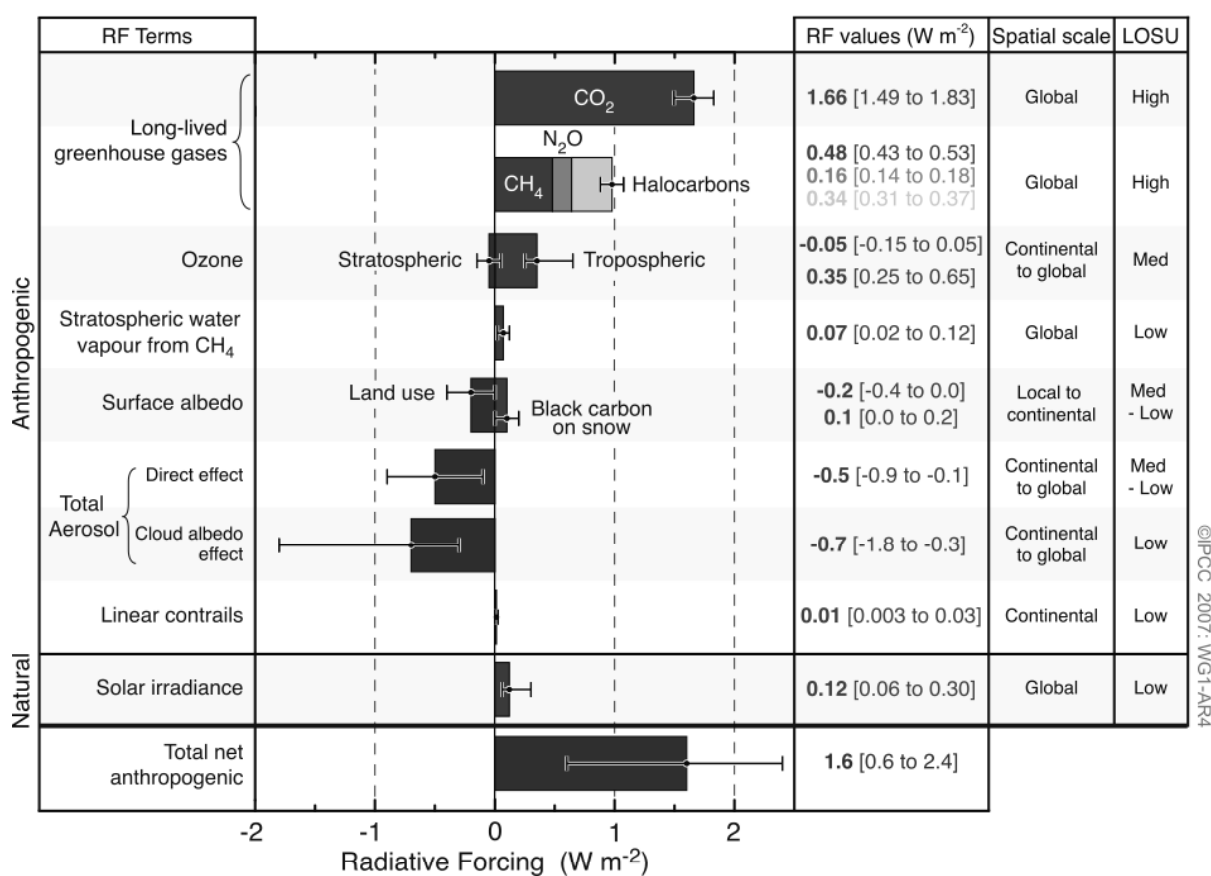


**Figure 3.1:** Global average RF estimates and ranges in 2005 for anthropogenic carbon dioxide (CO<sub>2</sub>), methane (CH<sub>4</sub>), nitrous oxide (N<sub>2</sub>O) and other important agents and mechanisms, together with the typical geographical extent (spatial scale) of the forcing and the assessed level of scientific understanding (LOSU) [IPCC 2007].

The increase of carbon dioxide, methane and nitrous oxide within the last 10,000 years is presented in Figure 3.2.

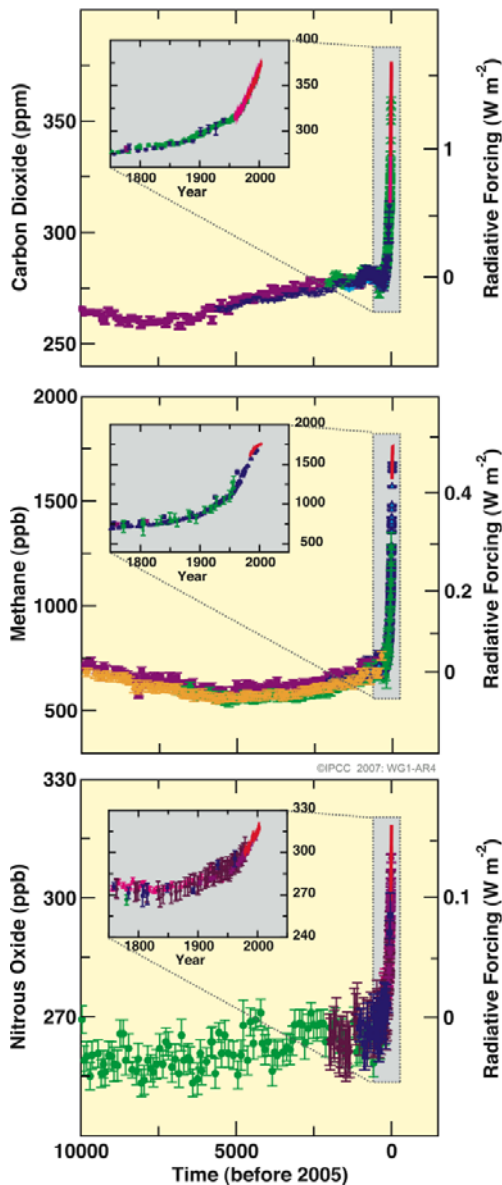


**Figure 3.2:** Atmospheric concentrations of carbon dioxide, methane and nitrous oxide over the last 10,000 years (large panels) and since 1750 (inset panels). Data shown are from ice cores (symbols with different colors for different studies) and from atmospheric samples (red lines). The corresponding RF is shown on the right hand axes of the large panels [IPCC 2007].

It can be seen from the methane plot in Figure 3.2 that the methane concentration increased more than 150% during the last 255 years. Although the concentration of methane in the atmosphere (1.8 ppm) is much less than that of carbon dioxide (370 ppm), its greenhouse effect is far from negligible. That is because the anthropogenic greenhouse effect caused by a molecule of methane is about eight times that of a molecule of carbon dioxide [Lelieveld et al. 1998]. To compare the RF of a unit mass of a given well-mixed greenhouse gas in the

present-day atmosphere integrated over a chosen time horizon, relative to that of carbon dioxide, the term “Global Warming Potential” (GWP) was introduced by the IPCC. The GWP represents the combined effect of the differing times these gases remain in the atmosphere and their relative effectiveness in absorbing outgoing thermal infrared radiation [IPCC 1990].

Although the total global methane sources are relatively well known, the strength of each source component and their trends are not. Thus, reliable methane measurements are needed to quantify the sources.

### 3.1.1 Methane

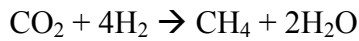
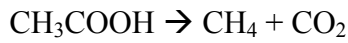
Methane (CH<sub>4</sub>) is one of the most common organic compounds. The four hydrogen atoms are located at the corners of a tetrahedron with the carbon atom in its center.

From ice core records it was detected that the atmospheric methane concentration over the last 650,000 years varied from 400 ppb up to 770 ppb [Spahni et al. 2005]. In the year 1750, the reference year for the RF calculation, the atmospheric methane concentration was  $715 \pm 4$  ppb [Etheridge et al. 1998]. As shown in the inset panel for the atmospheric methane concentration of Figure 3.2 a continuous increase in concentration from the year 1750 to 2005 is observable. The concentration in 2005 was about 1774 ppb corresponding to an increase of about 150% within the last 255 years. The RF for methane in 2005 was  $0.48 \pm 0.05$  W m<sup>-2</sup> which is the second-largest RF behind CO<sub>2</sub>. The GWP for one kg emitted CH<sub>4</sub> compared to one kg CO<sub>2</sub> is 72 for a given time horizon of 20 years [IPCC 2007]. This is due to the middle-infrared (MIR) and NIR absorption features of CH<sub>4</sub> molecules that are characterized by rotational-vibrational transitions. The main contribution of CH<sub>4</sub> to global warming comes from the  $\nu_4$  band at 1310 cm<sup>-1</sup> (7633 nm) in the atmospheric IR window between 700 and 1400 cm<sup>-1</sup> (7142 – 14285 nm). The strongest CH<sub>4</sub> absorption band is the  $\nu_3$  band at 3000 cm<sup>-1</sup> (3333 nm) [Bergamaschi et al. 1994].

Atmospheric methane originates from both non-biogenic and biogenic sources. Non-biogenic CH<sub>4</sub> includes emissions from fossil fuel mining and burning (natural gas, petroleum and coal), biomass burning, waste treatment and geological sources (fossil CH<sub>4</sub> from natural gas seepage in sedimentary basins and geothermal or volcanic CH<sub>4</sub>). Emissions from biogenic sources include wetlands, rice agriculture, livestock, landfills, forests, oceans and termites [Denman et al. 2007]. These biogenic sources account for more than 70% of the global total.

Methane is produced by primary fermentation of organic macromolecules to acetic acid (CH<sub>3</sub>COOH), other carboxylic acids, alcohols, CO<sub>2</sub> and hydrogen (H<sub>2</sub>), followed by

secondary fermentation of the alcohols and carboxylic acids to acetate, H<sub>2</sub> and CO<sub>2</sub>, which are finally converted to CH<sub>4</sub> by the so-called methanogenic Archaea [Conrad 1996].



Alternatively, the methane sources can be divided into anthropogenic and natural sources. Anthropogenic sources include rice agriculture, livestock, landfills, waste treatment, biomass burning and fossil fuel combustion. Natural sources of CH<sub>4</sub> emissions are wetlands, oceans, forests, fires, termites and geological sources [Denman et al. 2007].

Most of the atmospheric CH<sub>4</sub> is removed by reaction with the hydroxyl free radical, which is produced photochemically in the atmosphere. Further a fraction of about 7 – 11% is destroyed in the stratosphere and 1 – 10% is removed by bacterial consumption in soils [Lelieveld et al. 1998]. The average lifetime of methane in the atmosphere of about twelve years [Houghton 2004] is determined by the rate of these loss processes. An interesting observation is that the annual increase rate of CH<sub>4</sub> changed from greater than 1% yr<sup>-1</sup> (i.e. about 14 ppb yr<sup>-1</sup>) in the late 1970's early 1980's to close to zero towards the end of the 1990's (Figure 3.3a) [Dlugokencky et al. 1998; Simpson et al. 2002]. The interannual variability of this growth rate decrease is shown in Figure 3.3b. The reason for this decrease is not yet understood but it seems to be clearly related to the imbalance between CH<sub>4</sub> sources and sinks. Dlugokencky as well as Francey suggested that the slowdown in the growth rate reflects a stabilization of CH<sub>4</sub> emissions [Dlugokencky et al. 1998; Francey et al. 1999]. Some researchers consider that economic incentives have led to a reduction in CH<sub>4</sub> emissions [Hansen et al. 2000]. Furthermore the long-term change in its main sink, the hydroxyl free radical, implies that CH<sub>4</sub> emissions are not increasing anymore.

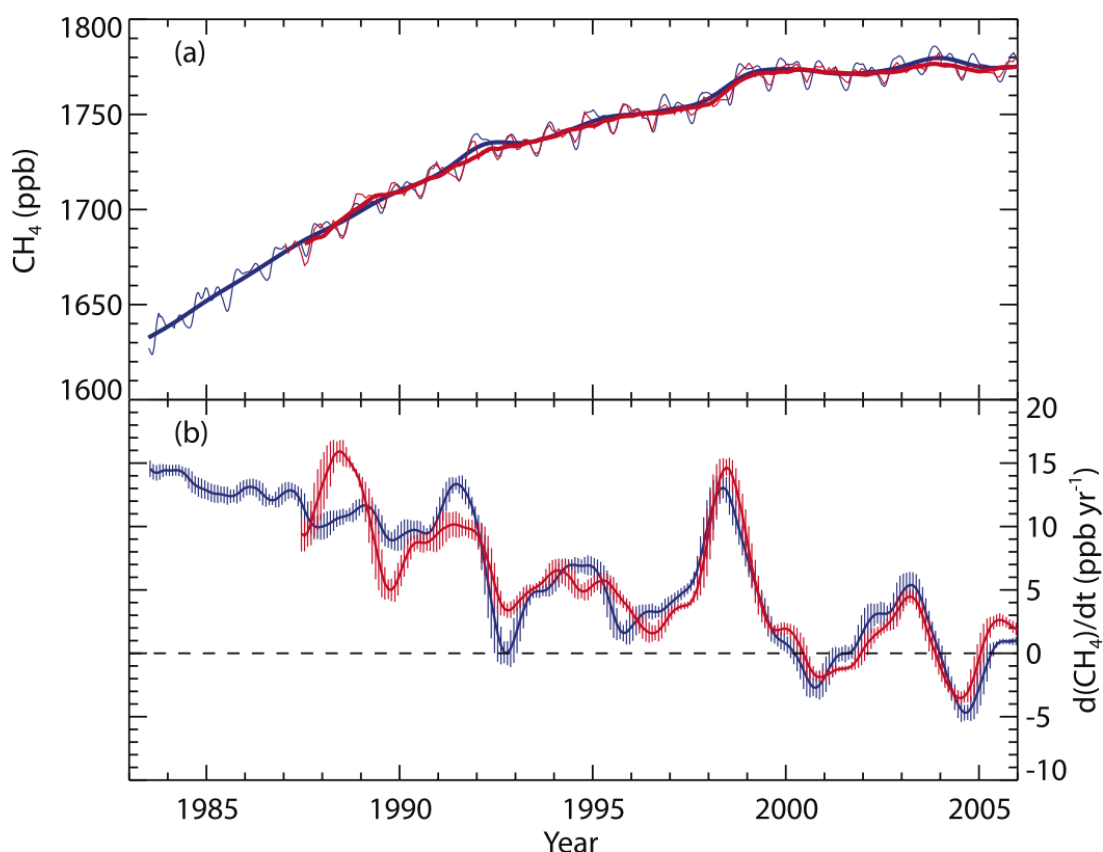


**Figure 3.3:** Recent  $\text{CH}_4$  concentrations and trends. (a) Time series of global  $\text{CH}_4$  abundance mole fraction (in ppb) derived from surface sites operated by NOAA/GMD (blue lines) and AGAGE (red lines). The thinner lines show the  $\text{CH}_4$  global averages and the thicker lines are the de-seasonalized global average trends from both networks. (b) Annual growth rate ( $\text{ppb yr}^{-1}$ ) in global atmospheric  $\text{CH}_4$  abundance from 1984 through the end of 2005 (NOAA/GMD, blue), and from 1988 to the end of 2005 (AGAGE, red). The vertical lines indicate  $\pm 2$  standard deviation uncertainties (95% confidence interval), and 1 standard deviation uncertainties are between 0.1 and 1.4  $\text{ppb yr}^{-1}$  for both AGAGE and NOAA/GMD. Note that the differences between AGAGE and NOAA/GMD calibration scales are determined through occasional intercomparisons [IPCC 2007].

Like mentioned above, the total global  $\text{CH}_4$  source is well known but the strength of each source component and their trends are not. Furthermore Keppler [Keppler et al. 2006] discovered methane emissions from living vegetation and leaf litter under aerobic conditions and estimated that this contributed to 10 – 30% of the global  $\text{CH}_4$  source. They calculated a source strength of 62 – 236  $\text{Tg yr}^{-1}$  for living plants and 1 – 7  $\text{Tg yr}^{-1}$  for plant litter [Keppler et al. 2006]. A newer study from Houweling calculated a new strength and limited this source to 125  $\text{Tg yr}^{-1}$  [Houweling et al. 2006]. Kirschbaum revised this estimate downwards to 10 – 60  $\text{Tg yr}^{-1}$  [Kirschbaum et al. 2006]. Table 3.1 summarizes actual values of sources and sinks of  $\text{CH}_4$ .

To date, experimental evidence has reported high levels of methane emissions [Keppler et al. 2006], moderate levels of methane [Wang et al. 2008] and no methane emissions [Dueck et al.

2007; Beerling et al. 2008] from living and dead plants. However, the conditions under which these measurements were made have not been standardized [Dueck et al. 2008]. In their most recent paper, Keppler showed that methoxyl groups in plant pectin are precursors of methane [Keppler et al. 2008] but the mechanism still reveals to be unraveled [Dueck et al. 2008].

**Table 3.1:** Sources, sinks and atmospheric budgets of CH<sub>4</sub> (Tg yr<sup>-1</sup>) according to IPCC [Lowe 2006].

	<b>Estimates</b>	<b>Range of estimates</b>
<b>Natural sources</b>		
Wetlands	145	92 – 237
Termites	20	20 – 20
Ocean	10	10 – 15
Hydrates (marine and terrestrial)	5	5 – 10
<b>Human-generated sources</b>		
Energy generation (coal mining, natural gas, petroleum industry)	95	75 – 110
Rice agriculture	60	40 – 100
Ruminant animals	93	80 – 115
Landfills	50	35 – 73
Biomass burning	52	23 – 55
<b>Total identified sources</b>	<b>530</b>	<b>500 – 600</b>
<b>Sinks</b>		
Tropospheric oxidation	507	450 – 510
Stratospheric loss	40	40 – 46
Soils	30	10 – 44
<b>Total identified sinks</b>	<b>577</b>	<b>460 – 580</b>
<b>Total sources-sinks</b>		
	<b>-47</b>	<b>-80 to +140</b>

As can be seen from this table the emissions from anthropogenic sources are the main contributor to atmospheric CH<sub>4</sub> budgets. Under these sources agriculture and animal husbandry are one of the main factors of methane emissions.

### 3.1.2 Ammonia

Ammonia ( $\text{NH}_3$ ) is the most abundant alkaline component in the atmosphere [Asman et al. 1998]. At ambient temperatures it is a gas with a characteristic pungent odor. At a concentration about 15 ppm the odor of  $\text{NH}_3$  in ambient air is not, at about 30 ppm barely, at about 60 ppm weakly and at about 120 ppm strongly noticeable.  $\text{NH}_3$  has a trigonal pyramid shape and the nitrogen atom in the molecule has a lone electron pair, so ammonia acts as a base, a proton acceptor. This shape gives ammonia an overall dipole moment and makes it polar so that it readily dissolves in water [Römpp 1995].

It reacts readily with acidic substances such as sulfuric acid ( $\text{H}_2\text{SO}_4$ ), nitric acid ( $\text{HNO}_3$ ), nitrous acid ( $\text{HNO}_2$ ), or hydrochloric acid ( $\text{HCl}$ ) to form ammonium salts that occur predominantly in the fine particle (size  $< 2.5 \mu\text{m}$ ) fraction [Finlayson-Pitts et al. 1999]. A small amount of  $\text{NH}_3$  (approximately 1%) reacts with hydroxyl radicals to form  $\text{NH}_2 + \text{H}_2\text{O}$ , which is subsequently oxidized to  $\text{NO}$  by  $\text{HNO}_3$  [Galbally et al. 1983]. The formation of fine particulate ammonium ( $\text{NH}_4^+$ ) salts is a very effective mechanism in removing gaseous  $\text{NH}_3$  from the atmosphere. This conversion is most effective in the lowest (100 m) layer of the atmosphere above the surface [Lenhard et al. 1980] and is much faster during the daytime than at night [Erisman et al. 1988].  $\text{NH}_4^+$  containing aerosol may both directly and indirectly affect light scattering and global RF, which is a regional scale problem [Sutton et al. 2001]. The lifetime of ammonia in the atmosphere is only a few hours to a few days [Olivier et al. 1998].

The surface exchange of  $\text{NH}_3$  with plants is essentially bi-directional.  $\text{NH}_3$  uptake depends on the concentration gradient between ambient air and mesophyll tissue (compensation point) of the plant. As long as ambient  $\text{NH}_3$  concentrations exceed the compensation point,  $\text{NH}_3$  uptake by the shoot will occur. If the internal mesophyll  $\text{NH}_3$  concentration of the vegetation exceeds the ambient level,  $\text{NH}_3$  is emitted by the plants. In general, the compensation point is larger for agricultural than for semi-natural plants, and varies with plant growth stage. However, exchange of  $\text{NH}_3$  does not only occur through the stomata, but it can also be deposited to leaf surfaces, as well as emitted back to the atmosphere from drying leaf surfaces [Asman et al. 1998]. Measurements from Sutton demonstrate the bi-directional nature of  $\text{NH}_3$  fluxes, with typically daytime emission and small nocturnal deposition [Sutton et al. 2001]. The deposition of  $\text{NH}_3$  is of major environmental concern, since this may lead to changes in plant species and soils through eutrophication and acidification [Fangmeier et al. 1994]. It is deposited rapidly within the first 4 – 5 km from its source [Krupa 2003]. While livestock dominate point source  $\text{NH}_3$  emissions, evidence suggests that exchange with vegetation plays a major role in

regulating both air concentrations and the extent of long-range transport [Langford et al. 1992].

$\text{NH}_3$  and subsequently derived  $\text{NH}_4^+$  are removed from the atmosphere both by dry and wet deposition. Dry deposition occurs by diffusion ( $\text{NH}_3$ ) and Brownian motion (fine particle  $\text{NH}_4^+$ ) and to a much lesser extent by sedimentation or impaction (coarse particles, size  $> 2.5 \mu\text{m}$ ) [Finlayson-Pitts et al. 1999]. The major portion of  $\text{NH}_4^+$  occurs in the fine particle portion. In contrast, wet deposition occurs by rainout (in-cloud processes) and by washout (below cloud scavenging). Dry deposition is more important in regions with high  $\text{NH}_3$  emissions and wet deposition in areas with low emissions [Krupa 2003]. Table 3.2 shows global sources of  $\text{NH}_3$ .

**Table 3.2:** Global sources ( $\text{TgN yr}^{-1}$ ) of  $\text{NH}_3$  for the 1990s [Asman et al. 1998; IPCC 2007].

Source	IPCC AR4	Asman
<b>Anthropogenic sources</b>		
Fossil fuel combustion & industrial processes	2.5	
Agriculture	35	
Dairy cattle		4.3
Non-dairy cattle		8.6
Buffaloes		1.2
Pigs		3.4
Poultry		1.9
Sheep/Goats		1.5
Other animals		0.7
<b>Subtotal domestic animals</b>		<b>21.6</b>
Fertilizers		9.0
Agricultural crops		3.6
Biomass and biofuel burning	5.4	4.1
Human excreta	2.6	
<i>Anthropogenic total</i>	<i>45.5</i>	<i>38.3</i>
<b>Natural sources</b>		
Soils under natural vegetation	2.4	
Oceans	8.2	8.2
Other sources		7.2
<i>Natural total</i>	<i>10.6</i>	<i>15.4</i>
<b>Total sources</b>	<b>56.1</b>	<b>53.7</b>

As can be seen from Table 3.2 more than between 70% [Asman et al. 1998] to 80% [IPCC 2007] of the global  $\text{NH}_3$  emission originates from anthropogenic sources. Of these sources agriculture is by far the most important one.

Since nitrogen is a limiting factor in biomass production, one of the most obvious plant responses following  $\text{NH}_y$  ( $\text{NH}_3 + \text{NH}_4^+$ ) assimilation is enhanced growth. This growth is mainly due to shoot growth response while root growth increases only slightly [Tisdale et al. 1993]. At excessive (toxic)  $\text{NH}_3$  concentrations growth is depressed.

Ammonia volatilization can occur whenever free  $\text{NH}_3$  is present near the soil surface. Ammonia losses from the soil can range between 3 and 50% depending on the texture of the soil and the type of N-fertilizer applied (urea,  $\text{NH}_4\text{NO}_3$  and  $(\text{NH}_4)_2\text{SO}_4$ ). When soil pH values change from acidic to basic,  $\text{NH}_4^+$  is converted to  $\text{NH}_3$ . Loss of  $\text{NH}_3$  increases with increasing soil temperature and the concentration of urea or  $\text{NH}_4\text{-N}$  added, but the proportion of N volatilization as  $\text{NH}_3$  is constant [Nelson 1982]. The lowest losses of ammonia occur from ammonium nitrate fertilizer of 1 – 2% directly after field application. Ammonium sulfate fertilizer show losses of 5 – 15% while those from urea show 20 – 30% [Erisman et al. 2002]. With all these fertilizers ammonia losses are unavoidable because the nitrogen use efficiency is much lower than 100%, which means that within the cascade nitrogen losses will occur [Galloway et al. 2003]. Socolow discovered that the first 100  $\text{kg ha}^{-1}$  of fertilizer N is three times as effective for crop growth as the second hundred [Socolow 1999]. The world average fertilizer use in 2001 was 90  $\text{kg ha}^{-1}$  in agricultural land, ranging from 0.2  $\text{kg ha}^{-1}$  in Congo to 562  $\text{kg ha}^{-1}$  in Ireland [Erisman et al. 2007].

Unfertilized terrestrial ecosystems are usually characterized by relatively closed N cycling, i.e. N input and output are comparably small in relation to N exchange in the soil-plant subsystem [Fenn et al. 1998]. In these ecosystems N is usually limiting for productivity and additional nitrogen is readily absorbed and utilized. If deposition exceeds the capacity to utilize N for a considerable period of time, over-saturation of the system indicated by N loss will occur. N loss may occur either by leaching of  $\text{NO}_3^-$  which is more mobile than  $\text{NH}_4^+$  or by denitrification, yielding  $\text{N}_2$  and some  $\text{N}_2\text{O}$ . The latter gas is emitted at higher rates from soils polluted with  $\text{NH}_4^+$  and contributes to the greenhouse effect and to the destruction of the stratospheric ozone layer [IPCC 1990]. In contrast to that, in nitrogen poor areas crop production might benefit from the ammonia emission [Erisman et al. 2007].

### **3.2 Optical Spectroscopy**

Optical spectroscopy (OS) is utilized in various fields of science, industry and medicine, particularly in (bio-) chemistry, biology, physics and astronomy. OS is highly specific, each substance is in principle distinguishable from all others by its spectral properties. Samples can be qualitatively and quantitatively analyzed. Measurements of various optical parameters as a function of wavelength/energy („spectrum“) or time („kinetics“) provide valuable insights that are not, or not readily, attainable by other analytical methods [Schmidt 2005].

The energy source for optical spectroscopic investigation covers the spectral range from the UV, followed by VIS up to the IR region.

OS has advantages compared to other analytical methods, e.g. it is not destructive or invasive. Moreover remote measurements are feasible, i.e., measurements ranging from distances of a few millimeters up to long distances, such as from airplanes or satellites, without any physical contact with the sample.

### 3.3 Photoacoustic Spectroscopy

The photoacoustic effect was first reported in 1880 by A.G. Bell. During his experiments with the “photophone” he noticed that a rapidly interrupted beam of sunlight focused on a solid substance produces an audible sound [Bell 1880]. His test arrangement is schematically shown in Figure 3.4. He discovered the PA effect in liquids and gases as well. Due to the limitations set by the light sources and sound detectors used in this early experiments the progress towards useful applications was inhibited. A blackbody IR source for radiation input and a microphone to detect the acoustic signal was first used by Viengerov in 1938 [Viengerov 1938]. Other researchers used two PA cells, one containing the gas mixture to be analyzed and the other the mixture without the substance of interest, to minimize the background noise [Luft 1943]. Kerr was the first to use a laser as radiation source reaching higher sensitivity and selectivity [Kerr et al. 1968]. Kreuzer introduced the PA technique for trace gas detection [Kreuzer 1971].

The progress achieved from the discovery of the PA effect discovered in 1880 to the nowadays used trace gas detection systems was due to the development of intensive radiation sources but also due to considerable improvements of the detection system (microphones and electronics). Compared to conventional light sources, lasers have superior beam quality and spectral purity, and can provide high power radiation. Temperature changes of as small as  $10^{-6}$  K and changes in power density of less than  $10^{-6}$  J cm<sup>-3</sup> s<sup>-1</sup> are measurable [Schmidt 2005]. For more detailed information about the principle of PAS see e.g. [Pao 1977; Rosencwaig 1980; Zharov et al. 1986].

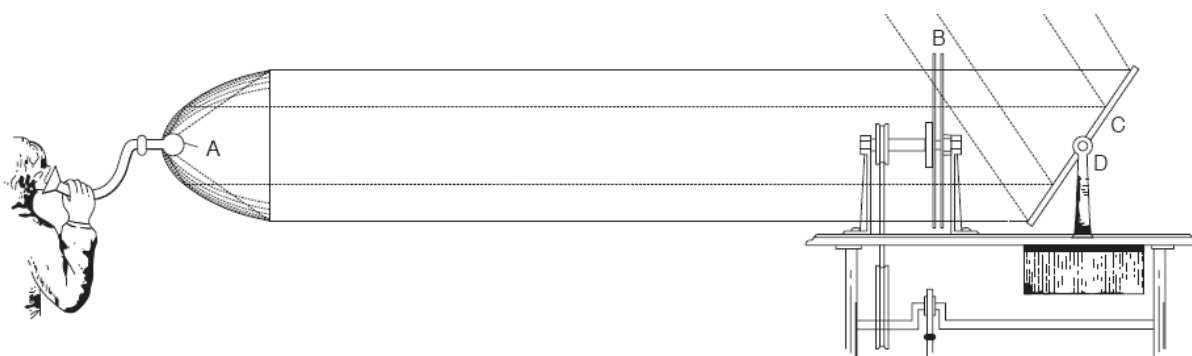


**Figure 3.4:** Sunlight is intercepted and aligned with a steering mirror (C, D), modulated with a chopper (B) and focused onto a glass bulb (A) [Bell 1881].

### 3.3.1 Photoacoustic Spectroscopy of Gases

Molecular absorption of photons results in the excitation of molecular energy levels (rotational, vibrational-rotational, electronic). The de-excitation of excited molecular energy levels can occur by radiant processes, such as spontaneous or stimulated emission, and by radiationless deactivation, which always channels at least part of the absorbed energy into the translational degrees of freedom of neighboring gas species. If the excitation energy is high enough, also direct photochemical decomposition of the excited molecule can occur. In the case of fundamental vibration excitation, radiative emission and chemical reactions do not play an important role, because the radiative lifetime of vibrational levels is long compared with the time needed for collisional deactivation at ordinary pressures normally used in PAS ( $\sim 10^5$  Pa). Furthermore the photon energy is too small to induce reactions [Hess 1992].

Thus, radiationless collisional deactivation always leads to heat production in the spatially confined irradiated region, appearing as translational (kinetic) energy of the gas molecules. This local heating effect generated with a short light pulse or a modulated light beam induces a local expansion process, which causes transient pressure change. The deposited heat power density is proportional to the absorption coefficient and the incident light intensity, [Rosencwaig 1980; Miklos et al. 2001]. Nowadays for the detection of gases lasers are predominantly used as light sources. A detailed scheme illustrating the series processes occurring during PA signal generation is presented in Figure 3.5.

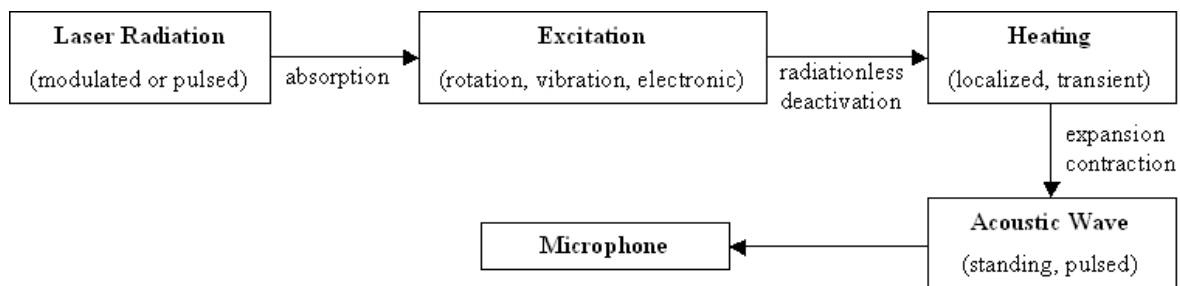


**Figure 3.5:** Scheme of the physical processes occurring after optical excitation of molecules. Modulated or pulsed laser radiation leads to the population of rotational, vibrational, and electronic states. Collisional radiationless deactivation leads to localized transient heating. The resulting expansion launches standing or pulsed acoustic waves, which are detected with a microphone.

### 3.3.2 Resonant and Nonresonant Photoacoustic Spectroscopy

PAS is subdivided into resonant and nonresonant. The main difference is the design of the PA cell and the modulation frequency of the incident light.

High detection sensitivities can be obtained with nonresonant PA technique by using a sample cell with a small volume of about 1 – 10 cm<sup>3</sup> and typical modulation frequencies of exciting radiation of up to 2 kHz. Such frequencies are in general far below the acoustic resonance of the cell so that standing waves cannot be formed. This setup for nonresonant PA experiments is extremely simple and highly sensitive due to the small volume. Typically, electret microphones are used as sensitive detectors for gas analysis. Lock-in technique (phase sensitive detection and amplification of the microphone signal) is standard for signal processing. The limiting factor for the sensitivity is the relatively large background signal caused by window and wall absorptions.

In contrast to the small volume PA cells for nonresonant experiments the cells employed for resonant PAS are in the range of 100 – 1000 cm<sup>3</sup>. The resonance enhancement, Q-factor (see chapter 3.3.3), is obtained by exciting acoustic resonances in the cavity. The Q-factor is depending on pressure and energy dissipation within the cavity. Thus, the losses in signal strength due to the larger volume may be compensated by the resonance amplification.

Advantages of resonant PA cells are:

- Improvement of the signal to noise ratio (SNR)
- Realization of a continuous gas flowing through the PA detector cell
- Minimization of adsorption of gaseous molecules under study on the PA cell walls
- Determination of the relaxation and thermodynamic characteristics of the gas under study

The principal cavity modes of a cylindrical chamber are schematically shown in Figure 3.6.

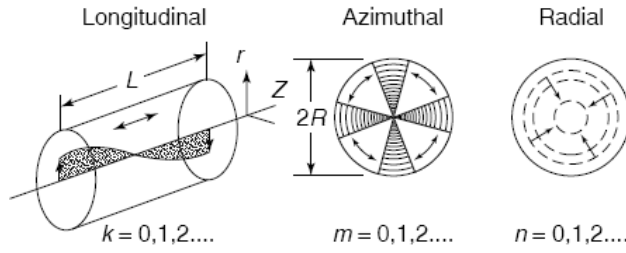


**Figure 3.6:** Resonant acoustic modes of a cylindrical closed chamber; the fundamental longitudinal, azimuthal and radial modes [Harren et al. 2000].

The normal vibration modes,  $p_j$ , of an enclosed cylinder of length  $L$  and radius  $R$  are described by the solution to the wave equation [Morse et al. 1986].

$$p_j = P_j \sin(m\phi) \cos(k\pi z / L) J_m(\alpha_{m,n} \pi r / R) \exp(-i\omega_j t) \quad (3.1)$$

$$\omega_j = \pi c_0 \left[ (k/L)^2 + (\alpha_{m,n}/R)^2 \right]^{1/2} \quad (3.2)$$

where  $\omega_j$  is the frequency of the  $j$ th mode;

$P_j$  is a normalization coefficient such that  $V_c^{-1} \int p_j^* p_k dV = 1$  for  $j = k$  and 0 for  $j \neq k$ ,

$V_c$  is the chamber volume, and  $p_j^*$  is the complex conjugate of  $p_j$ ;

$k, m, n$  are eigenvalues defining the longitudinal, azimuthal and radial modes, respectively;

$z, r, \phi$  are standard cylindrical coordinates;

$J_m$  is the Bessel function;

$\alpha_{m,n}$  is the  $n$ th solution of  $(dJ_m/dr) = 0$  at  $r = R$ ;

$t$  is time; and

$c_0$  is the speed of sound in the gas in the cylinder.

Optical excitation, e.g. by lasers, of the radial and longitudinal modes of the cell is achieved when the radiation is coincident with the radial axis of the cylinder, while the azimuthal mode excitation is maximized with radiation beam positioned near the end plate circumference and parallel to the radial axis [Adams 1988]; see Figure 3.7 for different resonant acoustic cell designs. In this work the PA cell design according to Figure 3.7e was applied.

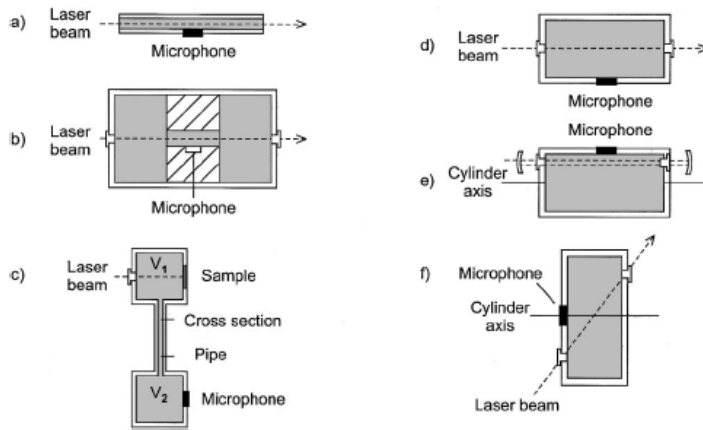


**Figure 3.7:** Resonant acoustic cell designs. a) Simple pipe (tube) for excitation of longitudinal modes, b) pipe with two buffer volumes, c) Helmholtz resonator with separate sample and detection chambers for solid samples, d) coaxial excitation (e.g., of radial modes) in a cylinder, e) asymmetric multipass arrangement for excitation of azimuthal modes in a cylinder, and f) cylindrical cell suitable for excitation of the first radial mode with suppression of the window noise [Miklos et al. 2001].

The ideal PA cell design for trace gas detection should amplify the generated sound originating from the molecular gas absorption while simultaneously rejecting acoustic and electric noise and in-phase IR absorption from other materials. Other requirements for PA cells are low gas consumption or a fast response. For this the active volume of the cell should be small so that no dilution can take place when the trace gas and its carrier flow through the acoustic cell [Harren et al. 2000]. Moreover the sound pressure is always proportional to the absorption coefficient and the laser power and is inversely proportional to an effective cross section defined by the ratio of the cell volume and length. In the case of modulated PAS the signal is in addition inversely proportional to the modulation frequency and proportional to the Q-factor of the resonance.

As an example Figure 3.8 shows the excitation of different acoustic modes in the PA cell by a test speaker and by a laser diode, respectively. As can be seen from this Figure the laser diode only excites the first, second and third azimuthal acoustic mode ( $m$ ), while the speaker excites longitudinal modes ( $k$ ) as well. This is attributed to the excentric irradiation of the laser beam into the PA cell.

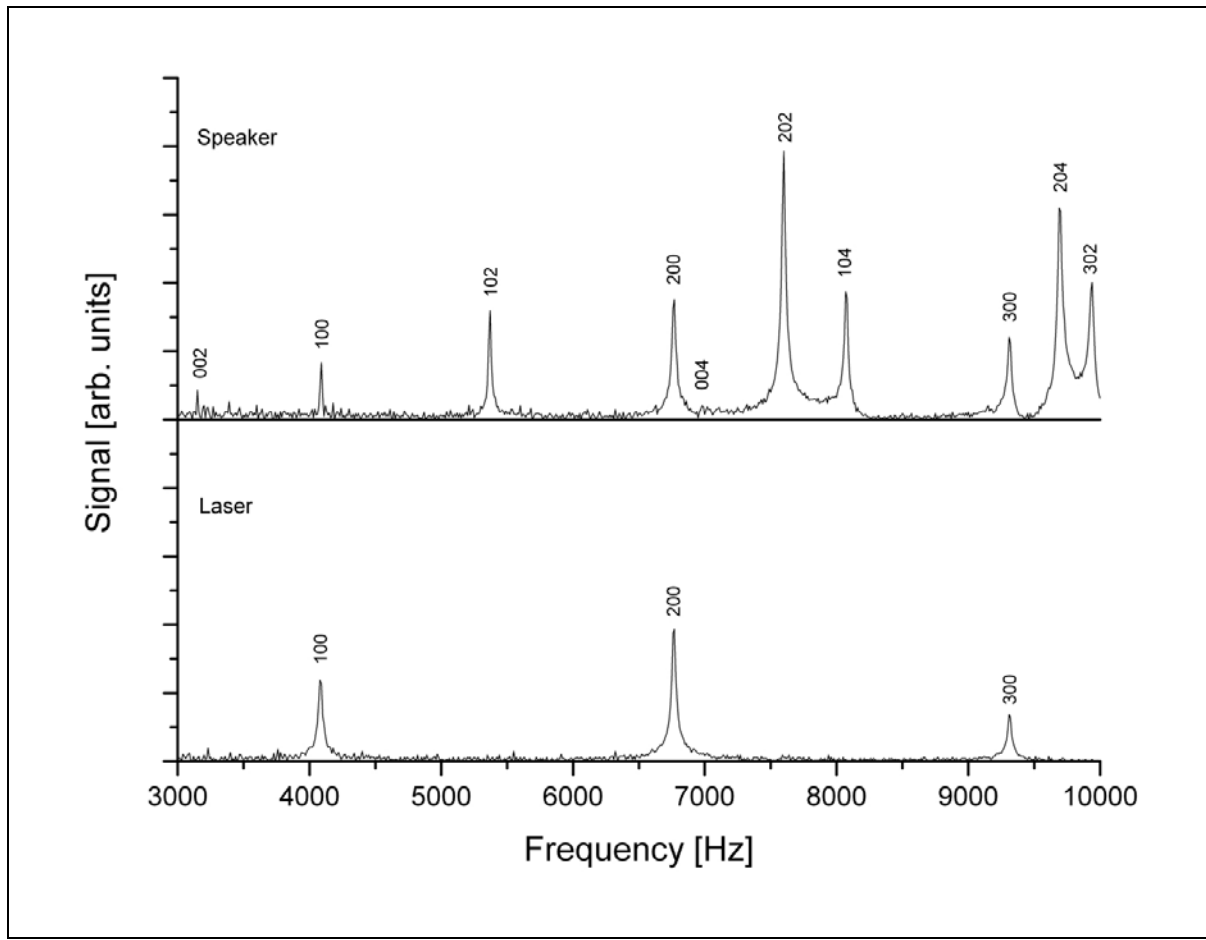


**Figure 3.8:** Acoustic spectrum of the PA cell for  $T = 294,5$  K and 100 ppm  $\text{NH}_3$ . Excited by speaker (top) and laser (bottom). The numbers represent the azimuthal ( $m$ ), radial ( $n$ ) and longitudinal ( $k$ ) acoustic modes.

### 3.3.3 Q-factor

The resonance enhancement is expressed by the Q-factor:

$$Q = \frac{\nu_0}{FWHM} \quad (3.3)$$

where  $\nu_0$  is the resonance frequency and FWHM full width at half maximum. Sound velocity, heat capacity, thermal conductivity, viscosity and the energies and relaxation times of molecular vibration-rotations are important parameters which determine the resonance frequencies as well as the quality factors of the resonances [Johnson et al. 1982].

The Q-factors of the PA cells used in this work were 180 for methane and 185 for ammonia, respectively. An example of the excitation of the second azimuthal mode by the laser diode is given in Figure 3.9 for ammonia.

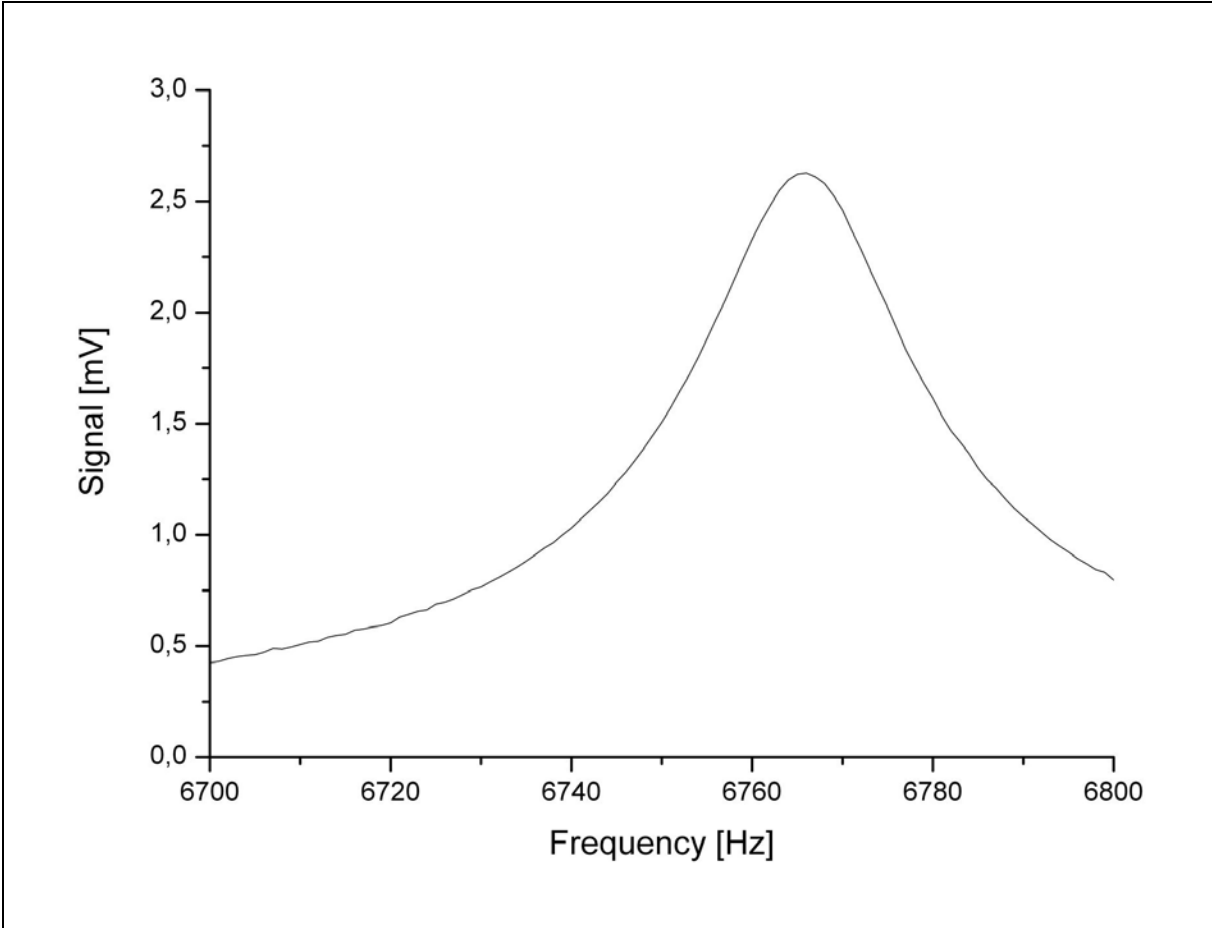


**Figure 3.9:** Excitation by the laser diode of the second azimuthal mode of a resonant cell filled with 100 ppm NH<sub>3</sub> depending of modulation frequency. The Q-factor is determined to Q = 185.04.

### 3.4 Trace Gas Measuring Devices

Nowadays there exist many different methods and analytical instruments for trace gas measurements, most of them applying absorption and photoacoustic spectroscopy. Like already mentioned in chapter 3.1.1 and 3.1.2 the fluxes of methane and ammonia are spatially variable. Therefore, reliable in situ measurements of these trace gases are needed. Only few of the developed instruments are capable of in situ trace gas measurements. An overview of the available devices for measuring methane and ammonia in ambient air is given in Table 3.3. Moreover it is indicated in that Table whether the devices are portable and therefore capable for in situ field measurements. Portable is defined that it should be possible to carry the device by hand. Moreover one should be able to use the device everywhere e.g. at the field. Some scientists improved their detection limit by calculating the  $1\sigma$  or  $2\sigma$  limit while others use  $3\sigma$ . In this work the  $3\sigma$  detection limit was solely used. Furthermore some of the devices shown in Table 3.3 are commercial devices. They are portable and very sensitive, some can even measure different gases at the same time, but the prices for these trace gas analyzers are very high so they do not fulfill the demand to be inexpensive.

A typical setup for resonant PA trace gas detection, as used in this work, is shown in Figure 3.10.

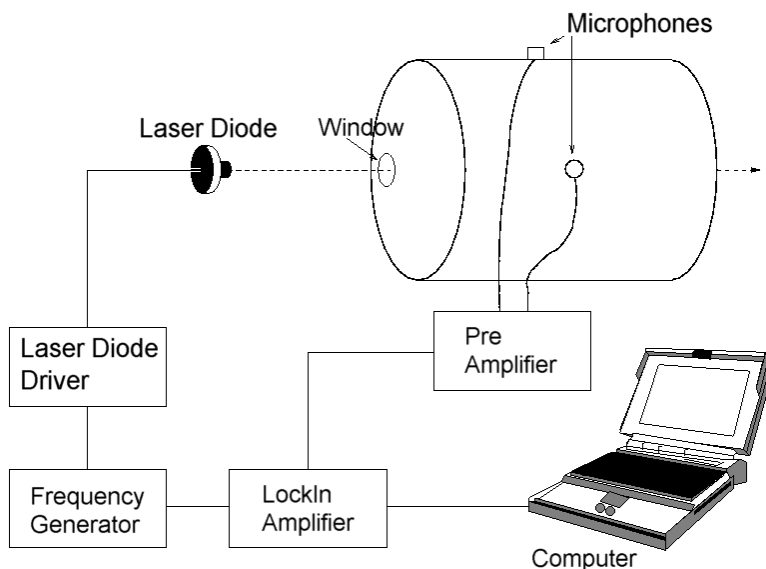


**Figure 3.10:** Schematic experimental setup of the TDL-PA device.

**Table 3.3:** Different ambient air methane and ammonia measuring devices. N/A = not applicable.

Species	Technique	Wavelength [nm]	Detection limit [ppb]	Real-time measurement	Portable	Reference
CH <sub>4</sub>	Gas Chromatograph with flame ionization detector	---	1	yes	yes	[Breuer et al. 2000]
CH <sub>4</sub>	Open path gas analyzer	N/A	10 – 1000 depending on path length	yes	yes	[Boreal-laser 2007]
CH <sub>4</sub>	Infrared Photoacoustic Spectroscopy	N/A	100	yes	yes	[Innova 2007]
CH <sub>4</sub>	Mid-infrared Spectroscopy	3314	0.4	yes	yes	[Maddaloni et al. 2006]
CH <sub>4</sub>	Mid-infrared Spectroscopy	7800	2	yes	yes	[Werle et al. 2002]
CH <sub>4</sub>	Cavity ring-down Spectroscopy	3221	0.16	yes	no	[Ngai et al. 2006]
CH <sub>4</sub>	Cavity ring-down spectroscopy	~3000	< 1	yes	no	[Kleine et al. 2001]
CH <sub>4</sub>	Intra-cavity Photoacoustic Spectroscopy	7655	10 <sup>+</sup>	yes	no	[Bijnen et al. 1996]
CH <sub>4</sub>	Absorption Spectroscopy	1653	< 5000 <sup>+</sup>	yes	yes	[Iseki 2004]
CH <sub>4</sub>	Absorption Spectroscopy	7900	4 <sup>+</sup>	yes	no	[Nelson et al. 2004]
CH <sub>4</sub>	Absorption Spectroscopy	1651	30	yes	yes	[Nadezhdinskii et al. 1999]
CH <sub>4</sub>	Absorption Spectroscopy	3290	500 <sup>*</sup>	yes	yes	[Töpfer et al. 1997]
CH <sub>4</sub>	Photoacoustic Spectroscopy	7827	34 <sup>+</sup>	yes	no	[Grossel et al. 2007]
CH <sub>4</sub>	Photoacoustic Spectroscopy	1651	80	yes	no	[Besson et al. 2006b]
CH <sub>4</sub>	Photoacoustic Spectroscopy	---	< 1	N/A	N/A	[Koskinen et al. 2006]
CH <sub>4</sub>	Photoacoustic Spectroscopy	1651	180 <sup>*</sup>	yes	no	[Schilt et al. 2006]
CH <sub>4</sub>	Photoacoustic Spectroscopy	1635	6000 <sup>*</sup>	no	no	[Scotoni et al. 2006]
CH <sub>4</sub>	Photoacoustic Spectroscopy	2298	20000	no	no	[Civis et al. 2005]
CH <sub>4</sub>	Photoacoustic Spectroscopy	1651	23 <sup>*</sup>	yes	yes	[Link 2005]
CH <sub>4</sub>	Photoacoustic Spectroscopy	1651	115 <sup>*</sup>	yes	yes	[Sauter 2004]
CH <sub>4</sub>	Photoacoustic Spectroscopy	1651	300	yes	no	[Zeninari et al. 2003]
CH <sub>4</sub>	Photoacoustic Spectroscopy	1653	5000	yes	no	[Kapitanov et al. 2002]

+ = 1  $\sigma$  detection limit, # = 2  $\sigma$  detection limit, \* = 3  $\sigma$  detection limit

Species	Technique	Wavelength [nm]	Detection limit [ppb]	Real-time measurement	Portable	Reference
NH <sub>3</sub>	Open path gas analyzer	N/A	10 – 1000 depending on path length	yes	yes	[Boreal-laser 2007]
NH <sub>3</sub>	Dräger-tubes	---	0.25	no	yes	[Drägerwerk 1994]
NH <sub>3</sub>	Tungstic acid denuder	---	0.04	no	yes	[Williams 1992]
NH <sub>3</sub>	Wet trapping	---	0.5	no	yes	[Denmead et al. 1977]
NH <sub>3</sub>	Photofragmentation/two photon laser-induced fluorescence	---	0.01	yes	no	[Schendel et al. 1990]
NH <sub>3</sub>	Photothermal Interferometer	9220	0.066 <sup>#</sup>	yes	no	[Owens et al. 1999]
NH <sub>3</sub>	Absorption Spectroscopy	2005	25 <sup>+</sup>	yes	yes	[De Tommasi et al. 2006]
NH <sub>3</sub>	Absorption Spectroscopy	1531	700 <sup>*</sup>	yes	yes	[Claps et al. 2001]
NH <sub>3</sub>	Cavity-enhanced Absorption Spectroscopy	1522	100 <sup>+</sup>	yes	no	[Peeters et al. 2000]
NH <sub>3</sub>	Infrared Photoacoustic Spectroscopy	N/A	200	yes	yes	[Innova 2007]
NH <sub>3</sub>	Quartz-enhanced Photoacoustic Spectroscopy	---	0.5 <sup>+</sup>	yes	no	[So et al. 2007]
NH <sub>3</sub>	Quartz-enhanced Photoacoustic Spectroscopy	2005	3000 <sup>+</sup>	yes	no	[Lewicki et al. 2007]
NH <sub>3</sub>	Quartz-enhanced Photoacoustic Spectroscopy	1531	650 <sup>+</sup>	yes	no	[Kosterev et al. 2004]
NH <sub>3</sub>	Fiber-amplifier enhanced photoacoustic Spectroscopy	1531	120 <sup>+</sup>	yes	yes	[Webber et al. 2005]
NH <sub>3</sub>	Photoacoustic Spectroscopy	---	0.1	yes	yes	[Omnisens 2007]
NH <sub>3</sub>	Photoacoustic Spectroscopy	1531	12	yes	no	[Besson et al. 2006a]
NH <sub>3</sub>	Photoacoustic Spectroscopy	9555	30 <sup>+</sup>	yes	no	[Filho et al. 2006]
NH <sub>3</sub>	Photoacoustic Spectroscopy	1635	60000 <sup>*</sup>	no	no	[Scotoni et al. 2006]
NH <sub>3</sub>	Photoacoustic Spectroscopy	2298	1000	no	no	[Civis et al. 2005]
NH <sub>3</sub>	Photoacoustic Spectroscopy	10784	0.032 <sup>+</sup>	yes	no	[Pushkarsky et al. 2003]
NH <sub>3</sub>	Photoacoustic Spectroscopy	1531	100 <sup>*</sup>	yes	yes	[Reinhardt 2002]
NH <sub>3</sub>	Photoacoustic Spectroscopy	1531	200 <sup>+</sup>	yes	no	[Schmohl et al. 2002]
NH <sub>3</sub>	Photoacoustic Spectroscopy	9220	1 <sup>+</sup>	yes	no	[Rooth et al. 1990]

+ = 1  $\sigma$  detection limit, # = 2  $\sigma$  detection limit, \* = 3  $\sigma$  detection limit

For detailed information about the PAS devices used in this work see [Reinhardt 2002; Sauter 2004; Link 2005]. The instruments had been successfully used in many different field experiments. Their reliability was demonstrated either by comparison with commercial devices or with gas chromatographic techniques [Reinhardt 2002; Jungkunst et al. 2006].

### 3.5 Semiconductor Laser

The principle of semiconductor lasers was introduced by Basov in 1961 who suggested that stimulated emission of radiation can also occur in semiconductors by the recombination of charge carriers (electrons and holes) injected across a p-n junction. In 1962 this concept was realized as a pulsed system by Hall [Hall et al. 1962]. In 1969 the simple p-n junction was replaced by multiple semiconductor layers of different compositions (heterostructures). Due to this heterostructures it was possible to develop lasers that were capable of running continuously at room temperature. The nowadays used semiconductor material depends on the emission wavelength of the laser diode which ranges from UV over VIS to the NIR region.

The advantages of semiconductor lasers over other types of lasers are e.g. a small size with only several cubic millimeters; highest efficiency (often more than 50%) and a long lifetime compared with other lasers.

Most state-of-the-art semiconductor diode lasers use forward biased double hetero p-n structures to achieve carrier inversion. In this type of structure, an undoped semiconductor layer with a direct band gap is sandwiched between p-doped and n-doped material with a higher band gap. When the junction is forward biased, this region acts as a laser-active layer which amplifies optical radiation by stimulated emission. There are different types of optical resonators creating optical feedback, e.g. Fabry-Pérot, Distributed Feedback (DFB) and Distributed Bragg Reflector.

Detailed information about the concept of semiconductor lasers can be found in the literature, e.g. see following references [Siegmann 1986; Chow et al. 1997; Diehl 2000; Kneubühl et al. 2005].

The emission wavelengths of semiconductor laser diodes can be continuously adjusted over the range of some nanometers by either changing the operating temperature or the injection current. Changing the operating temperature leads to a slow and broad adjustment while changing the injection current leads to a fast and fine tuning of the emitted wavelength. By doing so it is possible to reach every wavelength that is required for e.g. PA trace gas detection. In this work the used laser diodes were DFB-lasers with an emission at 1651 nm and 1512 nm for detection of CH<sub>4</sub> and NH<sub>3</sub>, respectively.



## **4 Material and Methods**

In this chapter the experimental field station Dongbeiwang, where the trace gas exchange measurements were conducted, is characterized. Moreover its pedological as well as climatological properties are presented in chapter 4.1.

The TDL-PA measuring device used for methane and ammonia detection is introduced in chapter 4.2.

The selection process of suitable absorption lines for the methane and ammonia PA detection as well as the applied laser diodes are given in chapters 4.3 and 4.4, respectively, while the details about the calibration can be found in chapter 4.5.

The already mentioned new developed mobile closed chambers are introduced in chapter 4.6.

## 4.1 Experimental Field Station Dongbeiwang

The experimental field station DBW is located in the Haidian District in the north-west of Beijing. The coordinates are  $40^{\circ}$  N and  $116.3^{\circ}$  E, approximately 3.2 km north of the CAU as shown by the map in Figure 4.1.

The elevation is 50 m above sea level. The groundwater table was 22 – 24 m below surface during the experimental period. The experiments were conducted in the years 2006 and 2007.



**Figure 4.1:** Satellite image of Beijing, including Dongbeiwang and China Agricultural University. Image provided by Google Earth.

Analysis of the soil properties in Dongbeiwang were conducted by Mack during a previous project. He classified the loamy and silty alluvial soil as a Calcaric Cambisol according to the FAO classification [FAO 1998]. The pH is 7.9. It had partly been influenced by human deposits, impairing the natural development of the profile. Below 80 cm depth the Calcaric Cambisol showed calcareous concretions of different size and share. Bioturbation by earthworms was intense. Shallow sand and clay layers alternated irregularly inside the silt-dominated soil profile [Mack 2005]. Soil properties in detail for selected layers are listed in Table 4.1.

**Table 4.1:** Soil properties of the experimental field DBW [Mack 2005].

Depth	cm	0 – 15	15 – 30	30 – 60	60 – 90	90 – 120
Sand	%	27	28	22	30	25
Clay	%	16	16	18	14	12
Silt	%	57	56	60	56	63
Water Content (WC) at pF 2.0	Vol.-%	34.2	34.2	33.2	33	33.9
WC at pF 4.2	Vol.-%	12.1	13	12.9	10.1	16.7
WC at pF 2.0 – WC at pF 4.2	Vol.-%	22.1	21.2	20.3	22.9	17.2
Plant available soil water content	mm	33.2	31.8	60.9	68.7	51.6
Bulk density	g cm <sup>-1</sup>	1.34	1.34	1.51	1.42	1.52
Saturated hydraulic conductivity	cm h <sup>-1</sup>	10.88	9.25	8.29	9.79	10.21
CaCO <sub>3</sub>	%	5	5	7	9	15
C <sub>org</sub>	%	2.6	2.8	0.4	0.4	0.2

The climate in Dongbeiwang is a monsoon-influenced humid continental climate, according to the Köppen climate classification “Dwa”. It is characterized by hot, humid summers due to the East Asian monsoon and harshly cold, windy, dry winters that reflect the influence of the vast Siberian anticyclone [Köppen 1918].

Climate measurements conducted in Dongbeiwang show that the average temperatures in January are between –7 to –4°C, while average temperatures in July are about 25 to 26°C. Calculation of the long-term temperature reveal an average of about 11.5°C. The average long-term annual precipitation is about 649 mm. More than 75% of this precipitation is falling during summer.

In the years 2006 and 2007 the average temperature in Dongbeiwang was about 13.5°C with a precipitation below 600 mm. Therefore, these two years were warmer and drier compared with the long-term average.

## **4.2 Tunable Diode Laser Photoacoustic Measuring Device**

The TDL-PA measuring devices used in this work were home-made [Reinhardt 2002; Sauter 2004; Link 2005]. Here only a short summary about the system and its main components will be given. The PA system contains following parts:

- PA detection unit
- Temperature control unit
- Electronic unit
- External laser diode driver (optional)
- Data capture unit
- Gas flow accessories

All the devices including marking and manufacturers are listed in Table 4.2.

### **4.2.1 Photoacoustic Detection Unit**

The PA detection unit is housed in a compact thermally stabilized box. The walls inside the box are covered by an insulation material. Six Peltier-Elements mounted inside of the unit can either be cooled or heated depending on the ambient condition. The typical working temperature is between 293 and 303 K, controlled by an installed Pt100 temperature sensor, to keep the variation in temperature within 0.1 K. A proper intermixture of the enclosed air is provided by two fans.

The laser diode is mounted in a home-made housing and separately temperature stabilized [Uhl 2001] by a Peltier-Element and can furthermore be water-cooled. The laser diode temperature is controlled by a temperature sensor either of the type AD590 or thermistor. The laser beam is collimated by an adjustable anti reflex coated lens. The laser diode housing is mounted on a translation stage for three dimensional adjustment.

**Table 4.2:** Overview of the used devices and components for CH<sub>4</sub> and NH<sub>3</sub> measurements.

<b>Device</b>	<b>Marking and Manufacturer</b>
<b>Laser Diode Driver</b> ITC 110 PRO 800 Series	OEM Laser Diode and Temperature Controller, Thorlabs Inc. LDC 8002 and TED 8020, Thorlabs Inc.
<b>Lock-in Amplifier</b> Femto	LIA-BVD-150 Single-Board Lock-in Amplifier, FEMTO Messtechnik GmbH
<b>Microphones</b> Sennheiser Conrad	KE 4-211-2 electret microphone capsule, Sennheiser electronic GmbH & Co KG 302007-62, Conrad
<b>Differential Amplifier</b> INA111	Self-made based on IC-Amplifier INA111AP, Burr-Brown Corporation
<b>Peltier Controller</b> Peltron	PRG H 400, Peltron GmbH
<b>Wavemeter</b> Burleigh	WA-1500, Burleigh
<b>Power Meter</b> Fieldmaster	Fieldmaster with LM-1 measuring head, Coherent Inc.
<b>A/D Converter</b> Meilhaus	USB-Mini-Messlabor RedLab 1008, Meilhaus Electronic
<b>Gas Humidifier</b> Nafion Humidifier	Perma Pure Nafion Humidifier MH-070-12, Ansyco GmbH
<b>Temperature Sensor</b> Pt100 Testo	Pt100-sensor, RS-Components GmbH Testo 110, Testo AG
<b>Temperature/Humidity Sensor</b> Testo	Testo 605-H1, Testo AG
<b>Flowmeter</b> Rotameter L2,5 Rotameter L0,25 Rotameter L1,6 ABB	L2,5/100-12039, Rota Wehr GmbH L0,25/14-4375, Rota Wehr GmbH L1,6/70-6697, Rota Wehr GmbH Snap-In Flowmeter, ABB Company
<b>Pump</b> KNF	Diaphragm pump N86 KT.18, KNF Neuberger GmbH
<b>Valves</b> Balzers Messer Aero Brightly	EVN 116, Balzers FM 62 and E 61, Messer Group Aero Brightly Regulator A-1H, National Research Center for Certified Reference Materials (NRC CRM)
<b>Filter</b> Pall	Acro50 Vent Device 0,2 µm, Pall Corporation
<b>Fan</b> Axial Flow Fan	Axial Flow Fan 220V/79,8m <sup>3</sup> /h, Sunon Group
<b>Computer</b> Samsung	P35 XVM 1600 II, Samsung

The PA cell is made from high-grade steel. It is a hollow cylinder with a length of 10 cm and an inner radius of 2.5 cm leading to a total volume of 196 cm<sup>3</sup>. Both sides of the cell are covered by caps sealed with o-rings. Gas inlet and outlet pipes are fixed to the center of these caps. According to the used wavelength, anti reflex coated windows are installed off-center close to the cell walls to excite the second azimuthal acoustic mode by the incident laser beam. A microphone adapted as a speaker is mounted at one cap so that the acoustic characteristic of the cell can be tested. In the middle of the cylinder in axial direction two electret microphones are mounted flush to the wall and perpendicular to each other. By this setup and an excitation of the second azimuthal acoustic mode of the cell the signals detected by the two microphones have a phase shifted of  $\pi$ . The differential input of the microphones pre-amplifier eliminates therefore on the one hand nonresonant background noise and on the other hand doubles the signal amplitude. A self-made differential amplifier is used.

To increase detection limit the absorption path length of the laser beam was extended to maximize the signal. Therefore, a multipass arrangement of the “White-type” [White 1942] was chosen as shown in Figure 4.2. Typically 28 transits are used, which is a total path length of about 5 m and about 2.8 m within the PA cell.

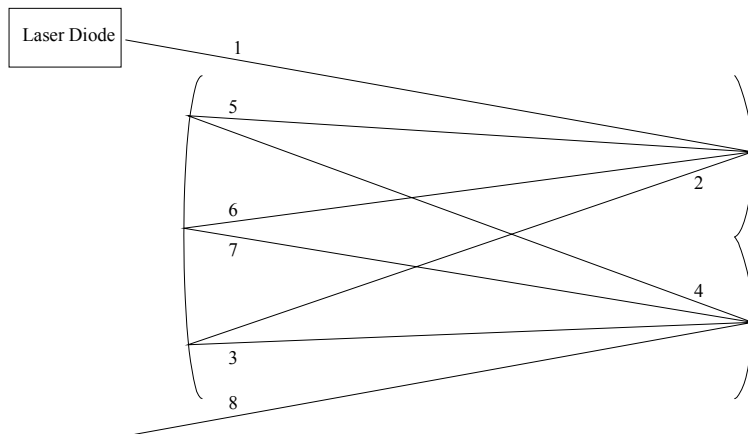


**Figure 4.2:** Scheme of the White-type multipass arrangement including beam numbers.

The PA detection unit for methane measurements, in contrast to ammonia measurements, contains a gas humidifier tube. It is a Teflon tube with a water filled Nafion membrane inside. The sampling air is led through the Teflon tube and the water diffuses through the membrane into the gas which is humidified to a level of about 75% relative humidity. So it is possible to avoid the effect of kinetic cooling. This effect lowers the signal, if the sampling air is dry, by quenching collisions. The excited methane molecules can transfer their energy by collision to oxygen molecules, exciting them to an energetic higher level close to the excited level of methane. The lacking energy difference is taken from the translation energy of the collision partners, resulting in a cooling of the gas. Details about this process can be found in the literature [Cottrell et al. 1965; Avramides et al. 1981; Hammerich et al. 1992; Schilt et al. 2005].

Two gas inlets and one outlet as well as a flowmeter and three connectors for the electronic unit are provided at the front side. At the back side one connector for the temperature control unit and some cooling fins are located. The dimensions of the whole unit are 520 x 420 x 400 mm (width x height x depth). The inner workings of the PA detection unit can be seen in Figure 4.3.

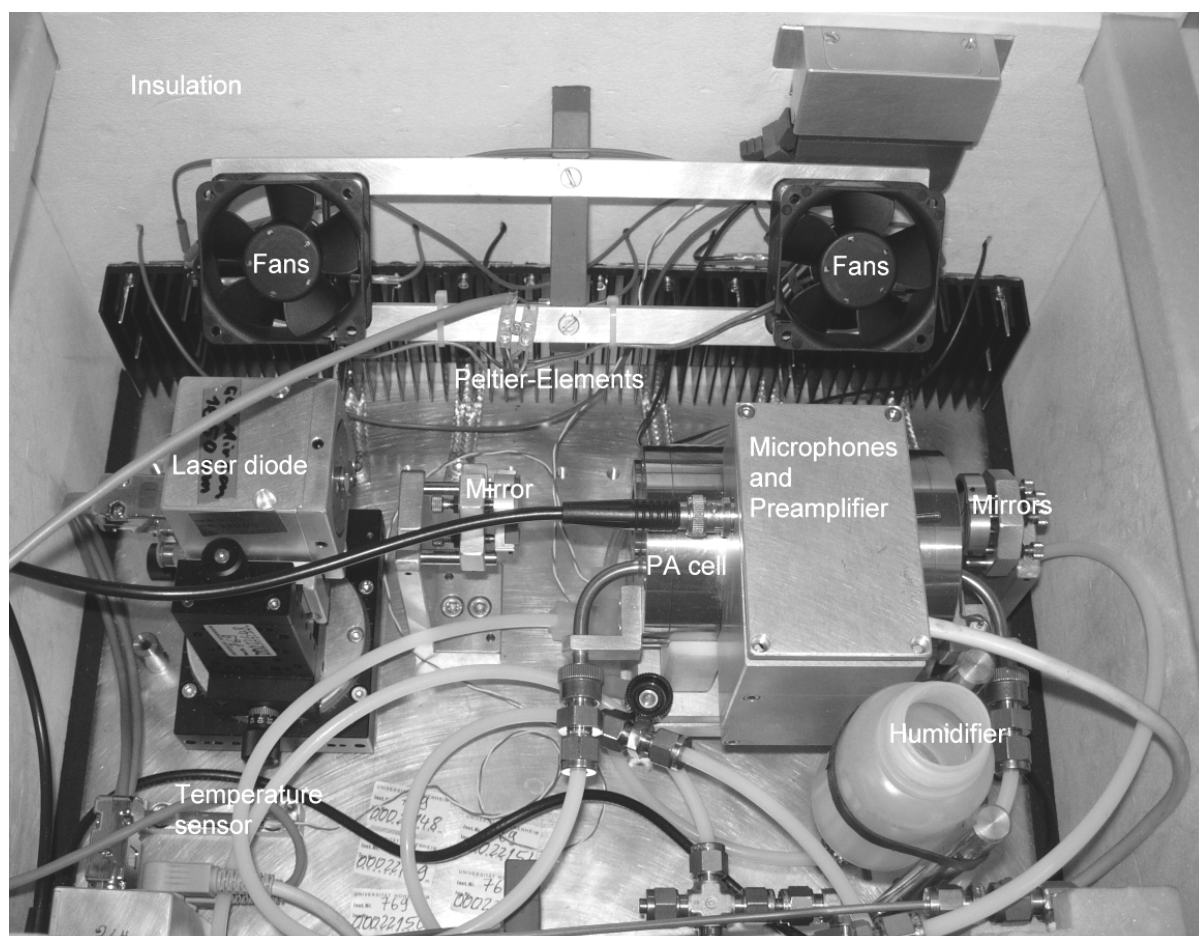


**Figure 4.3:** View into the open PA detection unit.

### **4.2.2 Temperature Control Unit**

The required temperature inside of the PA detection unit can be set with the temperature control unit. It is a commercial available device (Peltron) and controls the heating or cooling of the Peltier-Elements.

During the field measurements the set temperature was varied between 293 and 303 K according to the ambient temperature.

### **4.2.3 Electronic Unit**

The main components of the electronic unit are a laser diode driver, lock-in amplifier and the power supply for the fans and preamplifier. All of this equipment is installed on single Euro-boards and housed in a compact 19 inch rack.

The laser diode driver is used to control the temperature and current of the laser diode. The temperature and current can be set within a range between 253 to 353 K and from 0 to 1000 mA, respectively. The type of temperature sensor (AD590 or thermistor) depends on the laser diode and can be easily switched by jumpers on the board.

For ammonia detection an external laser diode driver is connected to the electronic unit (see chapter 4.2.4).

The lock-in amplifier acts as a phase sensitive detector of the modulated acoustic signal detected by the microphones. The primary electric signals of opposite phase of the two microphones are pre-amplified by a differential amplifier. The output of the pre-amplifier (difference signal of both microphones) is delivered as an AC signal to the input of the lock-in amplifier as well as a reference signal generated by a laptop. This reference signal is also used as modulation frequency of the injection current of the laser diode. The output of the lock-in provides a phase sensitive detected and amplified DC signal which is A/D converted and stored in a laptop.

#### **4.2.4 External Laser Diode Driver**

As mentioned above there is a laser diode driver installed in the electronic unit. Due to its maximum current of 1000 mA it is used with the laser diode for methane detection. The applied current for this laser diode is about 230 mA.

The external laser diode driver (Pro 800 series, Thorlabs) provided a maximum current of 200 mA and is used with the laser diode for ammonia detection. For this laser diode a current of about 190 mA is applied.

#### **4.2.5 Data Capture Unit**

The laptop on the one hand provides the modulation frequency for the incident laser beam, on the other hand it is used to start and control the measurement and to store the data.

First the resonance frequency must be checked before a measurement can be conducted. For that purpose a user-written program in LabView 7 express is started which allows the identification of the resonance frequency. A start and stop frequency can be set and the step size and delay as well as the sensitivity of the lock-in amplifier can be defined. The signal is then generated by the laptop and transferred to the test-speaker in the PA cell and to the lock-in amplifier, respectively. The discovered maximum frequency, normally in the range of 6700 Hz, is then applied as modulation frequency of the laser diode. Due to the fact that the resonance frequency is dependent on temperature, humidity, atmospheric composition and pressure of the sampled air, the maximum frequency must be checked before and during measurements, respectively. The procedure takes about one minute until completion. A screenshot of the user interface can be found in Figure 4.4.

Second another user-written LabView program is started. With this program the sensitivity of the lock-in amplifier in mV, the measuring frequency in Hz and the data storage path is set. Furthermore the values obtained by calibration of the system can be inputted in the program so that the PA signal is automatically converted into concentrations of the unit ppm. Moreover the actual concentration is displayed on the screen and the data is stored on the laptop for further analysis. For information about the calibration process see chapter 4.5. A screenshot of the user interface is presented in Figure 4.5.

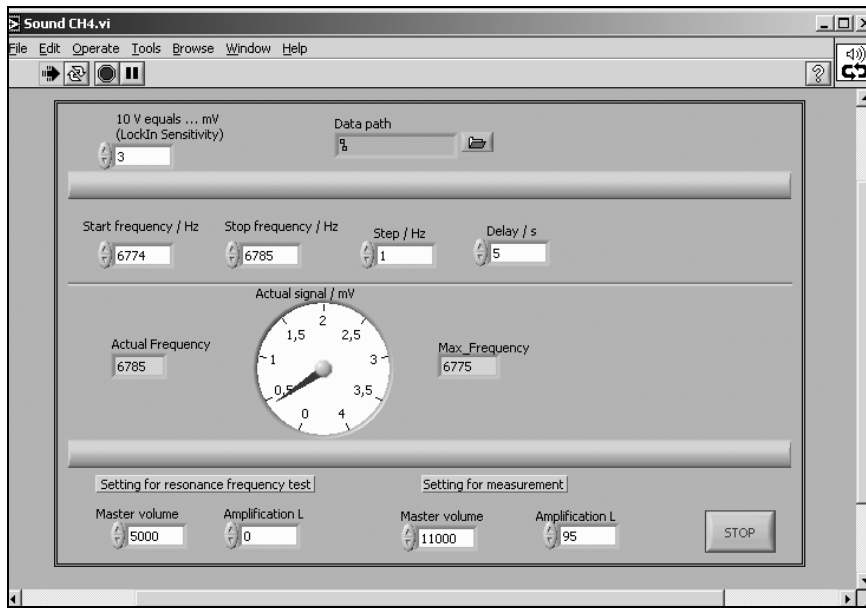


Figure 4.4: Screenshot of the LabView user interface controlling the frequency.

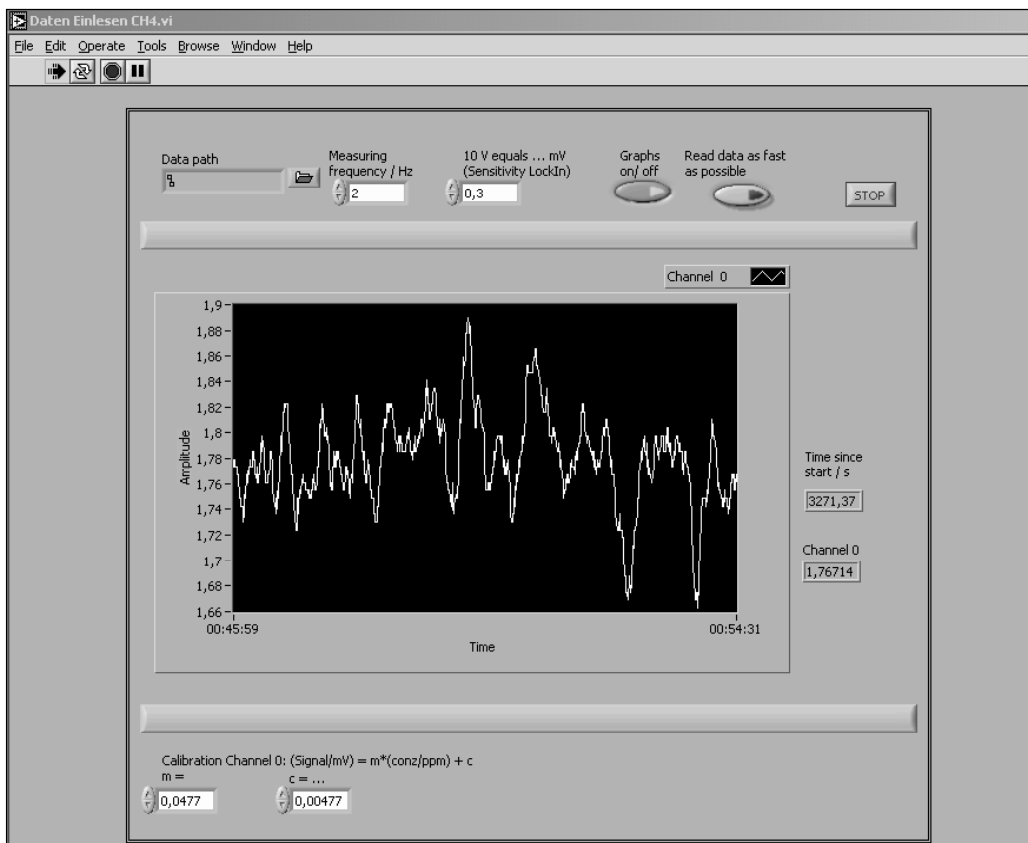


Figure 4.5: Screenshot of the LabView user interface for measurement and data storage.

#### **4.2.6 Gas Flow Accessories**

For a constant flow of the sample gas through the PA cell a diaphragm pump is used. To avoid both contamination of the samples and interferences, the pump is placed behind the gas outlet of the PA detection unit sucking the sample gas through it. For conditioning of the sample gas to the temperature inside of the thermally stabilized unit a 2 m long stainless steel capillary is integrated. The flow rate is typically set to  $0.5 \text{ l min}^{-1}$  and verified by a flowmeter installed in the PA detection unit. If trace gas exchange measurements are conducted, the pump outlet is connected with the inlet of the closed chambers via Teflon tubes.

To prevent dust and other particles from entering the system a membrane filter with  $0.2 \mu\text{m}$  pore size is installed at the gas inlet of the PA detection unit.

To avoid disturbances of the pump during field measurements a stainless steel cylinder with a volume of about  $100 \text{ cm}^3$  is installed between the exit of the PA detection unit and the pump. By doing so the flow of the sampling air through the detection unit is made laminar.

The relative humidity of the gas after exiting the PA detection unit is sporadic checked with a Testo temperature and humidity measuring stick at the pump outlet.

### 4.3 Selection of Absorption Lines

To detect sensitively and selectively the two analyte gases methane and ammonia, respectively, the utilizable absorption wavelengths in the NIR of the two gases had to be determined using the HITRAN database, inter alia. The fundamentals of the HITRAN database to calculate the absorption behavior of an analyte gas are [Rothman et al. 2003; Rothman et al. 2005]:

- Pressure of gas mixture: 101.325 kPa
- Temperature: 296 K
- Absorption length: 100 m
- Peak slope: Voigt-profile
- Cross-checked molecules: all molecules listed by HITRAN database in the spectral range of interest

For methane the HITRAN database could be directly used to find suitable wavelengths without interferences of e.g. water vapor or carbon dioxide. Information about absorption lines of ammonia in the NIR were only available from the literature [Lundsberg-Nielsen et al. 1993] and had to be cross-checked for interferences with other gases taking the HITRAN database as well. The selected absorption peak wavelengths were at 1650.957 nm for methane detection and for ammonia at 1512.2126 nm and 1512.2377 nm, respectively. As can be seen in Figures 4.6 and 4.7 no interferences with other relevant gases are to be expected, as confirmed by an experimental check later on.

Detailed information about the selection of absorption lines are also given by Reinhardt [Reinhardt 2002], Sauter [Sauter 2004] and Link [Link 2005].

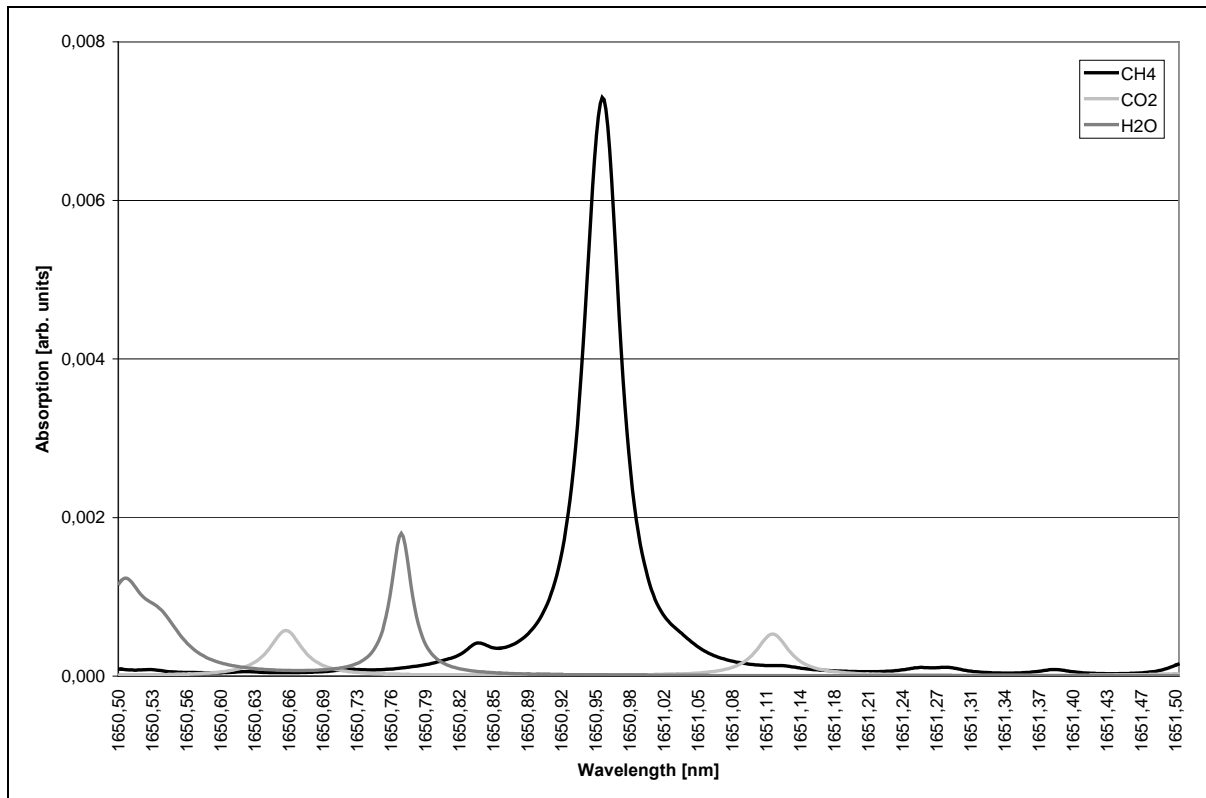


**Figure 4.6:** Absorption profile of methane at about 1650 nm (peak maximum at 1650.957 nm) and of carbon dioxide and water vapor, respectively, taken from the HITRAN database.

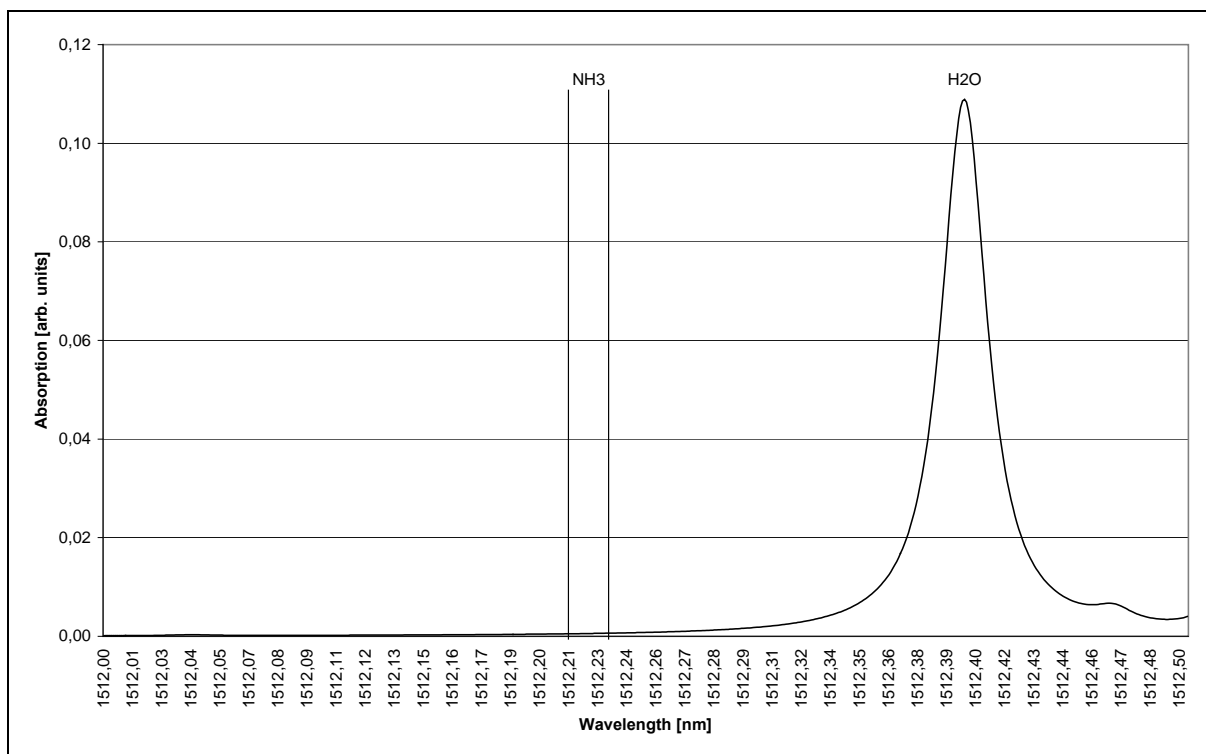


**Figure 4.7:** Absorption peak of water vapor near the two absorption lines of ammonia at 1512.2126 nm and 1512.2377 nm, respectively [Lundsberg-Nielsen et al. 1993]. Water vapor data were taken from the HITRAN database.

## **4.4 Laser Diodes**

As mentioned in chapter 3.3.2, a high output power of the laser diode guarantees in principle an improvement of the detection limit of the trace gas analyzed. For this reason the available commercial laser diodes with the highest possible output power were used.

### **4.4.1 Laser Diodes for Methane Detection**

The laser diode first used for methane detection was a DFB laser diode (SPEC DILAS D-1651-MTE-E, Laser Components) emitting at 1651 nm with an output power of typically > 20 mW. The reduced detection limit for methane as well as some other technical problems with this laser diode implied the necessity to replace it by another laser diode emitting at 1651 nm as well. It was a DFB laser diode manufactured by GEC Marconi (LD 6204/30/1651/1/4) and was housed in a TO 5.6 package for protection purposes. The output power at 1650.957 is about 48.5 mW. An external Peltier-Element, controlled by an AD590 sensor, keeps the temperature stable while the injection current of typically 234 mA is modulated. Due to its higher output power compared to the first used laser diode a better detection limit could be achieved from about 250 ppb to about 80 ppb.

### **4.4.2 Laser Diodes for Ammonia Detection**

For ammonia detection a SPEC DILAS-DFB laser diode (D-1512-MTE-E, Laser Components) emitting at 1512 nm is used with an output power of about > 20 mW. It is housed in a SOT-9 package and the temperature is checked by a thermistor controlling the built in Peltier-Element. In comparison with the already existing laser diode emitting at 1531.68 nm (GEC Marconi LD 6204) no significant change in the ammonia detection limit was observed. This can be explained by the stronger absorption lines at 1512 nm compared with 1531 nm [Lundsberg-Nielsen et al. 1993].

#### 4.5 Calibration of the Tunable Diode Laser Photoacoustic System

A fundamental precondition for quantitative trace gas measurements is a sound and reliable calibration of the detection systems. Whenever the system parameters such as temperature inside of the PA detection unit, laser diode current and temperature or the adjustment of the laser beam are changed a new calibration has to be carried out. The calibration procedure for methane and ammonia detection is the same for both gases. Due to the calibration the readings of the further investigations can automatically be converted into the unit ppm. Certified gas mixtures of different concentrations (about 100, 10 and 1 ppm) of methane and ammonia in nitrogen 5.0, respectively, were used for calibration. The used certified gas mixtures are listed in Table 4.3.

**Table 4.3:** Overview of the certified gases used for calibration.

<b>Gases used in Germany</b>	<b>Specification</b>
Synthetic Air	Synthetic Air, Nitrogen 79,1%, Oxygen 20,9%, Sauerstoff-werke Friedrichshafen GmbH (SWF)
Nitrogen	Nitrogen 5.0, SWF
Methane 102.6 ppm	102.6 ppm Methane in Nitrogen 5.0, SWF
Methane 99 ppm	99 ppm Methane in Nitrogen 5.0, SWF
Methane 10.9 ppm	10.9 ppm Methane in Nitrogen 5.0, SWF
Methane 0.99 ppm	0.99 ppm Methane in Nitrogen 5.0, SWF
Ammonia 100.2 ppm	100.2 ppm Ammonia in Nitrogen 5.0, SWF
Ammonia 10.2 ppm	10.2 ppm Ammonia in Nitrogen 5.0, SWF
Ammonia 1.5 ppm	1.5 ppm Ammonia in Nitrogen 5.0, SWF
<b>Gases used in China</b>	<b>Specification</b>
Nitrogen	Nitrogen 5.0, National Research Center for Certified Reference Materials (NRC CRM) Beijing, China
Methane 102 ppm	102 ppm Methane in Nitrogen 5.0, NRC CRM
Methane 98.9 ppm	98.9 ppm Methane in Nitrogen 5.0, NRC CRM
Methane 10.3 ppm	10.3 ppm Methane in Nitrogen 5.0, NRC CRM
Methane 10 ppm	10 ppm Methane in Nitrogen 5.0, NRC CRM
Methane 0.98 ppm	0.98 ppm Methane in Nitrogen 5.0, NRC CRM
Ammonia 101 ppm	101 ppm Ammonia in Nitrogen 5.0, NRC CRM
Ammonia 100.8 ppm	100.8 ppm Ammonia in Nitrogen 5.0, NRC CRM
Ammonia 10.1 ppm	10.1 ppm Ammonia in Nitrogen 5.0, NRC CRM
Ammonia 5 ppm	5 ppm Ammonia in Nitrogen 5.0, NRC CRM

By diluting the gas with nitrogen other concentrations could be produced. In Germany this was achieved by two-stage fine regulating valves connected to the gas bottles. Unfortunately these valves did not fit the Chinese gas bottle threads and in 2006 single-stage valves had to be used first but by constructing suitable adapters the two-stage valves could advantageously be used in China too, avoiding contamination of the gas mixtures by residual air and water vapor. By a flowmeter of the rotameter type, installed at the gas outlet of the PA detection unit, the gas flow was set to  $0.5 \text{ l min}^{-1}$  because all trace gas measurements were conducted with this flow rate. Another rotameter was placed between the nitrogen gas bottle and the gas inlet controlling the dilution of methane and ammonia, respectively.

Each gas concentration was led through the system for five minutes (calibration of methane) or ten minutes (calibration of ammonia) while the resonance frequency was determined. Afterwards the measurement was started and the data were recorded for five minutes. With a sampling rate of 2 Hz in five minutes in total 600 data points were obtained during one measurement. Due to signal fluctuations in the first 40 seconds after starting the measurement the first 120 data points were omitted. Each gas concentration was measured ten times distributed over two or three days of calibration. This led to 4800 data points for each concentration which were summarized and the mean value as well as the standard deviation were calculated. The blank value was similarly detected by using pure nitrogen 5.0. The mean of the blank value was then subtracted from all other measurements and a linear regression was applied. According to the German Institute for Standardization (DIN) the detection limit was calculated using the following relation [DIN-32645 1994]

$$\chi_{\text{DL}} \approx 3 \frac{s_0}{b} \quad (4.1)$$

$s_0$  is the standard deviation of the blank value and  $b$  the slope of the regression line. As already mentioned above the  $3 \sigma$  detection limit was exclusively calculated.

A typical result from calibration of methane and ammonia is shown in Figures 4.8 and 4.9, respectively.

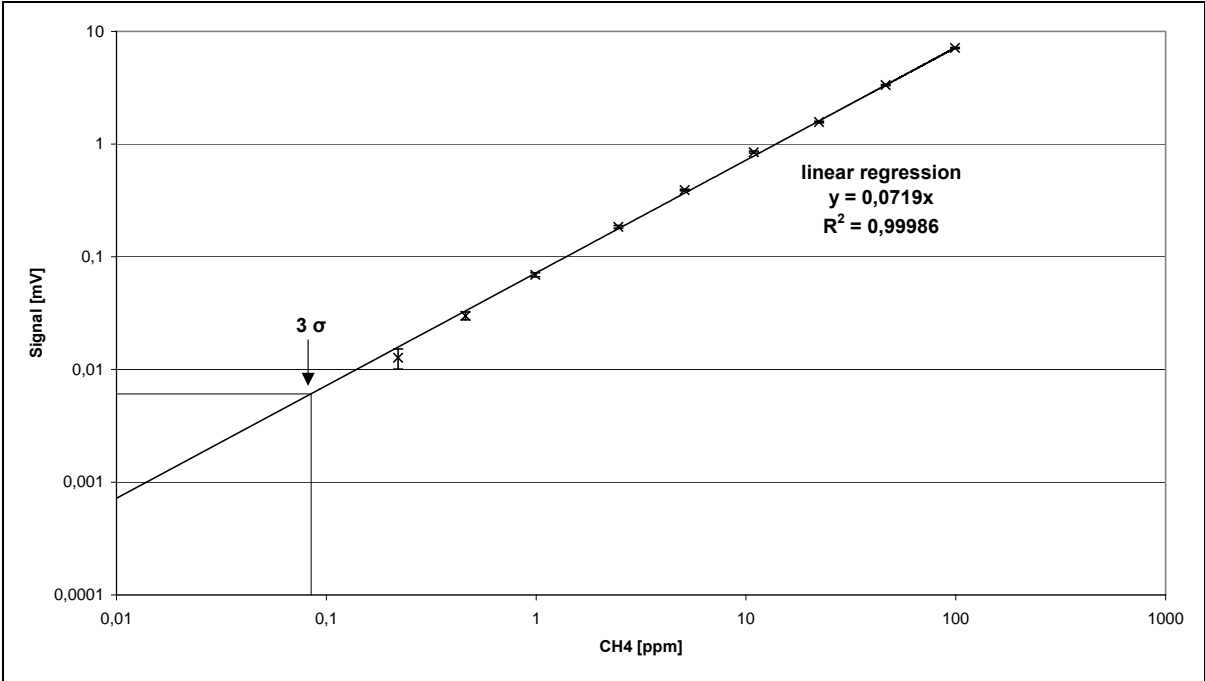


Figure 4.8: Calibration of the methane PA system. The calculated  $3\sigma$  detection limit is 85 ppb.

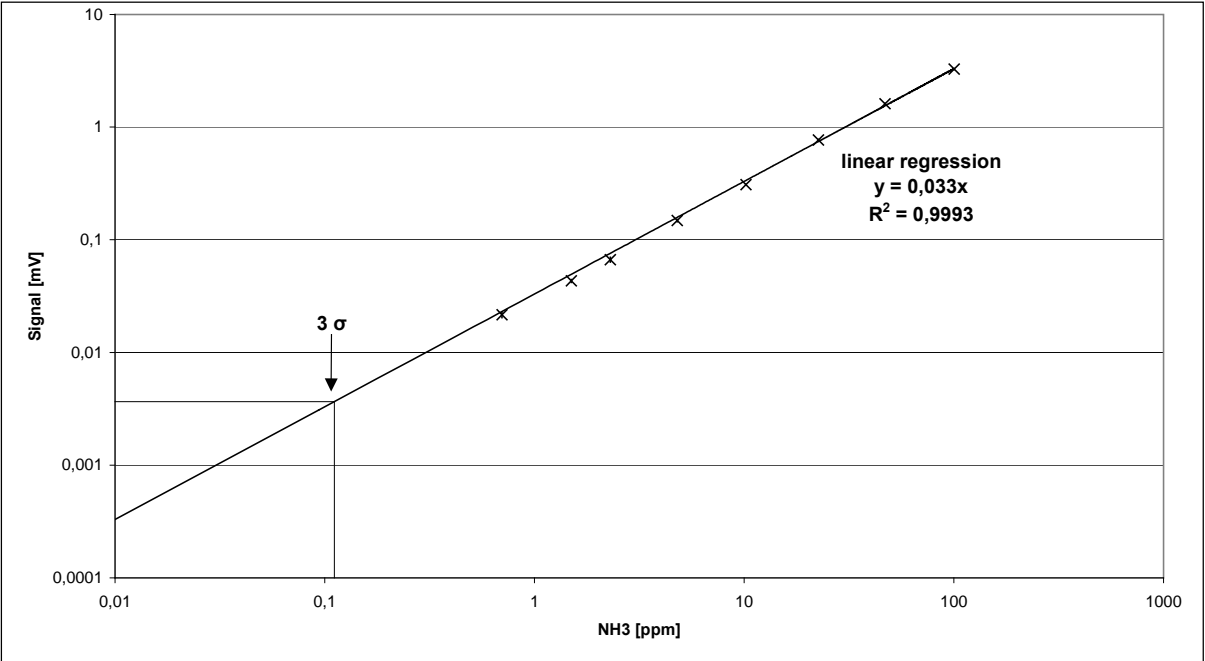


Figure 4.9: Calibration of the ammonia PA system. The calculated  $3\sigma$  detection limit is 111 ppb.

#### **4.5.1 Problems During Ammonia Calibration**

Especially for ammonia it was crucial to use two-stage valves. After connecting them to the gas bottle they first had to be thoroughly flushed with nitrogen to get rid of water vapor. Only afterwards the bottle with the certified gases could be opened.

Because of the high adsorbing power of ammonia all tubes used inside of the detection system as well as the connection tubes between the detection unit and the gas bottles were made from stainless steel. To get rid of water vapor in the system it had to be purged with either nitrogen or synthetic air. At all measurements the relative humidity of the sample gas flowing through the system was controlled. When the relative humidity was below 0.1% the calibration was started. This procedure had to be repeated each time a different gas bottle was connected.

## 4.6 Closed Chamber Technique

The closed chamber method is a very often used and simple technique. In principle, a container of definite dimensions is sealed over the soil surface for periods usually of the order of 20 – 60 minutes. During closure the change in concentration with time of a gas emanating from the soil or being absorbed by the soil from the enclosed air in the box is measured.

Mostly closed chambers consist of two parts: One frame installed permanently in the soil and a hood placed on it during the measurement and removed afterwards again. Tightness between the hood and the frame is normally achieved by water-filled channels where the hood fits in or by rubber seals glued onto either the frame or the hood. This approach has advantages when it is necessary to avoid shading of growing plants between measurements, because the frame protrudes only a few cm above the surface. Moreover it allows the use of hoods of different heights on the same bases so that a complete vegetation cycle can be studied.

When operated in the static mode, gas samples are taken from the chamber headspace at intervals during the closure period. The samples are usually withdrawn through a septum and collected in gas tight syringes, evacuated vials, Vacutainers or Tedlar (polyvinyl fluoride) gas sample bags. The samples are then analyzed off-line in the laboratory typically by GC. It is recommended to analyze the samples within a few hours or days after collection, depending on the sample containers used, because otherwise gas exchange between the sample container and the outside atmosphere could occur leading to errors in the flux rate calculation [Smith et al. 2004].

Closed chambers may also be operated in the dynamic mode, in which the air in the chamber is circulated through a gas analyzer and the increase or decrease in concentration with time is determined. The main advantage of this method is that the change in concentration of the gas can be measured in real-time making the above mentioned errors negligible as long as the whole system can be considered tight.

In this work the TDL-PA detection system for methane was operated together with self-developed closed dynamic chambers. The air was sucked out of the chamber and through the PA detection unit and blown back into the chamber.

#### **4.6.1 Advantages and Disadvantages of Closed Chambers**

Closed chambers have the advantage that they are capable of measuring very small fluxes and the source of the flux is well defined. The technique can be applied in conventional experimental designs for example in replicated field plots. Furthermore the construction of the chambers is relatively cheap.

The main disadvantage is the potential to influence the magnitude of the flux that is to be measured. The gas transport between soils and the atmosphere can be affected by covering the surface with a chamber and circulating the air within it. In a closed chamber a rise in temperature can be induced, affecting the rate of production or consumption of the target gas.

#### **4.6.2 Self-developed Closed Dynamic Chambers**

The hoods and frames used in this work were developed at the University of Hohenheim within the subproject of the IRTG. The construction of the hoods was done by a German company (Junker Kunststoffverarbeitung, Esslingen). Altogether seven frames were constructed by a company located in Beijing.

The hoods are made from 8 mm colorless Plexiglas (type GS 233). This material has the following positive characteristics:

- High transparency
- Absolute resistance to weathering
- Good scratch resistance
- High break resistance
- Little weight

For optimal stability and accuracy grade the Plexiglas panels were mitred and agglutinated to hoods with colorless glue applied from the inside. To be able to do continuous measurements during the whole vegetation period three hoods of different heights were constructed. The dimensions are 600 x 600 mm with heights of 250, 500 and 1000 mm, leading to volumes of 90, 180 and 360 l, respectively. To ensure tightness, a semicircular rubber seal was affixed at their bases. For easy and safe handling handholds were attached to two sides of each hood. Gas inlet and outlet were drilled into the other two sides and shut by stainless steel tube

fittings from Swagelok. For easy and stable fixation of the hoods onto the support plate, tension clamps were attached in the middle of all four sides near the hood base. They provide enough contact pressure to firmly press the rubber seal on the plate and guarantee gas tight connection between hood and frame. See Figure 4.11 for a schematic diagram of hoods and frame.

The frames were constructed of stainless steel and made up of two parts. The support socket (see Figures 4.10 and 4.11) which is installed in the soil and the support plate (see Figures 4.11 and 4.12) screwed on top of it.

The reversed L-shaped support socket has dimensions of 740 x 740 mm at the bottom, 800 x 800 mm on top and a height of 250 mm (see Figure 4.11). It is installed about 150 mm deep into the soil and therefore contains more than 25 bore holes, 30 mm in diameter, in the lowest 150 mm on each side allowing lateral water flow under the surface. The area covered by the frame is 0.74 m<sup>2</sup>.

The support plate has dimensions of 800 x 800 mm with a free area of 500 x 500 mm. Therein agricultural crops could be planted. The latch of the tension clamps were screwed on the support plate (see Figure 4.12). The bearing area between support socket and frame was caulked by rubber seal.

All screws and nuts of both support socket and support plate were sealed by silicone to improve gas tightness.

To guarantee a proper intermixture of the air inside of the closed chambers two fans with an airflow of about 80 m<sup>3</sup> h<sup>-1</sup> were mounted on tent pecks. They could be easily inserted in as well as removed from the soil. The power cable for the fans was buried in the soil before installation of the frames.

The special feature of the frame is the possibility to insert up to eight cooling packs that cool down both the support plate and the enclosed air in the chambers via the two fans. With this method the temperature inside of the chamber can be adapted close to ambient conditions. To the best of the author's knowledge this is the first time that a closed chamber was designed which can be cooled by cooling packs inserted in the support socket. The main advantage of this setup is the long-term benefit of the cooled down support plate in cooling the air while the

plants inside can still receive sunlight. Other methods to minimize a temperature increase are e.g. shading the chambers or construct them from opaque [Matthias et al. 1980], reflective [Hutchinson et al. 1981] or insulating materials [Hutchinson et al. 1992].

A schematic diagram of the support socket can be found in Figure 4.10. Figure 4.11 provides a cross section of support socket, support plate and hood. A picture of one of the frames installed in DBW is shown in Figure 4.12.

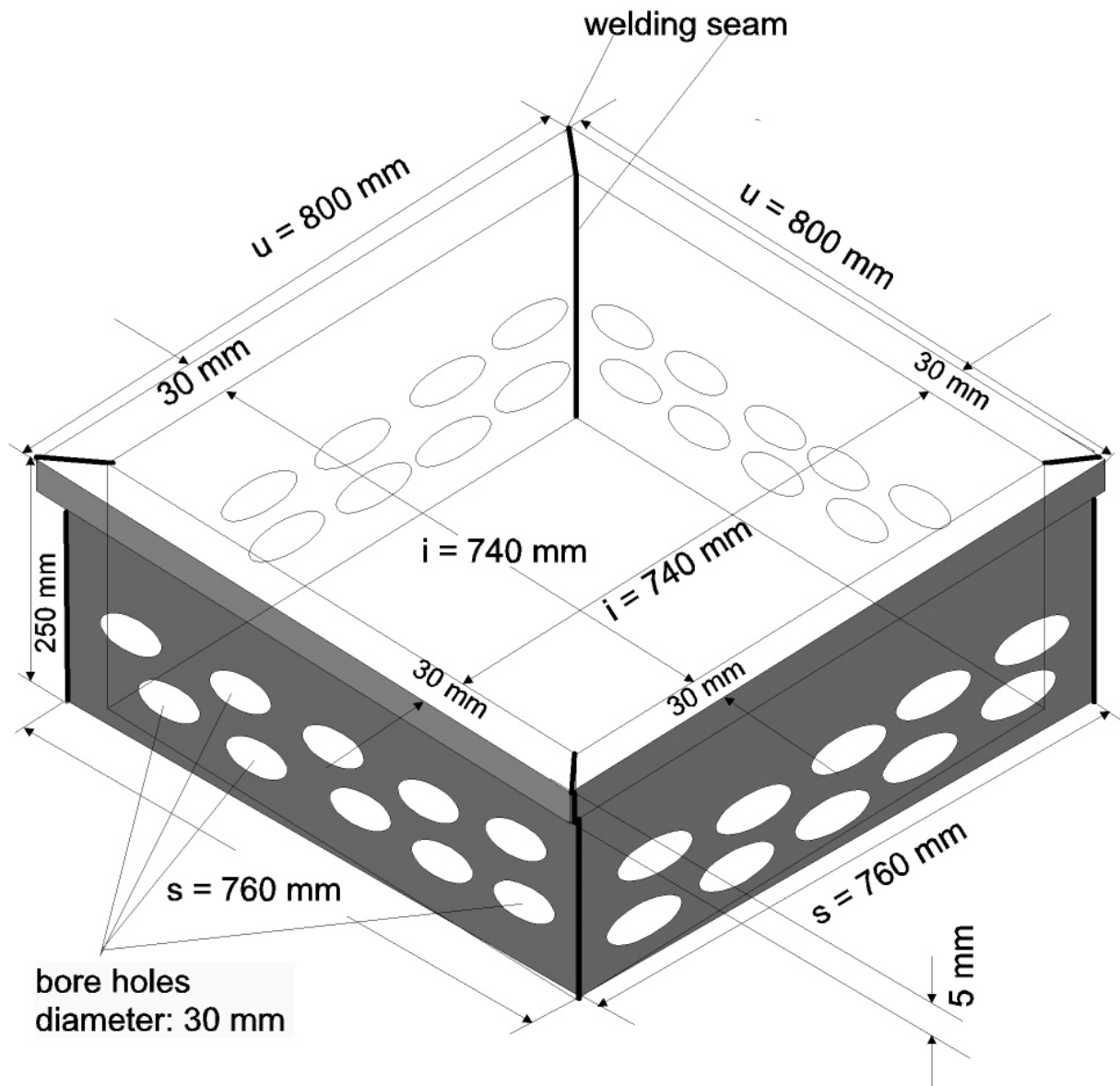


Figure 4.10: Schematic diagram of the support socket.

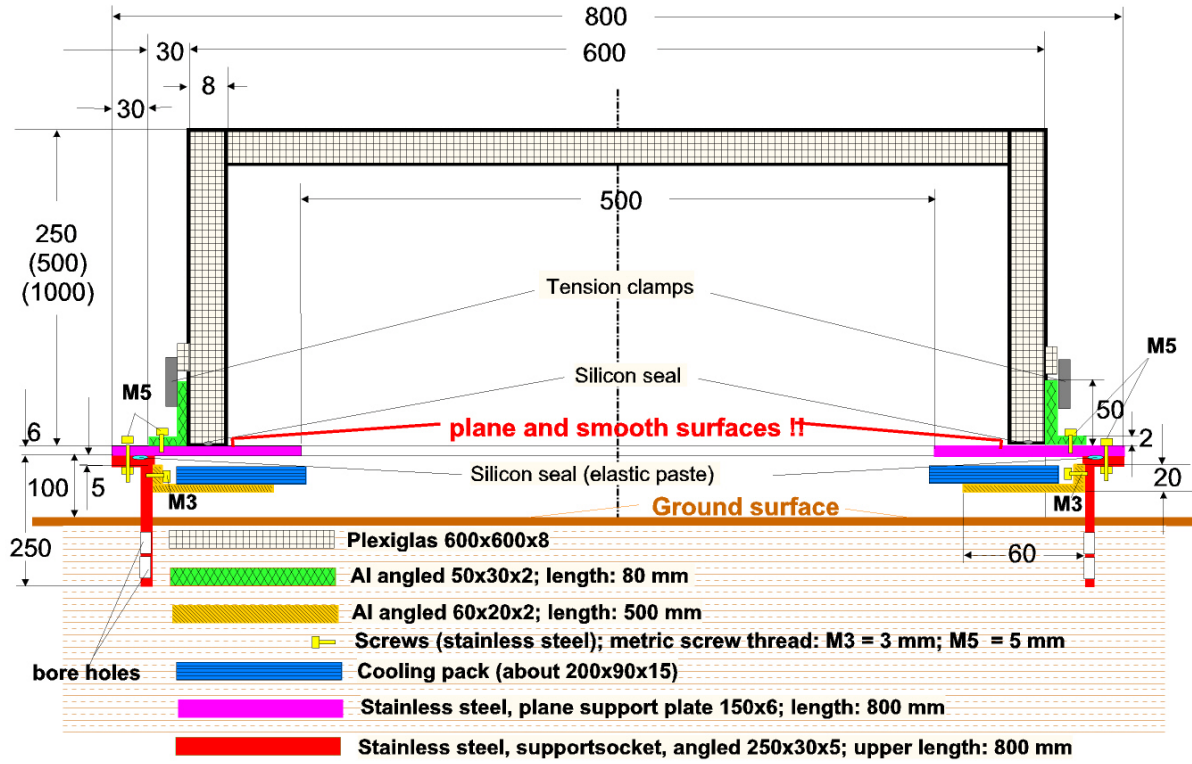


Figure 4.11: Cross section of support socket, support plate and hood (all values in mm).

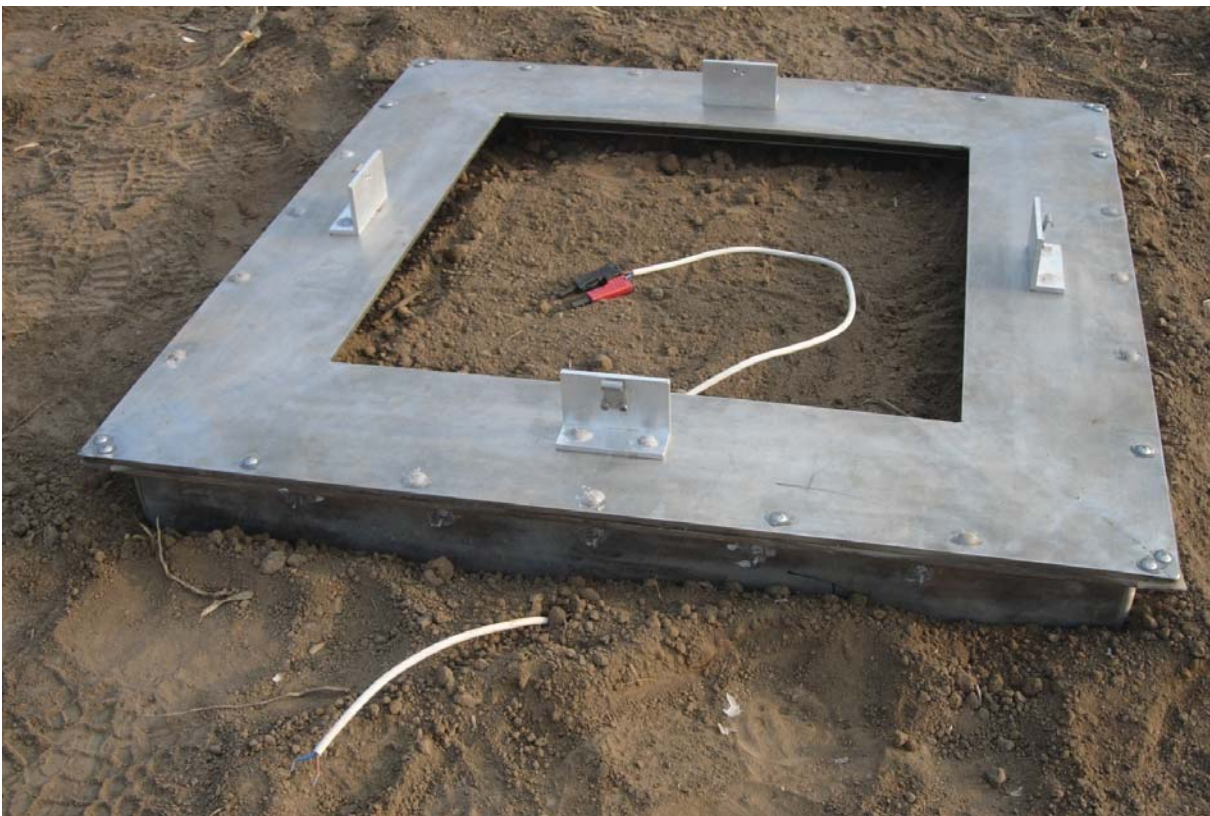


Figure 4.12: Picture of an installed frame at the experimental field Dongbeiwang.

### 4.6.3 Tightness Test

After installation of the closed chambers a test checking the gas tightness had to be performed. With this test leakages of the frames, hoods and tubes should be discovered.

This was usually done by injection of a gas into the closed chambers which is not a component of ambient air. If the loss of the injected gas was lower than 10% after one hour of closing, the system could be considered tight.

The injected gas was ethane ( $C_2H_6$ ) that meets the following requirements. It is not:

- Chemically or biologically oxidized during the test
- Produced by soil organisms or plants in the chamber
- A component of the ambient air

For these tests the GC in the measuring container in DBW was used, connected by Teflon tubes to the closed chambers. The hood of 1 m height was placed on one of the frames and affixed by the tension clamps. After connecting the gas outlet of the closed chamber with the GC, 2 ml ethane were injected at the gas inlet via a syringe and the fans were started to guarantee a proper intermixture in the volume. Directly after injection the gas inlet was shut with a blank plug and the enclosed air was pumped out of the chamber to the GC ( $0.5 \text{ l min}^{-1}$ ). The ethane concentration decrease after one hour of closure time was calculated. This procedure had to be done for all of the seven frames and each time they were reinstalled in the soil. For every measurement the loss was lower than 10% so the chambers could be considered tight. The result of one of the tightness tests is presented in Figure 4.13.

Unfortunately the 25 cm as well as the 50 cm hood could not be tested directly with this setup because the volume of air sucked out of the chambers within one hour was about 30 l. Taking the volume of the 25 cm hood (90 l) and of the 50 cm hood (180 l) into consideration more than 16% or 33% of the total air volume were sucked out of the closed chamber, respectively. This led to a low-pressure in the chambers and therefore to biased GC results. Moreover during gas exchange measurements the closed chambers were operated in the dynamic mode so the sample air was sucked out of the chamber, through the PA system and blown back into the chamber avoiding such pressure differences between inside and outside of the chambers. However the tightness could be proved indirectly by comparing the methane exchange results obtained with the two smaller hoods with the gas exchange data obtained with the 1 m hood. There were no differences detectable so the hoods could be considered tight.

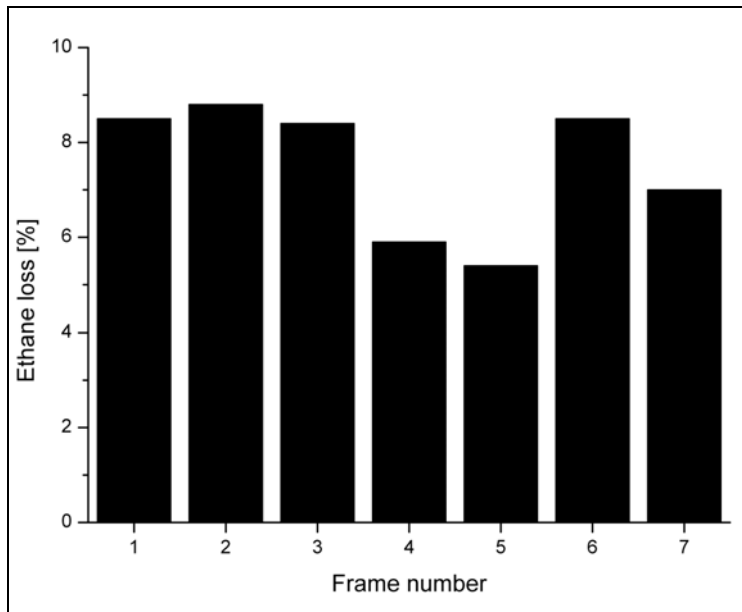


**Figure 4.13:** Gas tightness test result from the 25<sup>th</sup> – 26<sup>th</sup> of October 2006.

#### 4.6.4 Cooling of the Closed Chambers

As already mentioned above, the design of the frames allow to install up to eight cooling packs under the support plate. By the implementation of two fans, mounted on tent pecks plunged in the soil, a proper intermixture of the enclosed air inside of the chambers was guaranteed. Twenty cooling packs were stored in the freezing compartment and twelve in the refrigerator provided inside of the container in DBW. So there were enough cooling packs available for stabilizing the temperature inside of the closed chambers during the course of the full-time measurements. Sunshine and ambient air temperature were the decision criteria for using cooling packs. If necessary they were installed some minutes before closure of the chamber.

Comparison measurements with and without applying cooling packs showed their advantage in minimizing the temperature increase inside the closed chamber. In both cases the hood with 25 cm height was used and the temperature was measured within the chamber approximately 10 cm above soil. The particular temperature is shown in Figure 4.14, the resulting difference between both situations in Figure 4.15.

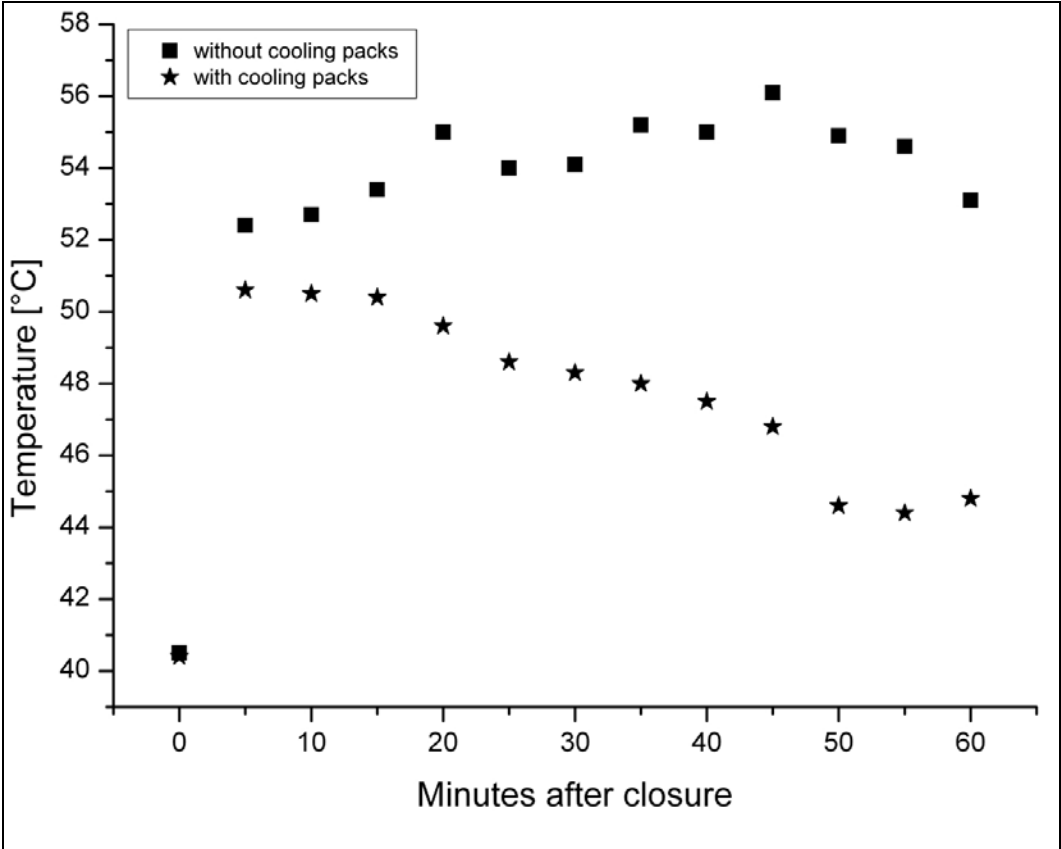


**Figure 4.14:** Temperature profile inside of the closed chamber with and without applying cooling packs. As a control mean ambient air temperature 3 cm above soil was measured close to the climate station in Dongbeiwang. Ambient air temperature at beginning of this study 31°C and at the end of this study 30.5°C.

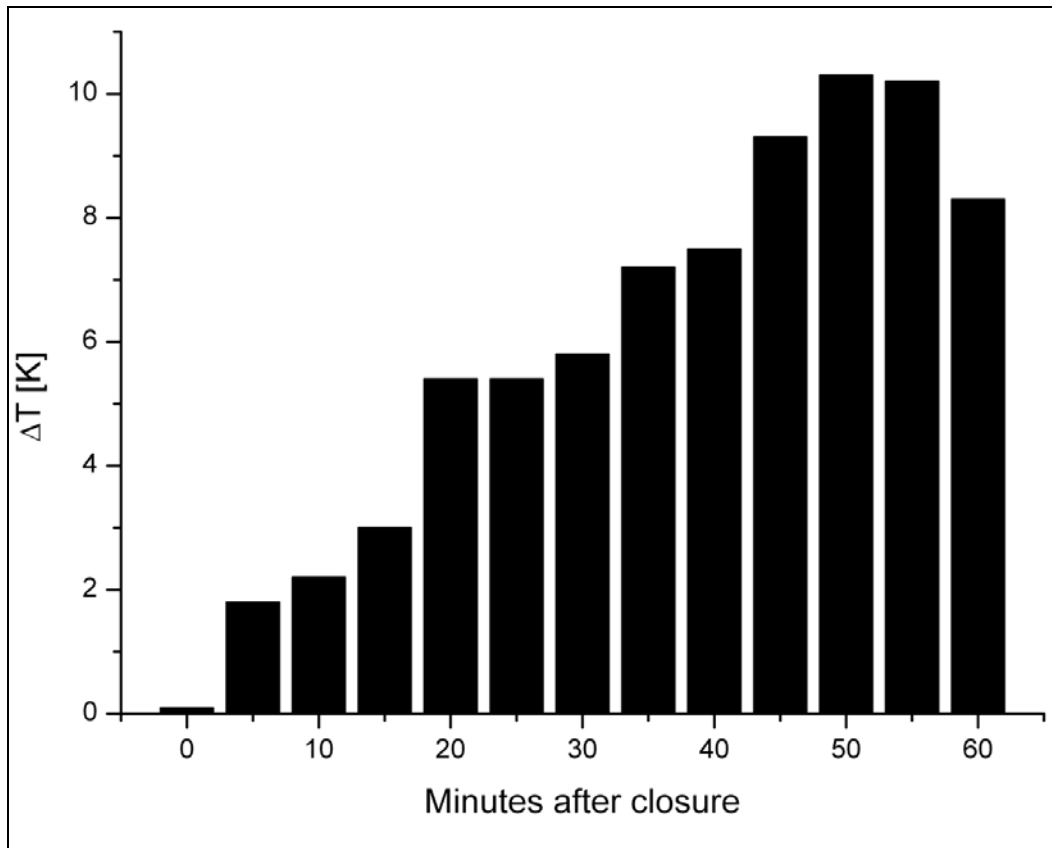


**Figure 4.15:** Temperature difference between the situation without cooling packs and the situation with cooling packs.

As can be seen in Figure 4.14 the initial temperature directly after closing of the chamber was about 40.5°C in both cases. In the first five minutes after closure both temperatures were rising above 50°C but then the cooling effect of the cooling packs was clearly visible. Without cooling packs the temperature was still rising up to 56°C and after 60 minutes it was still at about 52°C. By applying the cooling packs the temperature remained first stable at about 50°C for ten minutes and decreased steadily afterwards until it reached about 44°C after one hour of closure, only about 4 K above ambient temperature within the chamber before closure. The temperature difference between both situations was increasing up to 10 K (Figure 4.15). According to the ambient air temperature measurement 3 cm above soil at the climate station in DBW a decrease of only 0.5 K occurred during the closed chamber period. Taking the starting temperature inside the chamber as reference value this test shows that the temperature of the enclosed air can be considered near ambient condition.



## **5 Results and Discussion**

### **5.1 Soil-Atmosphere Exchange of Methane**

For investigations of the soil-atmosphere trace gas exchange, the above-mentioned newly developed and constructed closed dynamic chambers were used together with the TDL-PAS detection system. The results of the experimental field DBW were then compared with data obtained by already existing static chambers connected to the GC in the container. These static chambers were constructed and installed during a previous project and were automatically opening and closing. With an inner area of 1.96 m<sup>2</sup> and heights adjustable from 250 mm up to 2250 mm their volumes were up to twelvefold that of the new chambers.

#### **5.1.1 Closed Chamber Measurements in Dongbeiwang**

As mentioned above agricultural crops could be planted within the frames. The planting and irrigation scheme of the main field experiment was adopted to make a statement about the soil-atmosphere exchange of methane of the main field experiment. For that purpose winter wheat and summer maize were planted in October 2006 and June 2007, respectively. Due to the lack of adequate precipitation winter wheat had to be irrigated by flooding (border irrigation). Summer maize had to be irrigated only directly after fertilizing. Two fertilization schemes were applied which differed on the amount of N-fertilizer used. One scheme was the farmers practice applying 100 kg N ha<sup>-1</sup> and the other scheme was a reduced input of 50 kg N ha<sup>-1</sup>. Both schemes were used for the closed chamber measurements.

All seven frames were installed in October 2006 and six of them were planted with winter wheat. The seventh frame was the control plot containing bare soil. The winter wheat was harvested in June 2007 and summer maize was planted one week later. The two fertilization schemes were applied to summer maize. Farmers practice (chambers 1 – 3) and reduced input (chambers 4 – 6) with amounts of N-fertilizer of 100 kg ha<sup>-1</sup> and 50 kg ha<sup>-1</sup>, respectively. Directly after the fertilizer input the field as well as the plots were irrigated with an amount of water of 30 mm. This was done at the 22<sup>nd</sup> of July 2007.

Due to the fact that the TDL-PA systems were brought back to Hohenheim for examination and overhauling from November 2006 until March 2007 no gas exchange data could be collected with the chambers during that time. In 2007 the chamber measurements were

interrupted at the end of July 2007 due to the urgent necessity of ambient air methane concentration analysis (see chapter 5.5). Because of this all winter wheat and summer maize data obtained by the different chambers can be regarded as the same treatment.

Further chamber measurements were impossible because in the middle of October 2007 the research field DBW was abandoned due to the spreading of Beijing county area.

If not stated otherwise the TDL-PA systems were placed in the container and two Teflon tubes, each about 20 m in length, were connected to the chambers inlet and outlet, respectively. The gas was then pumped in a closed circuit with a flow rate of 0.5 l min<sup>-1</sup>.

### 5.1.2 Flux Calculation

Due to the fact that the soil in DBW was a net sink for methane an exponential decrease of the concentration within the chamber was assumed. So all methane fluxes were calculated applying the following formula [Smith et al. 2004].

$$F = \alpha * C_0 * \frac{h * M}{V_m} * \frac{273}{T} \quad (5.1)$$

with:

$F$  gas flux rate [mg CH<sub>4</sub>-C m<sup>-2</sup> d<sup>-1</sup>]

$\alpha$  degradation rate constant

$C_0$  concentration at the time of closure [ppm]

$h$  chamber height [m]

$M$  molecular weight of methane = 12 [g mol<sup>-1</sup>]

$V_m$  volume occupied by 1 mol of methane at standard pressure = 22.4 [l mol<sup>-1</sup>]

$T$  ambient air temperature [K]

For each dataset the correlation coefficient was calculated. Unfortunately there existed no standardized threshold value of the correlation coefficient beneath which the data must be omitted. Some scientists used an absolute value < 0.9 [Matson et al. 1995] while others used < 0.8. If the change in concentration is analyzed discontinuously, e.g. by manually taking samples and analyzing them by GC, only about five to twenty data points per hour closure time will be obtained. In contrast to that the measurement by TDL-PAS with 2 Hz, as applied

in this study, yielded 7200 data points per hour. Therefore, the correlation coefficient was below 0.9 most of the time but the flux rate values could be used. In this study the threshold value beneath the data were omitted was defined as  $< 0.3$ . An example of the different  $R^2$  of the same dataset is given in Figure 5.1. Due to Smith the uptake of methane is an exponential function [Smith et al. 2004] which can be seen in Figure 5.1.

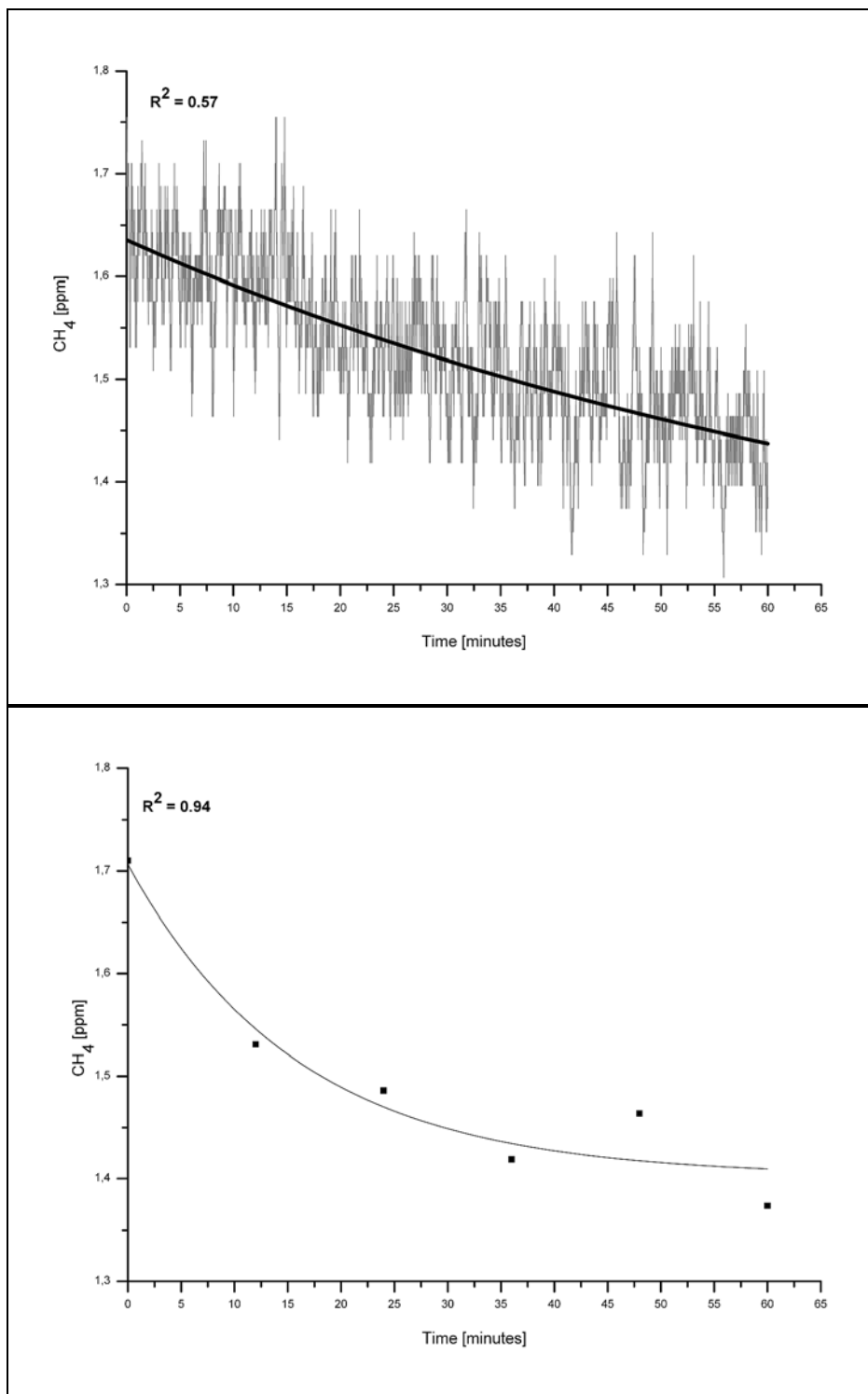


**Figure 5.1:** Correlation coefficient of the same dataset. Raw data (top) and 12 minutes data points (bottom).

### 5.2 Soil-Atmosphere Exchange of Methane during Winter Wheat Growing Season

The winter wheat was planted inside of the chambers in October 2006. Only first measurements could be started until middle of October 2006. In 2007 at the 25<sup>th</sup> of April the winter wheat was irrigated with an amount of water of 12 mm and the measurements were restarted at the 30<sup>th</sup> of April. At the 21<sup>st</sup> of May the winter wheat was irrigated with an amount of water of 13.5 mm. Harvest was at the 16<sup>th</sup> of June.

Methane exchange data using the 1 m hood and six planted frames as well as the control plot were available at different days from the 30<sup>th</sup> of April to the 7<sup>th</sup> of June 2007. For methane exchange rates with winter wheat planted mean values were calculated. The result is presented in Figure 5.2.

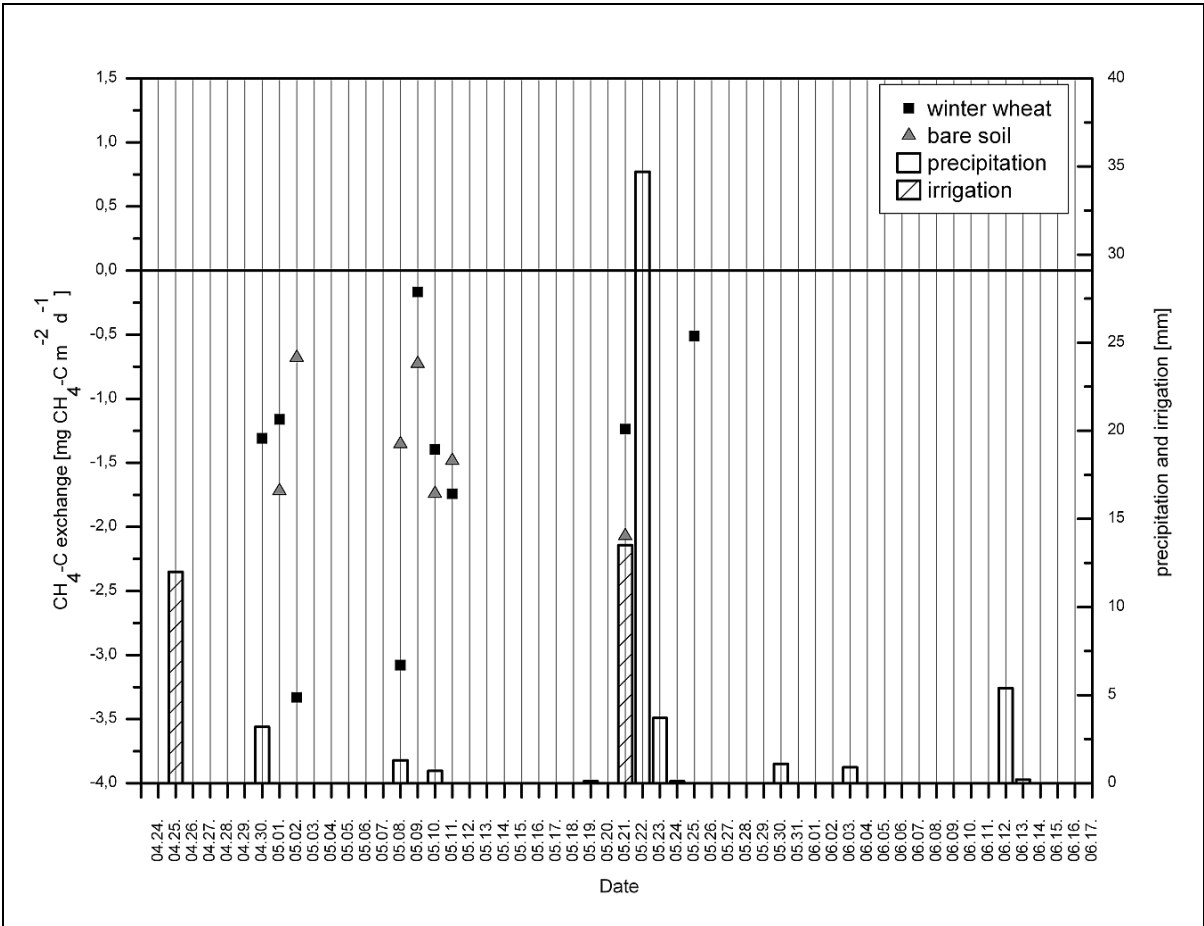


**Figure 5.2:** Daily sums of measured methane fluxes, precipitation and irrigation during winter wheat growing season from 24<sup>th</sup> of April to the 16<sup>th</sup> of June 2007.

As can be seen in Figure 5.2 the arable soil planted with winter wheat acted as a methane sink. The exchange rate ranged from -0.17 to -3.33 for winter wheat and from -0.68 to -2.07  $\text{mg CH}_4\text{-C m}^{-2} \text{d}^{-1}$  for bare soil, respectively. These values were higher compared to the findings of Kogge who used the large automatic chambers and GC analysis technique in 2002. He calculated an exchange rate of -0.25  $\text{mg CH}_4\text{-C m}^{-2} \text{d}^{-1}$  for winter wheat in DBW [Kogge 2002]. His daily mean values ranged from 0 to -1.5  $\text{mg CH}_4\text{-C m}^{-2} \text{d}^{-1}$ .

The planted plots and the control plot showed a similar uptake pattern but there were differences in the uptake rate. At the 2<sup>nd</sup> of May the highest uptake rate in winter wheat occurred while it was lowest in the bare soil. This can be explained by the ambient air methane concentration at chamber closure. The higher this concentration the higher the value  $C_0$  in Formula 5.1. Moreover the uptake of  $\text{CH}_4$  during one hour of closure time was higher if there was more  $\text{CH}_4$  available in the ambient air. Figure 5.3 shows the situation at the 2<sup>nd</sup> of May.

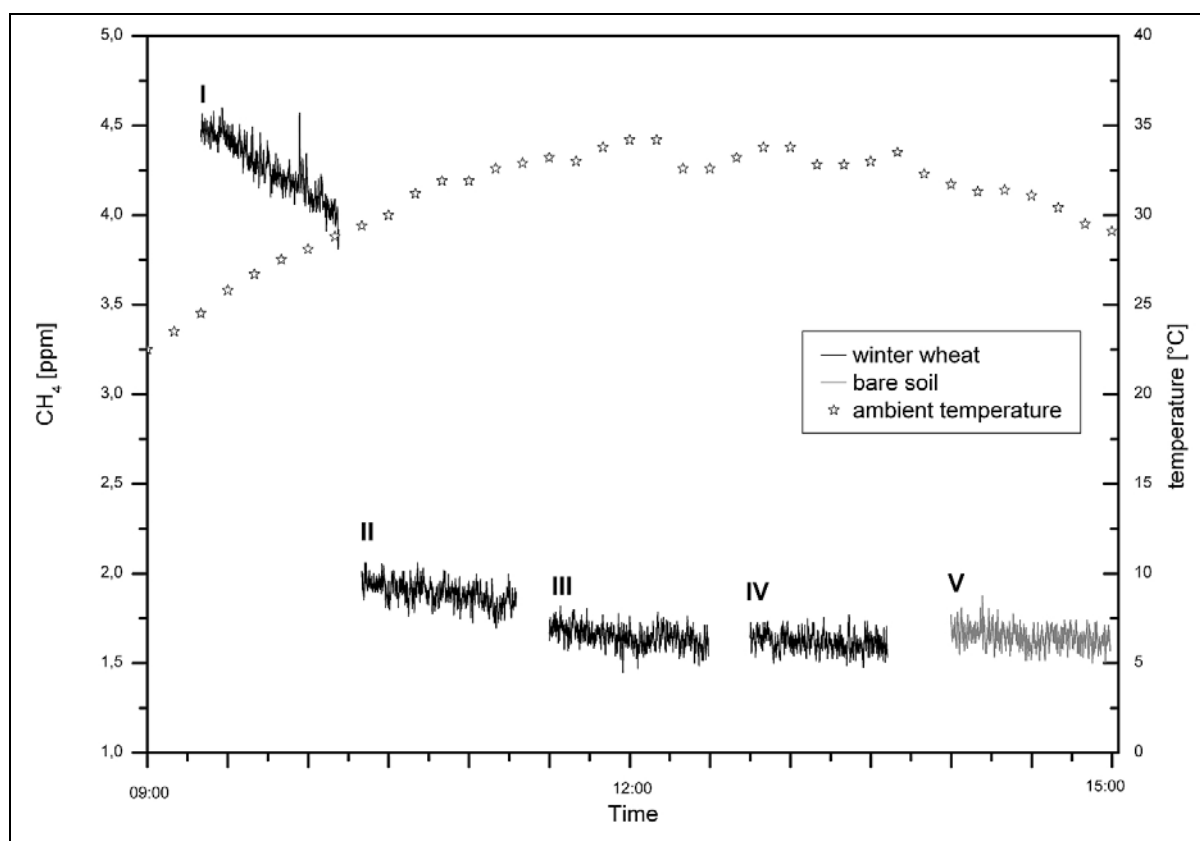


**Figure 5.3:** 2<sup>nd</sup> of May 2007 methane concentration pattern inside of the closed chamber planted with winter wheat (I – IV) as well as bare soil (V) at different closure times. Ambient temperature measured 3 cm above soil.

The winter wheat measurement (I) at 9:15 am started from an ambient air methane concentration of about 4.5 ppm. This was 2.5 times higher than the global methane concentration of about 1.8 ppm according to the newest IPCC report [IPCC 2007]. Within one hour closure time the concentration inside of the chamber decreased to a value of 3.9 ppm, which was a calculated exchange rate of  $-7.46 \text{ mg CH}_4\text{-C m}^{-2} \text{ d}^{-1}$ . In the same time the ambient concentration decreased to a value of about 2 ppm as was apparent from the beginning of the next chamber measurement (II). During noon and afternoon the uptake rate declined as well as the ambient air methane concentration. The calculated exchange rates for the measurements II to V were as follows:

-1.56 (II), -0.99 (III), -0.66 (IV) and  $-0.68 \text{ mg CH}_4\text{-C m}^{-2} \text{ d}^{-1}$  (V).

The consumption of  $\text{CH}_4$  occurs near the soil surface and hence is influenced by diurnal variation in temperature. This usually leads to exponentially increase in the enzymatic processes with rising temperature [Davidson et al. 1995] but could not be verified during this research. Here the temperature was not the limiting factor, in fact the ambient air methane concentration was the dominating process.

Another event with elevated ambient air methane concentration occurred at the 21<sup>st</sup> of May 2007 as shown in Figure 5.4. At that day all plots were irrigated with an amount of water of 13 mm and the measurements started one hour afterwards. Also here methane uptake occurred at a higher ambient air concentration level yielding in higher calculated uptake rates. The calculated exchange rates for the measurements I to V were as follows:

-2.83 (I), -1.57 (II), -1.19 (III), -0.95 (IV) and  $-1.34 \text{ mg CH}_4\text{-C m}^{-2} \text{ d}^{-1}$  (V).

It can be seen that during the course of the day the uptake rate decreased. During the last measurement of bare soil (V) methane uptake occurred but interestingly after 30 minutes methane was emitted instead of further being taken up. The exchange rate calculation for this measurement by applying the exponential function nevertheless revealed an uptake of methane by the soil.

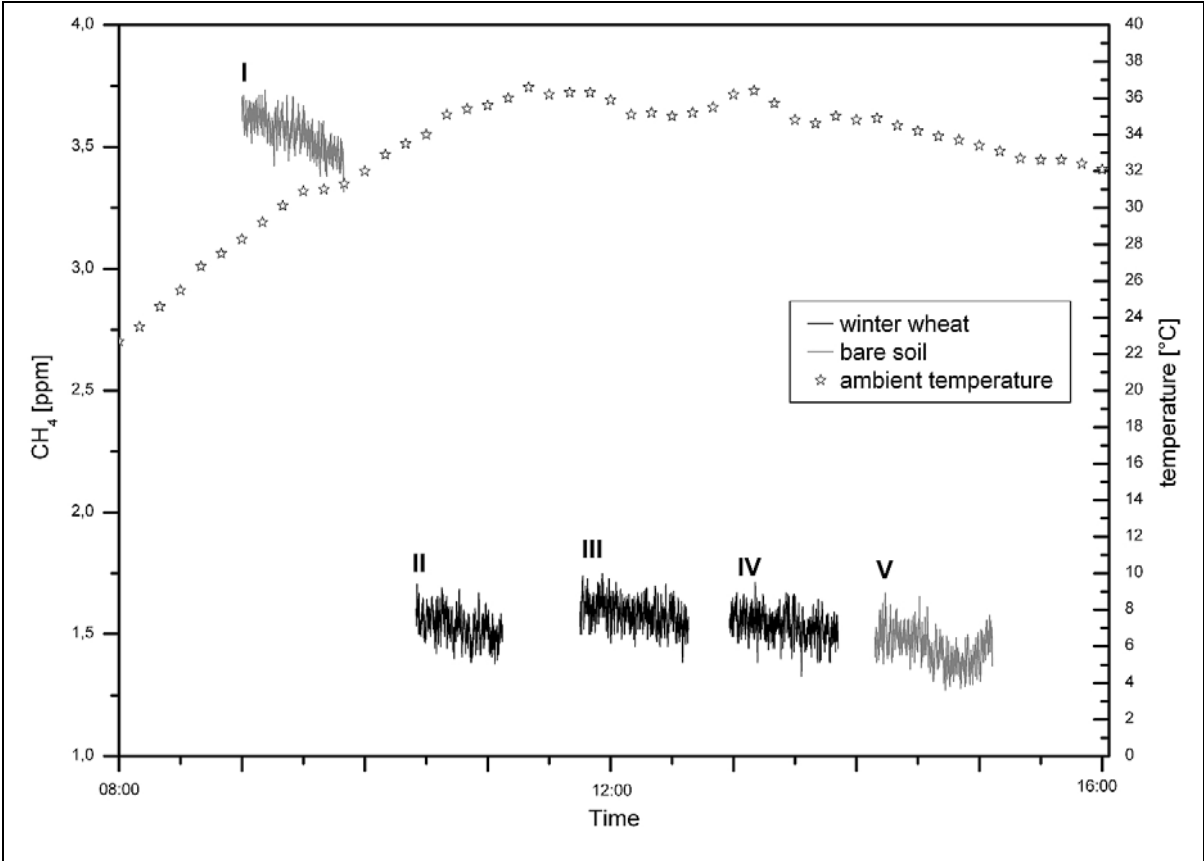


**Figure 5.4:** 21<sup>st</sup> of May 2007 methane concentration pattern inside of the closed chamber planted with winter wheat (II – IV) as well as bare soil (I and V) at different closure times. Ambient temperature measured 3 cm above soil. All plots were irrigated with an amount of water of 13 mm at 8 am.

### 5.3 Soil-Atmosphere Exchange of Methane during Summer Maize Growing Season

The summer maize was planted at the 25<sup>th</sup> of June 2007, one week after harvesting of winter wheat. Before seeding, the frames were removed from the soil and the plots were ploughed with a spade up to a depth of about 25 cm. Subsequently the frames were reinstalled and a gas tightness test was conducted as described in chapter 4.6.3. Since all frames could be considered tight, the summer maize was planted in six of the seven frames, four plants per frame. The seventh frame was the control plot containing just bare soil. The measurements were started at the 26<sup>th</sup> of June and stopped at the 24<sup>th</sup> of July. The results are shown in Figure 5.5.

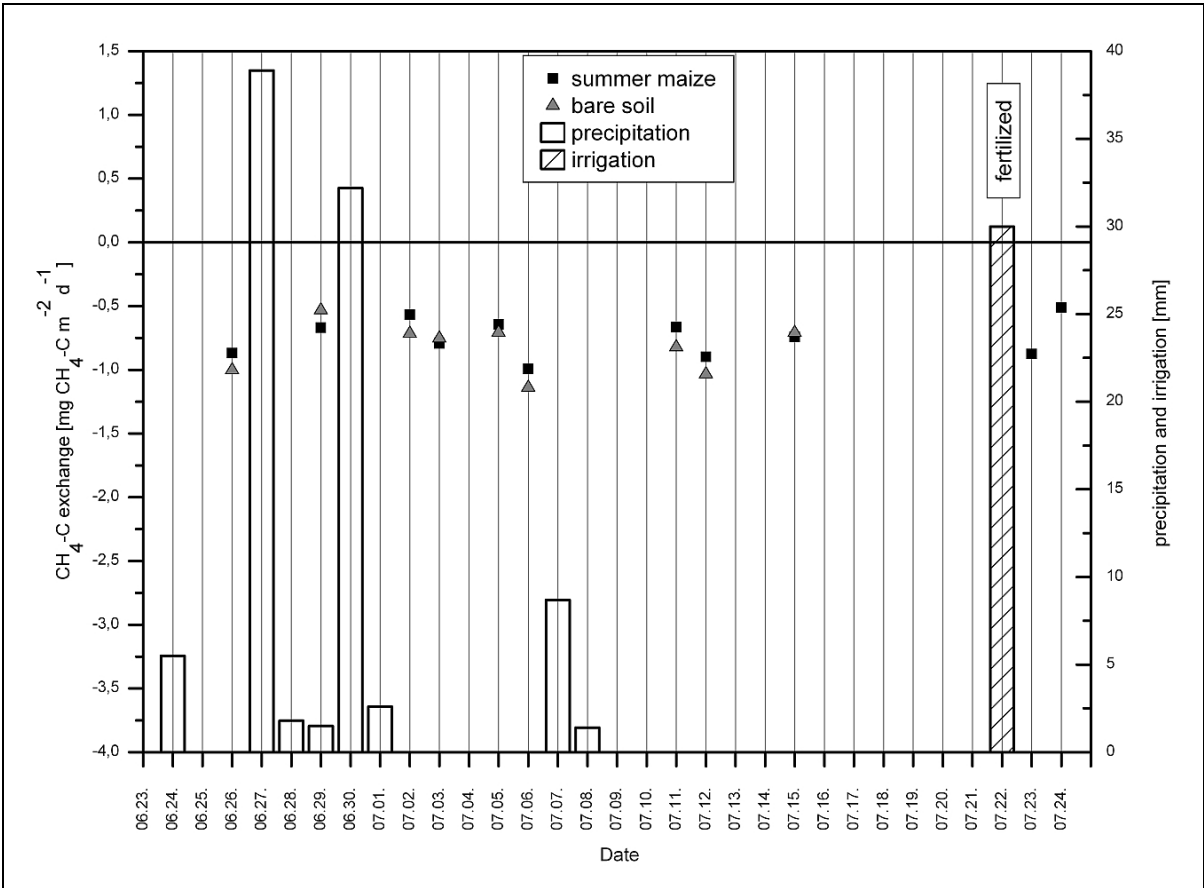


**Figure 5.5:** Daily sums of measured methane fluxes, precipitation and irrigation during summer maize growing season from the 26<sup>th</sup> of June to the 24<sup>th</sup> of July 2007.

The exchange of methane was negative all the time, meaning that uptake by the soil was taking place. The plots with summer maize and the bare soil correlated well with each other and showed the same pattern. The exchange rates ranged from -0.51 to -1.0 mg CH<sub>4</sub>-C m<sup>-2</sup> d<sup>-1</sup> for summer maize and from -0.53 to -1.14 mg CH<sub>4</sub>-C m<sup>-2</sup> d<sup>-1</sup> for bare soil. For the same period in 2002 Kogge calculated an exchange rate of about -0.8 mg CH<sub>4</sub>-C m<sup>-2</sup> d<sup>-1</sup> [Kogge 2002].

The precipitation data shown in Figure 5.5 were derived from the climate station at the research field DBW. Unfortunately at the 25<sup>th</sup> and 26<sup>th</sup> of June as well as from the 12<sup>th</sup> – 24<sup>th</sup> of July no precipitation data were available due to technical problems with the climate station. The main reasons for having only limited CH<sub>4</sub>-C exchange data obtained with the TDL-PA system and the new chambers were following: Multiple power breakdowns at the research field DBW caused by heavy rain led to measurement gaps by the hour or even by the day. Due to high relative humidity and temperature of the ambient air, condensation of water vapor in the tubes connecting the closed chambers and the TDL-PA system as well as in the PA detection system itself caused fluctuations in the experimental data resulting in a  $R^2 < 0.3$ .

### 5.3.1 24 Hour Measurement

In 2002 Kogge detected higher nighttime methane concentrations of up to 43 ppm during his measurements in DBW, but the fixed installation of his measurement equipment (GC) in the container in DBW did not allow him to do further research on that topic [Kogge 2002]. Other researchers detected a diurnal variation in ambient air methane concentration in Beijing as well but at a very low level. The methane concentration during their study fluctuated between 2.5 ppm (during nighttime) and 1.8 ppm (during daytime) [Su et al. 2002].

As shown in Figures 5.3 and 5.4 elevated methane concentrations at daybreak were detected during the exchange measurements at the plots planted with winter wheat as well as at the control plot. To verify and quantify the diurnal variation in methane concentration at DBW, one plot was selected for a 24 hour measurement campaign conducted from the 23<sup>rd</sup> – 24<sup>th</sup> of July 2007.

One day before the campaign the plots were fertilized with nitrogen fertilizer (urea 40.6% N) and irrigated with an amount of water of 30 mm. Three chambers were fertilized according to farmers practice (100 kg ha<sup>-1</sup>), three according to reduced input (50 kg ha<sup>-1</sup>), respectively.

Due to ease of handling only one plot, among farmers practice, was measured by using the 1 m hood. Because the purpose was to discover a diurnal variation in methane exchange, the chamber was closed and opened for one hour, respectively. During nighttime a sharp increase in the ambient air methane concentration was detected which proved that the methane was not emitted by the soils but must be emitted from somewhere else. The results are presented in Figure 5.6.

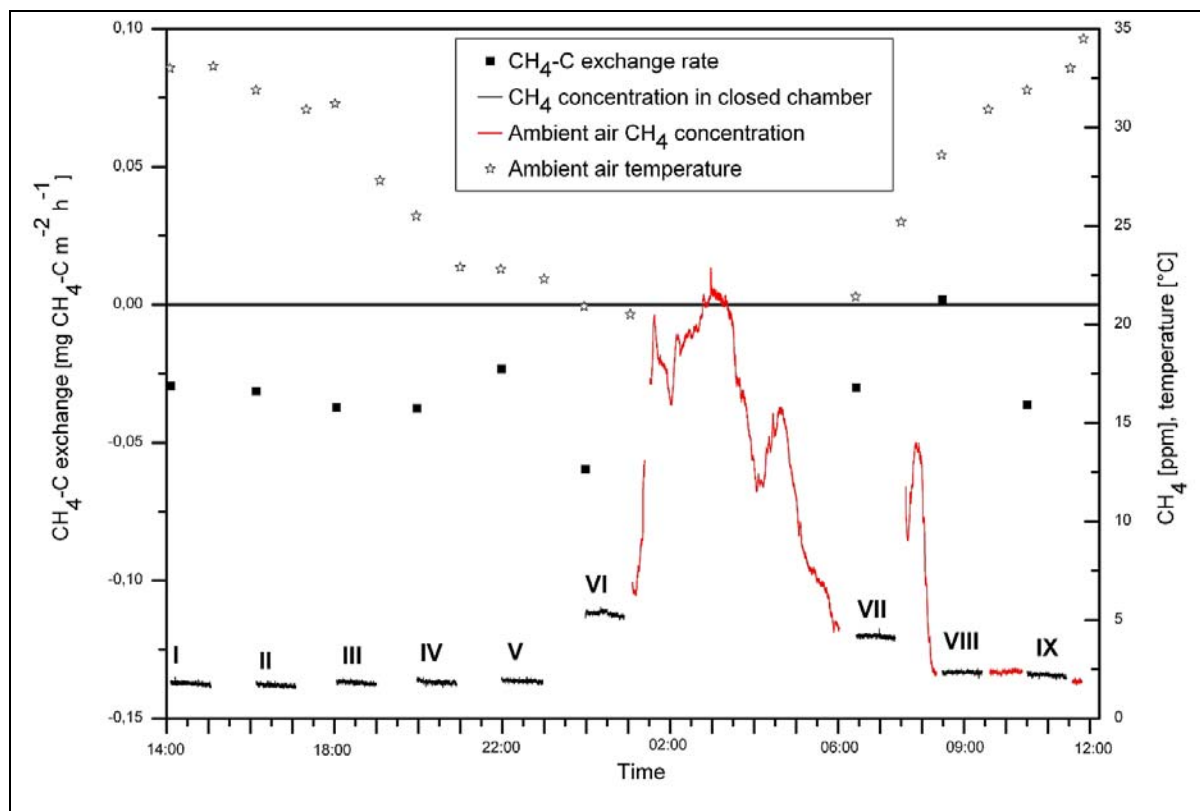


**Figure 5.6:** Measurement of methane concentration inside of the closed chamber (I – IX), ambient air methane concentration, temperature and hourly exchange rate from the 23<sup>rd</sup> – 24<sup>th</sup> of July 2007.

The chamber measurements were started at 2 pm (I) and the ambient air methane concentration, which was the initial value after closing of the chamber, was at normal level at about 2 ppm. The exchange rate remained stable at  $-0.03 \text{ mg CH}_4\text{-C m}^{-2} \text{ h}^{-1}$  for the first five chamber measurements (I – V), while the ambient air temperature decreased of about 10 K at the same time without an influence on the uptake rate. At midnight the next measurement (VI) was started and it can be seen that the ambient air methane concentration had doubled leading to an increase of the calculated uptake rate. The subsequent observation of the ambient air methane concentration conducted from 1 am until 6 am revealed a sharp increase to levels about 22 ppm, which was elevenfold the normal concentration. The chamber measurement at 6:30 am (VII) started at nearly the same methane concentration and ambient air temperature as the measurement before (VI) but the uptake rate was only half the amount. A possible explanation for this was that the soil consumed more methane during nighttime while there was a surplus of methane available so that the uptake rate during daytime was decreased. As can further be seen there was another methane peak of about 14 ppm at 8 am. The concentration stabilized afterwards at normal level at about 2 ppm (VIII, IX).

This 24 hour measurement showed the diurnal variation in ambient air methane concentration in DBW. Due to the fact that the methane was not emitted by the soil but originated from somewhere else it must be connected with the diurnal variation of the atmospheric boundary

layer. This is typical for urban heat islands, like Beijing, where stable atmospheric layering dominates during the night and a mixing layer during daytime. Liu studied the effect of the urban heat island in Beijing from 1995 – 2005 and found out that an inversion in the urban boundary layer was very favorable to the formation of the strong summer urban heat island [Liu et al. 2006]. According to Hu in summer the western part of Beijing, inter alia the Haidian district including DBW, is about 6 K warmer than the rest of Beijing. Moreover during daytime there is anabatic wind from the south while at nighttime the wind is katabatic from the north [Hu et al. 2005]. For details about the atmospheric boundary layer see chapter 5.4.

## 5.4 Atmospheric Boundary Layer

The result of the 24 hour measurement (see Figure 5.6) shows the diurnal variation of the atmospheric boundary layer. This is the lower portion of the troposphere where the atmospheric friction increases approaching the ground. This layer is capped by a static and stable air layer (temperature inversion) with intermittent turbulence where air exchange (entrainment zone) with the troposphere is taking place [Foken 2003]. The thickness of the atmospheric boundary layer is typically between 1 – 2 km. If the atmosphere is strongly stable layered the thickness can be only about 10 m. Moreover its diurnal variation is variable [Stull 1988]. After sunrise the atmosphere is heated up by turbulent heat flux from the basis dissipating the nocturnal inversion. A mixing layer is formed which is capped by the entrainment zone. Near sunset turbulence decays, leaving a residual layer in place of the mixed layer. During nighttime, the bottom of the residual layer is transformed into a statically stable boundary layer by contact with the radiative cooled surface [Seibert et al. 2000]. Zhang analyzed the atmospheric boundary layer in Beijing in autumn and calculated 1 km thickness during daytime and 200 – 400 m during nighttime [Zhang et al. 2006].

A strong and stable boundary layer leads to accumulation of trace gases, e.g. methane if emission sources are present. A diurnal variation in ambient air methane concentration was also detected by some researchers in Beijing but on a very low level. The methane concentration during their study fluctuated between 2.5 ppm (during nighttime) and 1.8 ppm (during daytime) [Su et al. 2002]. They took half-hourly samples at the Beijing University approximately 7 km south-east of DBW (see Figure 5.15).

For further analysis of the ambient air methane concentration, the mobile TDL-PA system was used to conduct measurements in DBW as well as at other places in the vicinity of DBW. To detect the source of the methane emission, wind direction and wind speed data were recorded by an ultrasonic anemometer that was combined with the TDL-PA system. That was why the methane exchange measurements were stopped at that point.

Further information about the ambient air methane concentration measurements are given in chapter 5.5.

## 5.5 Ambient Air Methane Measurements

### 5.5.1 Measurements of Methane at Dongbeiwang

After detection of the relatively high methane concentrations in DBW during the 24 hour measurement (see chapter 5.3.1) several multiple day campaigns were started. The methane concentration fluctuated between 1.4 ppm at daytime and up to 40 ppm at nighttime and early morning. By combining the TDL-PA system with an ultrasonic anemometer (Young 8100), provided by the Chinese counterparts, the correlation between high methane concentrations as well as wind direction and wind speed should be observed. For this purpose the anemometer was put on top of the container in DBW approximately 5 m above ground and a 10 m long Teflon tube with air filters (Pall Acro 50 Vent 0.2  $\mu\text{m}$ ) attached to both ends was connected to it and to the gas inlet of the TDL-PA device, respectively. The measurement rate was 4 Hz and the airflow was kept constant at 0.5  $\text{l min}^{-1}$  by sucking the air through the TDL-PA system. The results are presented in Figures 5.7 and 5.8.

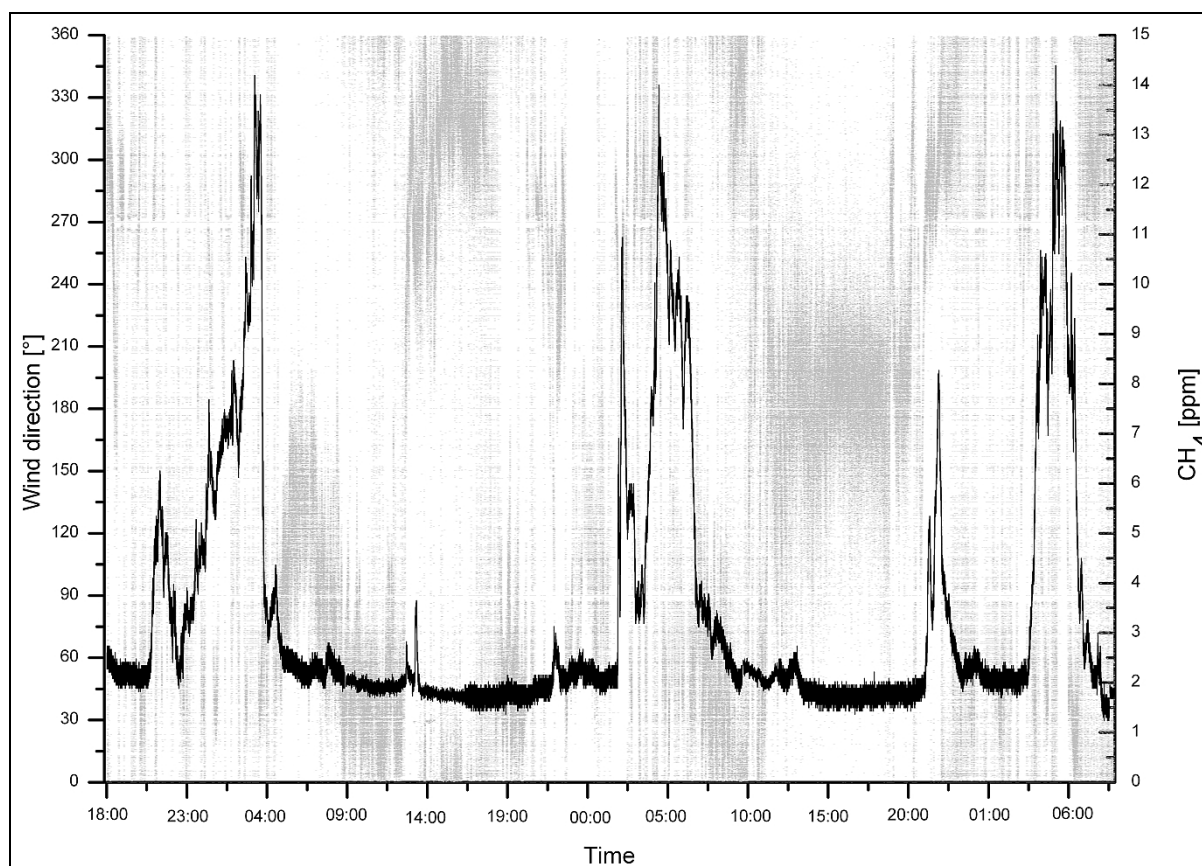


**Figure 5.7:** Measurement of methane concentration (black) and wind direction (gray) on top of the container in Dongbeiwang from the 6<sup>th</sup> – 9<sup>th</sup> of August 2007.

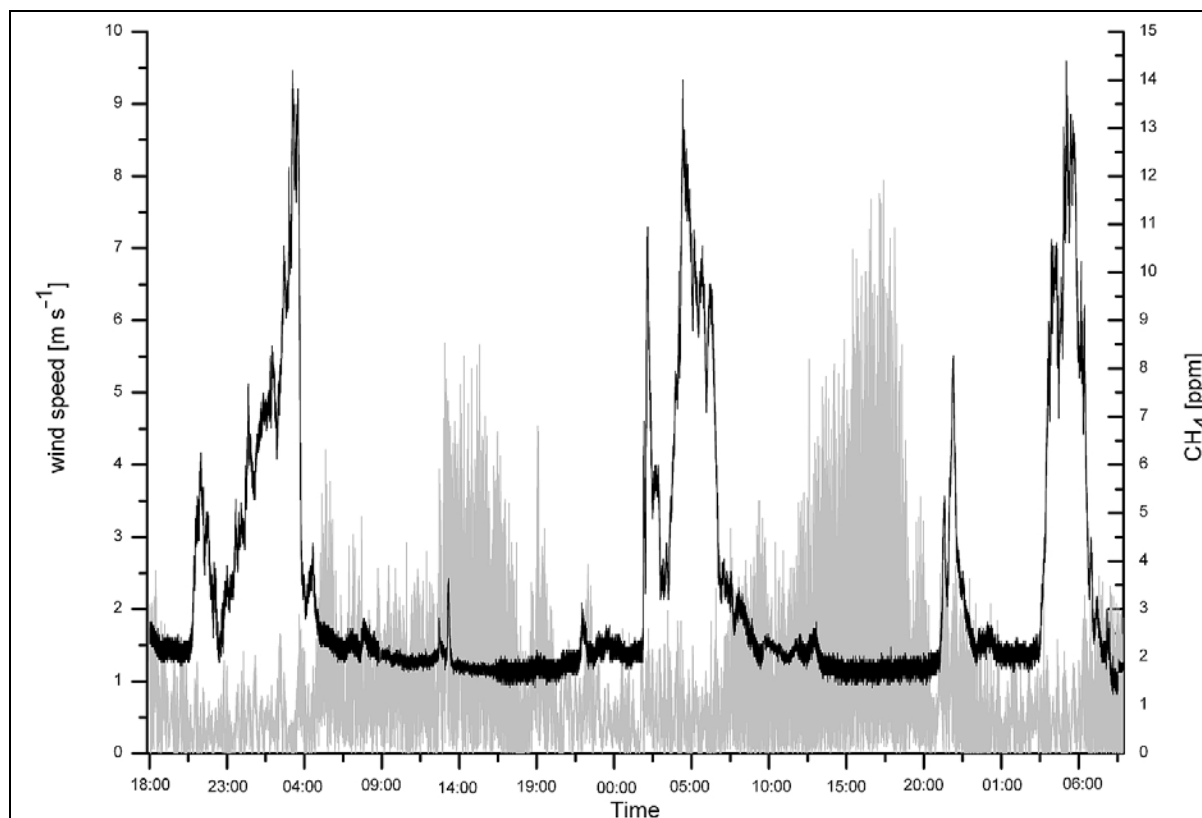


**Figure 5.8:** Measurement of methane concentration (black) and wind speed (gray) on top of the container in Dongbeiwang from the 6<sup>th</sup> – 9<sup>th</sup> of August 2007.

During the three nights of measurement elevated concentrations of methane were clearly visible. With 14 ppm the peak heights were at the same level differing only in the exact time reaching it. In the first night the concentration started to rise at about 9 pm and reached its maximum at 3 am. At 5 am the methane concentration was at normal level of 2 ppm because of increasing wind speed and thus mixing of the atmosphere. During daytime of the 7<sup>th</sup> of August the atmosphere was well mixed due to wind speeds ranging from 2 – 5 m s<sup>-1</sup> with a prevailing wind direction from west to north-west. There was a sharp increase in the concentration in the second night beginning at 2 am until 8 am with a maximum at 5 am. The wind speed was higher than the day before, up to 8 m s<sup>-1</sup>, with a prevailing wind direction from south. The 8 ppm methane peak at 10 pm (beginning of the third night) started with increasing wind speed and a change to western direction. The concentration dropped to about 2 ppm while the wind speed was decreasing without a distinct wind direction. At 4 am the methane concentration increased again to levels of about 14 ppm at 6 am. Afterwards turbulence started mixing the atmosphere resulting in lower concentrations of methane.

Conclusions about correlations between methane concentration, wind speed and wind direction should be drawn. Due to this fact all data with wind speeds  $< 0.3 \text{ m s}^{-1}$ , which is Beaufort number 0 (calm) according to the Beaufort scale, were omitted. As can be seen in Figure 5.9 elevated methane concentrations were correlated with wind blowing from north-east and west directions.

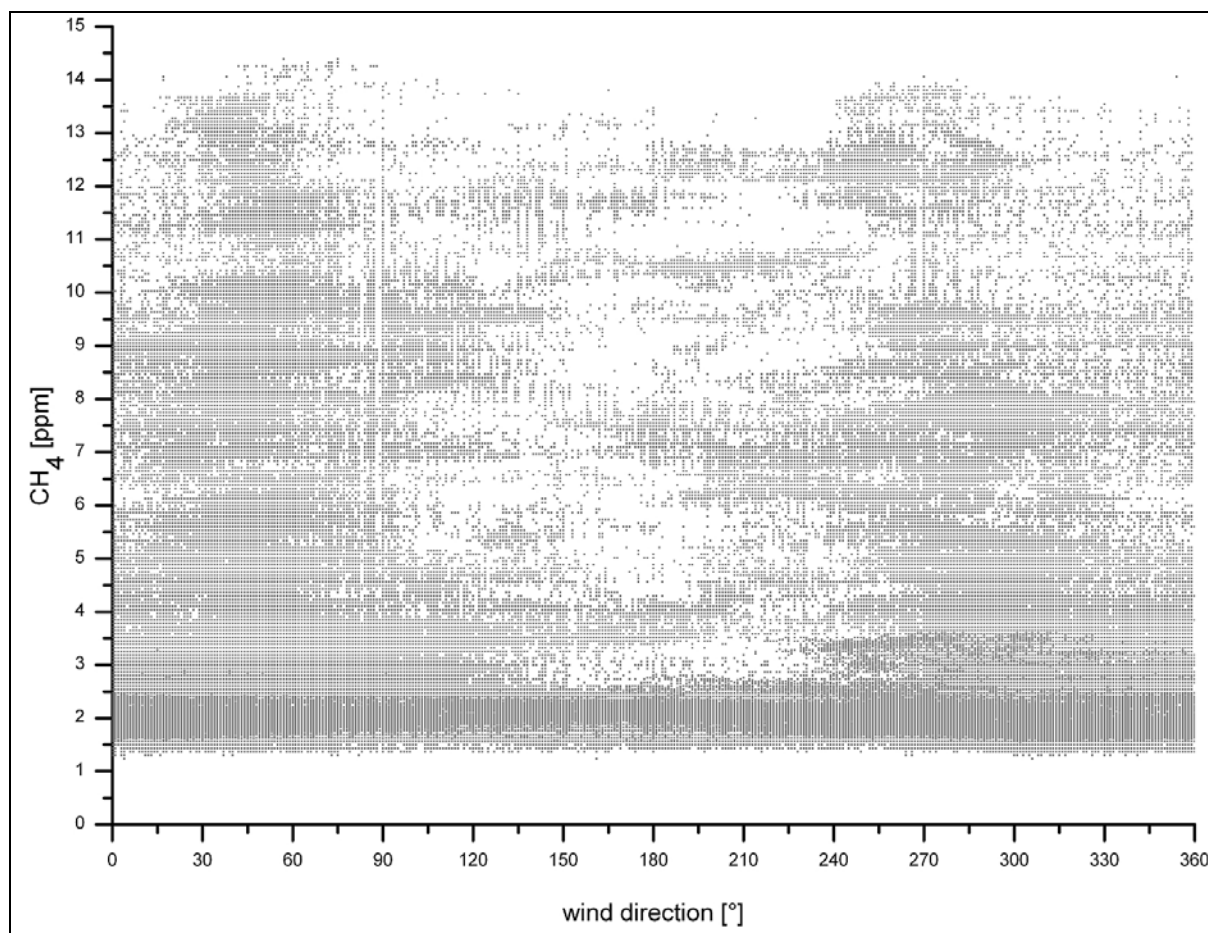


**Figure 5.9:** Correlation between methane concentration and wind direction measured on top of the container in Dongbeiwang from the 6<sup>th</sup> – 9<sup>th</sup> of August 2007. All data with a wind speed below  $0.3 \text{ m s}^{-1}$  were omitted.

The correlation between methane concentration and wind speed is shown in Figure 5.10 and between wind speed and wind direction in Figure 5.11. As expected it can be seen that higher methane concentrations were correlated with lower wind speeds. Winds with speeds about  $5 \text{ m s}^{-1}$  were blowing from southern and western directions while weak winds were blowing from north-east.

This supports the assumption of the statically stable boundary layer with lower wind speeds during nighttime where methane accumulation takes place.

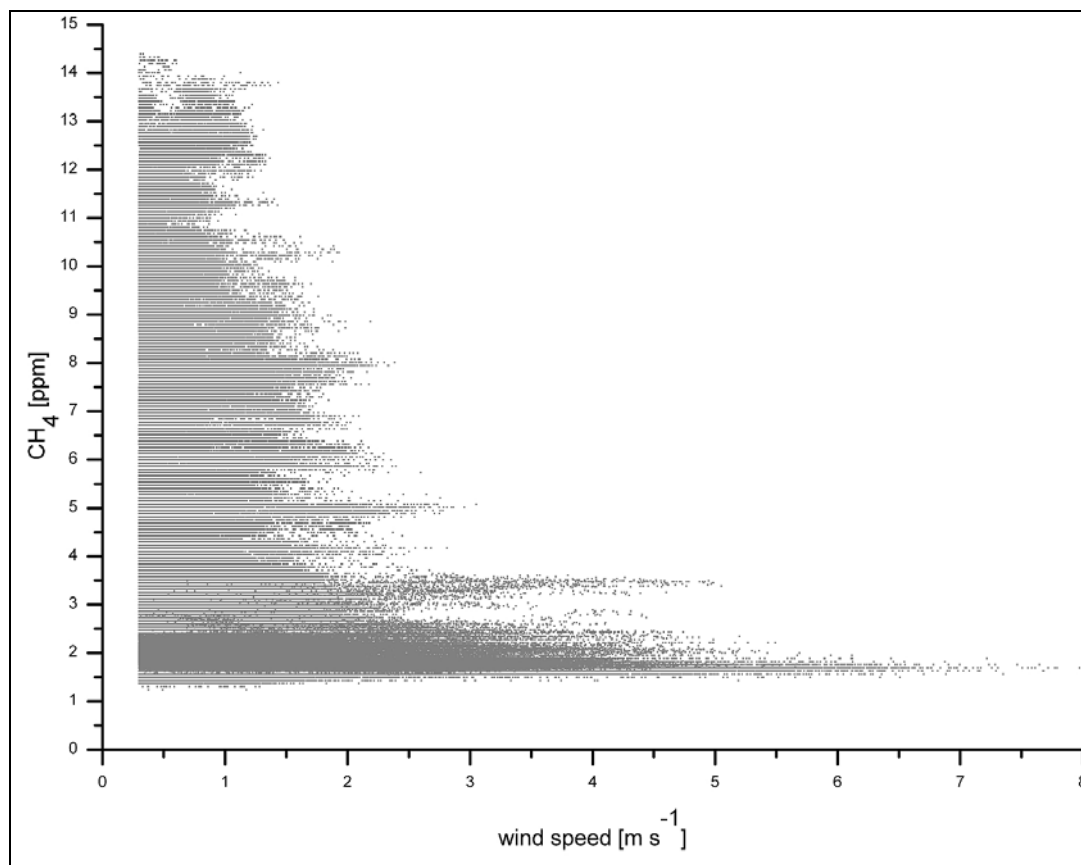


**Figure 5.10:** Correlation between methane concentration and wind speed measured on top of the container in Dongbeiwang from the 6<sup>th</sup> – 9<sup>th</sup> of August 2007. All data below 0.3 m s<sup>-1</sup> were omitted.

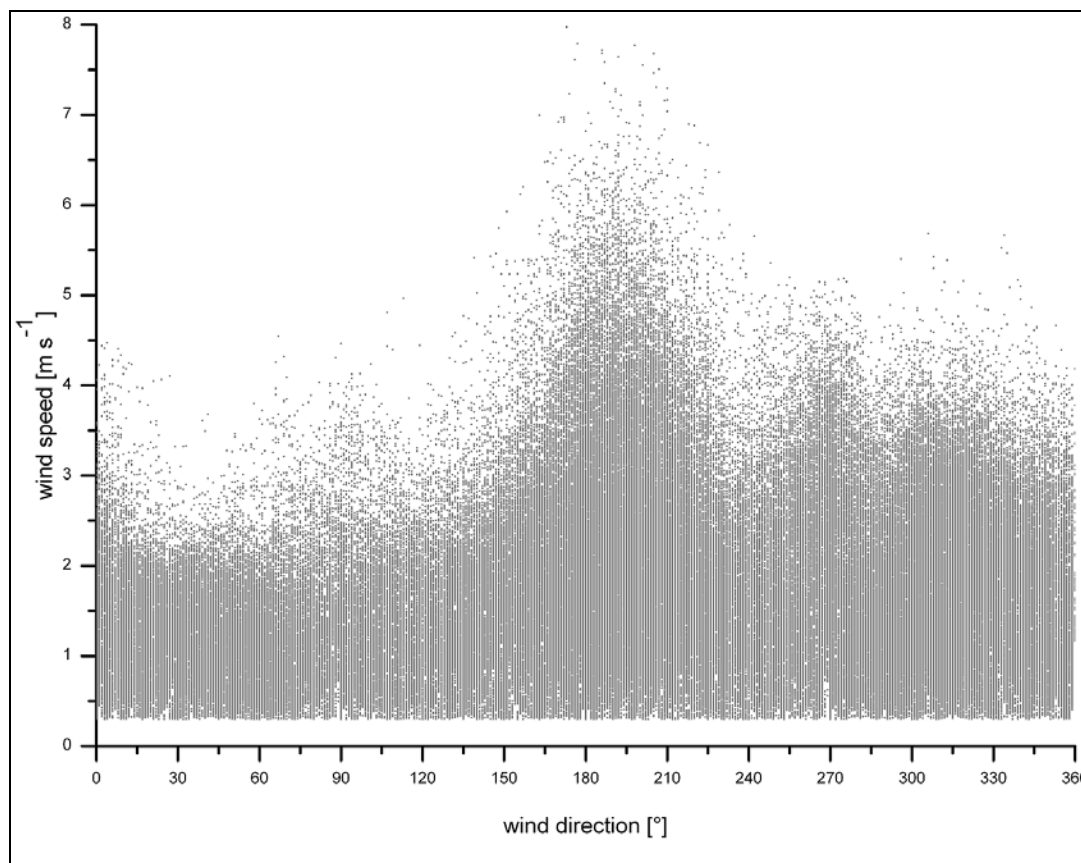


**Figure 5.11:** Correlation between wind speed and wind direction measured on top of the container in Dongbeiwang from the 6<sup>th</sup> – 9<sup>th</sup> of August 2007. All data below 0.3 m s<sup>-1</sup> were omitted.

Since that no such high methane emissions from the soil in DBW were detected during the chamber measurements it was assumed that there must be another source from where the methane originated. To check this assumption a three day measurement campaign at the campus of the CAU was conducted. The CAU was located about 3.2 km south of DBW (see Figure 4.1), surrounded by residential buildings and a main road was passing the university.

### 5.5.2 Measurements of Methane at the Campus of the China Agricultural University

The methane measurements were conducted from the 14<sup>th</sup> – 17<sup>th</sup> of August 2007 on the top of the main building at the campus of the CAU. A 20 m long Teflon tube with air filters (Pall Acro 50 Vent 0.2  $\mu\text{m}$ ) at both ends was connected to the head of the ultrasonic anemometer and the gas inlet of the TDL-PA system, respectively. The system was placed inside of the building. The airflow was set to 0.5 l min<sup>-1</sup> and the measurement rate to 4 Hz. The total height above ground was approximately 30 m. In the morning of the 16<sup>th</sup> of August at 7 am a half-hourly heavy rain caused technical problems with the ultrasonic anemometer. Therefore, from that time on neither wind nor temperature data were further available.

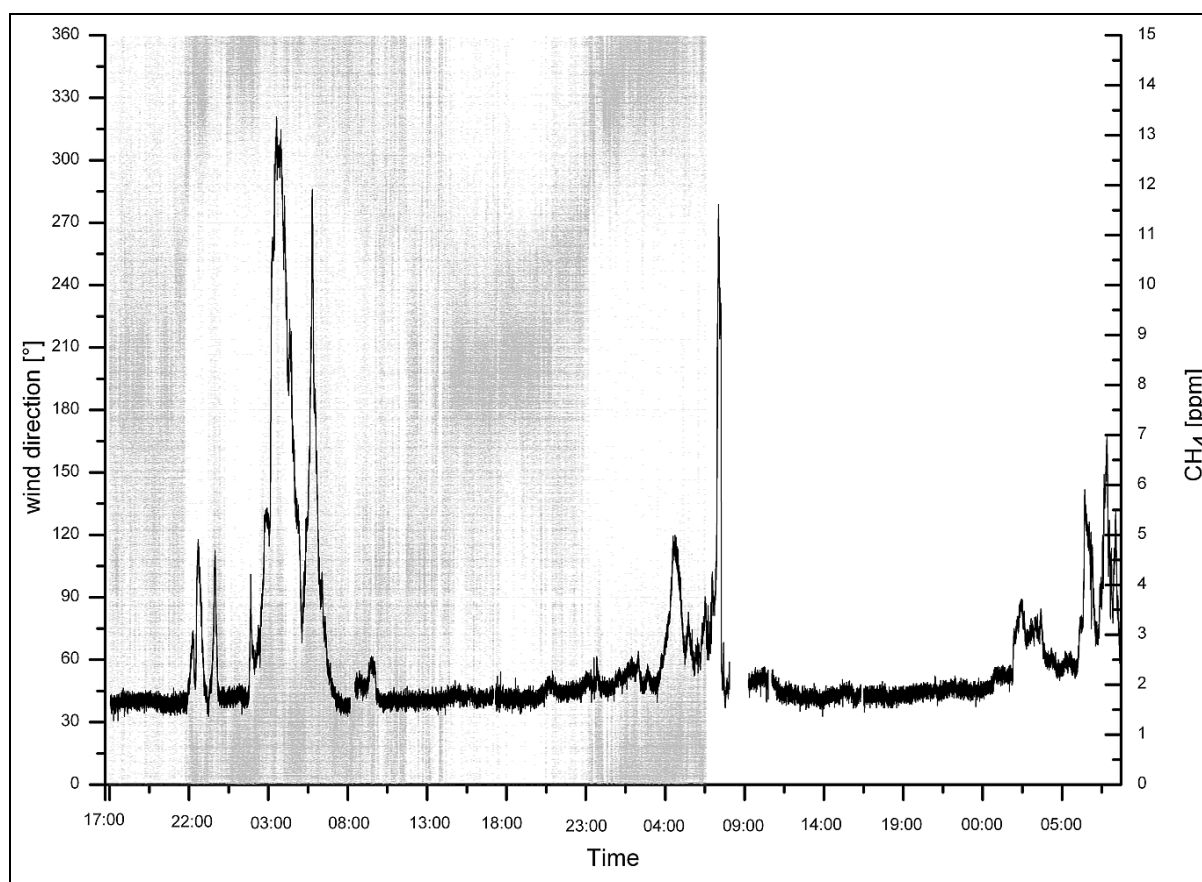


**Figure 5.12:** Measurement of methane concentration (black) and wind direction (gray) on the top of the China Agricultural University from the 14<sup>th</sup> – 17<sup>th</sup> of August 2007.

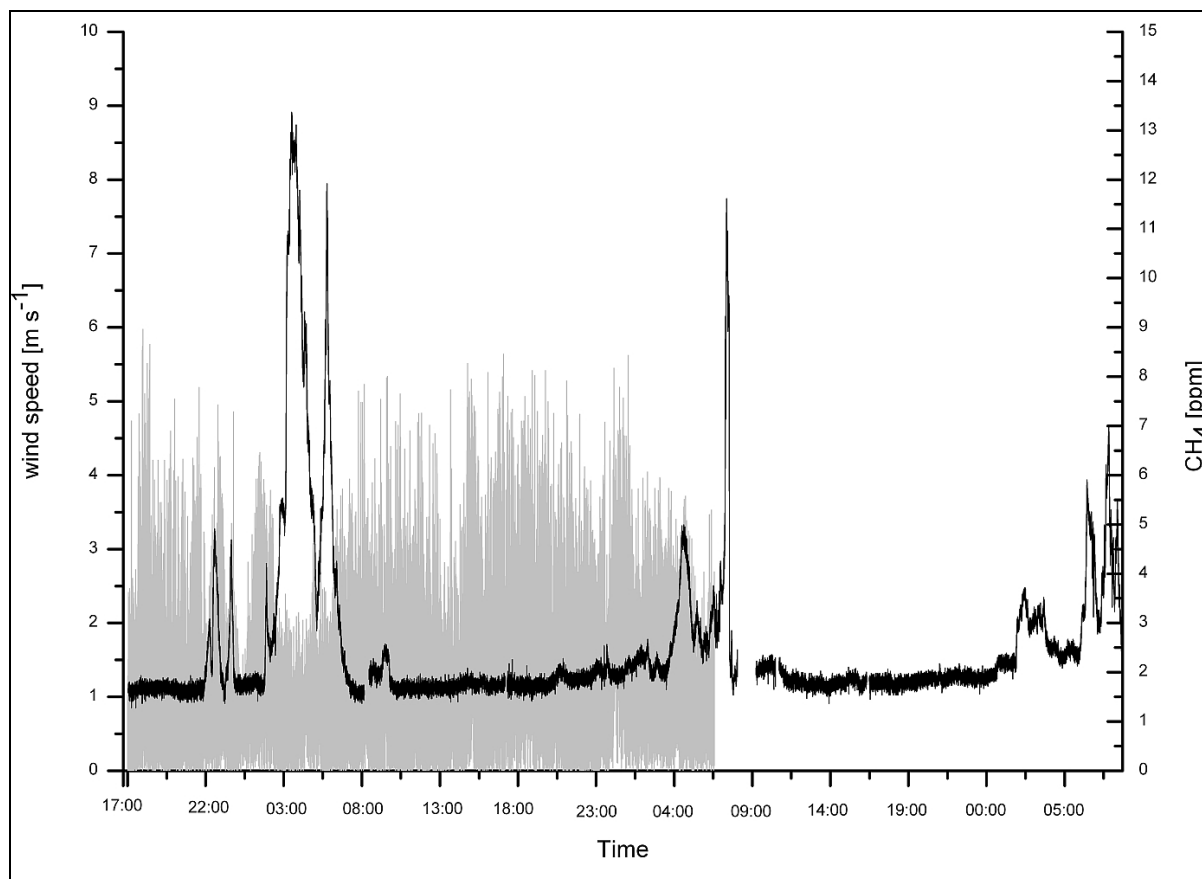


**Figure 5.13:** Measurement of methane concentration (black) and wind speed (gray) on the top of the China Agricultural University from the 14<sup>th</sup> – 17<sup>th</sup> of August 2007.

The results presented in Figures 5.12 and 5.13 show that during all three nights high methane peaks were observable but the concentration was decreasing from 13 over 12 to 7 ppm. Furthermore like in the experiments in DBW the exact time of the maximum concentration was shifted every night. At the first night the maximum was reached at 4 am with a second maximum at 6 am. At the second night the maximum was reached at 7 am and at about 8 am at the last day of measurement. Despite this the concentration pattern was similar. Comparing these three day measurements the result of the last day was outstanding. At the last day the methane peak was only half the amount of the two days before. The reason for this drastic reduction is quite a surprise. The third day of our measurements was the starting day of a four day traffic control campaign enacted by the Chinese government which we recorded by chance. Each day of this control 1.3 million cars were taken off from the roads of Beijing, a procedure to test the improvement of the air quality towards the Beijing Olympic Games 2008.

This observation induced the question of the influence of traffic on methane concentration in the atmosphere, and will be considered in chapter 5.6.

Regardless of a possible influence of the traffic to methane in the atmosphere the hypothesis of another methane source in the vicinity of DBW and CAU could not be excluded. The search for a potential emission source revealed a landfill approximately 6 km north-west of the CAU as well as 5.5 km west of DBW. Due to the fact that in linear distance between the university and the landfill hills with heights about 200 m were located, the direct flow was obstructed and modified. That was why there was no distinct correlation between the methane concentration at the CAU and the north-west wind direction but with north and north-east directions (see Figure 5.14). A map showing the locations of all measuring sites is presented in Figure 5.15. To obtain knowledge about the source strength a measuring campaign at the Liulitun landfill itself was carried out from the 3<sup>rd</sup> – 5<sup>th</sup> of September 2007 (see chapter 5.5.3).

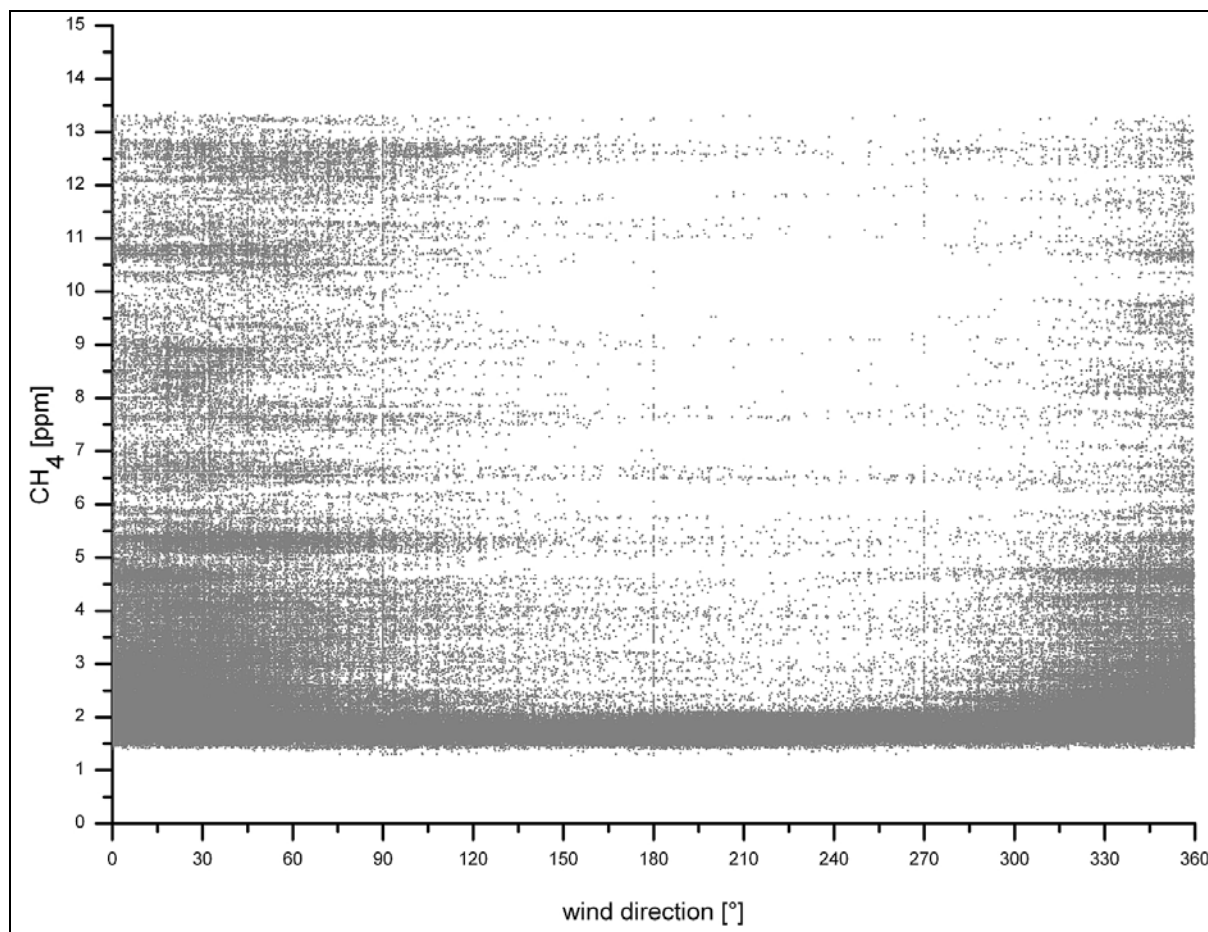


**Figure 5.14:** Correlation between methane concentration and wind direction measured on top of the China Agricultural University from the 14<sup>th</sup> – 17<sup>th</sup> of August 2007. All data with a wind speed below  $0.3 \text{ m s}^{-1}$  were omitted.



**Figure 5.15:** Overview of the measuring sites DBW, CAU, Liulitun landfill, Beijing University and Shang Zhuang for ambient air methane measurements. Image provided by Google Earth.

### 5.5.3 Measurements of Methane at the Liulitun Landfill

According to Pokhrel landfills produce in general following gases [Pokhrel et al. 2005]:

- Methane
- Carbon dioxide
- Carbon monoxide
- Nitrogen
- Hydrogen sulfide
- Ammonia

The percentage of the greenhouse gases methane and carbon dioxide on the total emitted landfill gas range from 40 – 60%.

The Liulitun landfill was a sanitary landfill for municipal solid waste (MSW). It covered an area of about 50 ha with a depth of excavation of about 22 m. Its operation started in 2002 and had the capacity of processing 2500 t of waste per day. One part of the landfill was already filled with waste and therefore covered with a plastic foil to stop gaseous emissions to the atmosphere. The gas was collected and pumped via pipes to a chimney where it was burned.

The other part of the landfill was still in use for storing waste and will be filled within the next four to five years. According to some online newspaper articles there were ten communities within a radius of 6 km around the landfill. The closest one was less than 300 m away. Many residents complained about a strong odor emanating from the landfill site especially during summertime. The governmental plan of constructing a waste incinerator plant at the landfill caused protests among the residents. In June 2007 its construction was suspended by Chinas State Environmental Protection Agency (SEPA) [China.org 2007; Sinofile 2007].

In 2006 Li studied the air quality at several MSW logistic facilities in Beijing. The Liulitun landfill was included in this study but methane emissions were not analyzed. At that landfill only the amount of totally suspended particles exceeded with  $1 \text{ mg m}^{-3}$  (24 hour average) the Chinese National Criteria for Standards of Environmental Air Quality of  $0.3 \text{ mg m}^{-3}$  totally suspended particles (24 hour average) [Li et al. 2007]. According to Xiao the proportion of organic substances and the calorific value of the MSW increased in Beijing from the year 1990 to 2003 leading to an increasing organic carbon content of the MSW and therefore to higher methane emissions [Xiao et al. 2007].

A satellite image of the landfill including the position of the TDL-PA device during the measurements on the landfill is shown in Figure 5.16. In that Figure the already filled as well as the still in use parts of the landfill can be seen.



**Figure 5.16:** Overview of the Liulutun landfill and the position of the TDL-PA system. Image provided by Google Earth.

The measurement was conducted from the 3<sup>rd</sup> – 5<sup>th</sup> of September 2007. The ultrasonic anemometer was placed on the plastic foil at the north-east corner of the landfill. A 20 m long Teflon tube led the sampling air to a container where the TDL-PA system was located. At both ends of the tube air filters were connected. For the first three hours the sampling rate was set to 2 Hz and changed to 4 Hz afterwards. The airflow was adjusted to  $0.5 \text{ l min}^{-1}$ . The result of the measurement is presented in Figure 5.17.

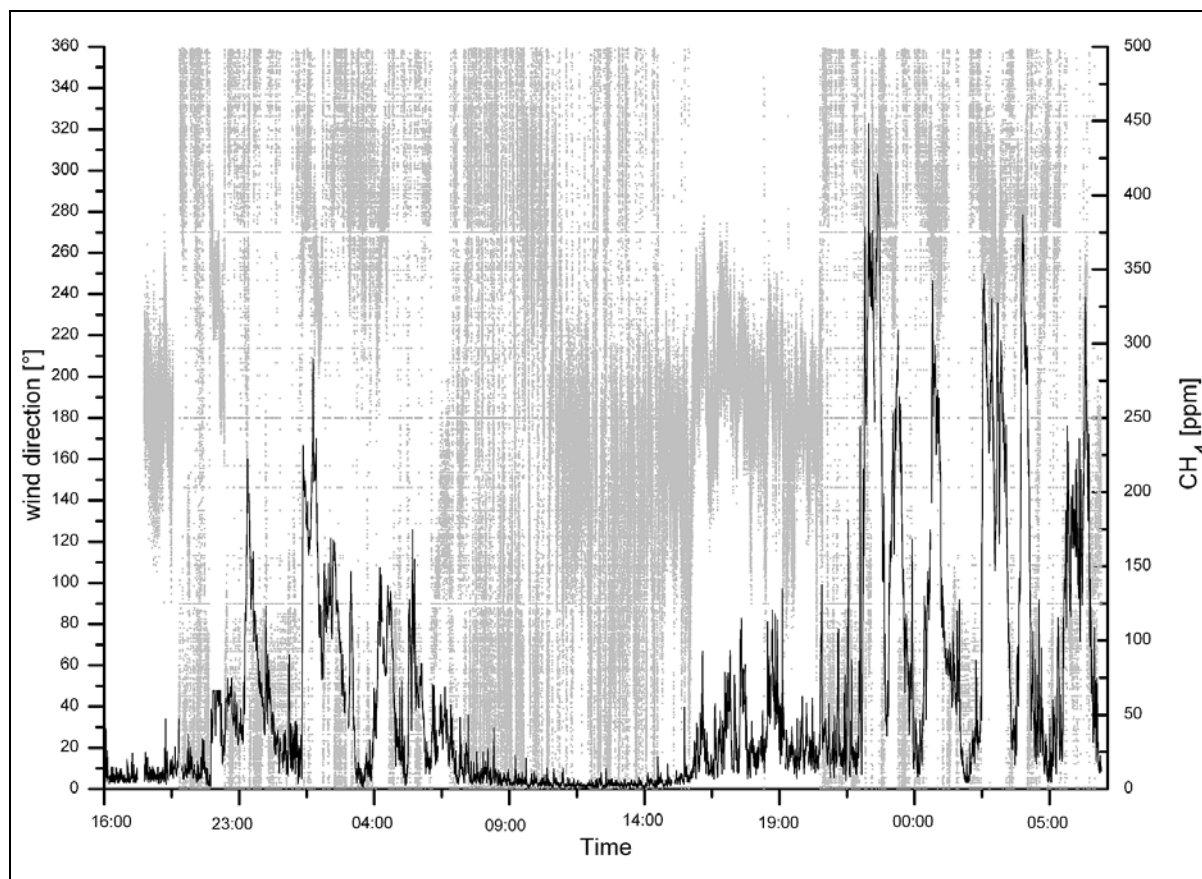


**Figure 5.17:** Measurement of methane concentration (black) and wind direction (gray) at the Liulitun landfill from the 3<sup>rd</sup> – 5<sup>th</sup> of September 2007.

The methane emission at the landfill showed a diurnal pattern. Compared to the concentrations measured at DBW and the CAU, respectively, it was five to thirty times higher. During daytime the concentration remained stable at about 10 ppm but in course of the evening and night it fluctuated between 25 and 450 ppm. The elevated daytime concentration confirmed that methane emission had taken place during the whole day but accumulation occurred only during nighttime due to the stable boundary layer. Moreover it can be seen that methane was emitted in plumes and transported away by eddies. Especially during both nights a pungent odor was observed by the author at some places of the landfill, supporting the plume hypothesis. Although it was said that the produced gas was collected and burned at the landfill site, still high amounts of methane were emitted to the atmosphere.

The methane concentration showed a good correlation with western wind directions where the waste was nowadays deposited (see Figure 5.18).

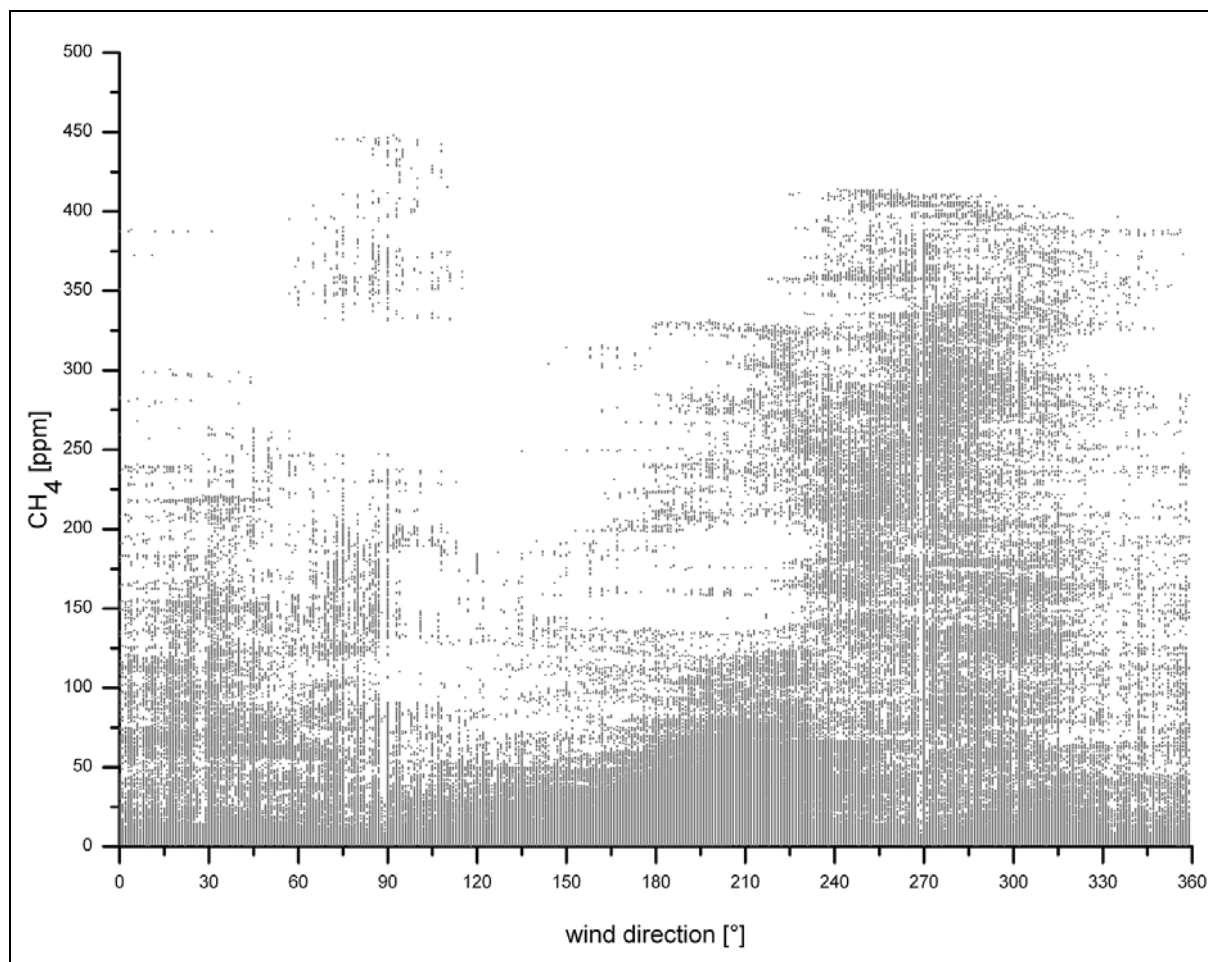


**Figure 5.18:** Correlation between methane concentration detected by the TDL-PA system and wind direction measured at the Liulitun landfill from the 3<sup>rd</sup> – 5<sup>th</sup> of September 2007. All data with a wind speed below  $0.3 \text{ m s}^{-1}$  were omitted.

For comparison purposes between the methane emissions from the landfill detected by the TDL-PA system and the ambient air concentration at DBW the GC in the container at DBW was adjusted to ambient air methane measurements. The sampling air was taken on top of the container and led to the GC. Thus, three minute mean values of the methane concentration were obtained and compared with the landfill data (see Figure 5.19). The GC data were provided by the Chinese counterparts.

It can clearly be seen that the methane concentration pattern at DBW was correlated with the methane emissions from the landfill. During the first night emissions occurred with maximum values ranged from 250 to 300 ppm at the landfill, leading to concentrations of about 6.5 ppm at DBW. The time shift between these two events was about three hours. Taking this time shift and the distance of 5.5 km between both sites into consideration a mean wind speed of  $0.5 \text{ m s}^{-1}$  was calculated. This was in good agreement with the wind speed data shown in Figure 5.19 obtained by the ultrasonic anemometer. The same conclusion corresponded to the

second night where higher methane emissions led to higher ambient air methane concentrations in DBW.

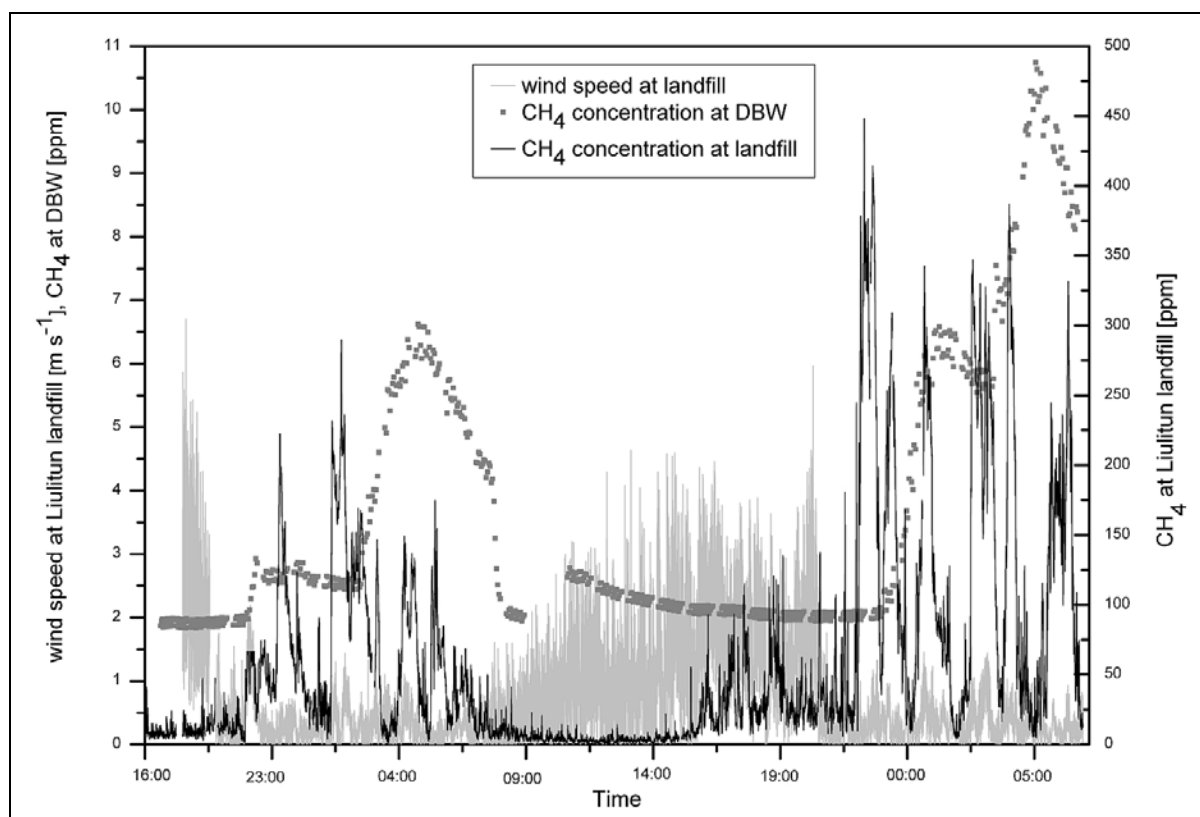


**Figure 5.19:** Comparison of methane concentration measured with TDL-PA and wind speed at Liulitun landfill and methane concentration measured with GC at Dongbeiwang from the 3<sup>rd</sup> – 5<sup>th</sup> of September 2007.

Another three day measurement was conducted at the campus of the Beijing University, which was in greater distance from the landfill. Due to the measuring site on top of a building the ultrasonic anemometer could not be used.

#### 5.5.4 Measurements of Methane at the Campus of the Beijing University

The measurements at the campus of the Beijing University were conducted from the 5<sup>th</sup> – 8<sup>th</sup> of September 2007 following the Liulitun landfill field campaign. One end of a 20 m long Teflon tube was placed on top of a building at the university approximately 20 m above ground the other end was led to the TDL-PA system inside of the building. To both ends of the tube air filters were attached. Data was collected with 2 Hz and the airflow was adjusted to 0.5 l min<sup>-1</sup>. Unfortunately the distance between the air intake and the TDL-PA unit was too long so that the ultrasonic anemometer could not be used. Therefore, only methane concentration data were available for the Beijing University measurement campaign.

For the purpose of comparison, methane concentrations were measured at DBW with the GC simultaneously (GC data provided by the Chinese counterparts). The Beijing University was located about 10.5 km south-east of the Liulitun landfill and 7 km south of DBW (see Figure 5.15). A main road was located 200 m east and the fourth ring road 500 m south of the university.

The obtained methane concentrations at Beijing University and DBW are shown in Figure 5.20.

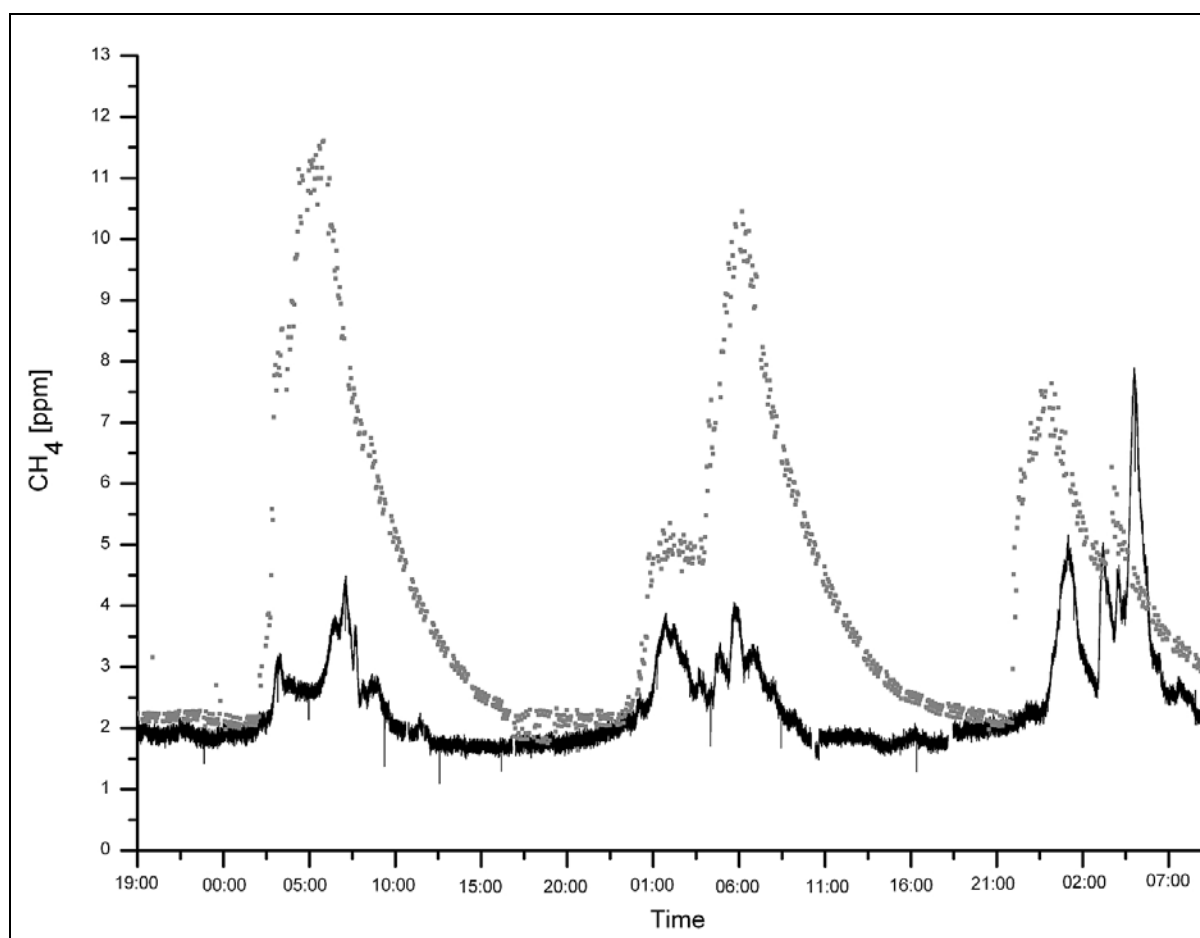


**Figure 5.20:** Comparison of methane concentration measured with TDL-PA at Beijing University (black) and methane concentration measured with GC at Dongbeiwang (gray) from the 5<sup>th</sup> – 8<sup>th</sup> of September 2007.

During the first seven hours of measurement the methane concentrations at Beijing University and DBW were at the same level. A concentration increase at 2:30 am at both locations was observable but it was two and a half times higher at DBW (11.5 ppm) compared to the Beijing University (4.5 ppm). Moreover it took about six hours longer for the methane concentration to decrease to levels of 2 ppm during daytime at DBW than at the Beijing University. There was a similar result for the second night with slightly lower maximum concentrations at both locations. The data from DBW showed a plateau lasting three hours before the concentration

increase continued. During the time of the plateau the data at the Beijing University reached a peak in methane concentration with a steady decrease afterwards. At the end of the plateau the concentration at the Beijing University rose again until the maximum of 4 ppm was reached. At the same time the maximum of 10.5 ppm was obtained at DBW. The situation changed during the last night. DBW and Beijing University reached the same maximum concentration of about 8 ppm but there was a time difference of about six hours between the maxima. Moreover the concentration pattern was reversed, showing the lowest methane concentrations of all three nights at DBW while it was the highest concentration at the Beijing University.

One possible explanation for this phenomenon could be lower methane emissions at the Liulitun landfill resulting in lower methane concentrations in the surrounding area. During the field campaign at the landfill this behavior was shown for DBW (see Figure 5.19). Due to the lack of data about wind direction as well as wind speed and methane emission data from the landfill this hypothesis could not be confirmed. An argument against this hypothesis was that the methane concentration at the Beijing University was highest at the same time.

Another possible explanation could be a local methane emission source near the Beijing University. As mentioned above there were two main roads adjacent to the university. Maybe methane emissions from cars and trucks were recorded because freight vehicles were only allowed to drive through Beijing between midnight and 6 am. Normally these trucks were not equipped with a diesel catalytic converter leading to higher methane concentrations (see also chapter 5.6).

Because of the lack of wind data none of the two hypothesis could be excluded so presumably both arguments combined led to these methane emission patterns. To check methane emissions from cars a pilot study with the TDL-PA system and a passenger car equipped with a catalytic converter was carried out in Germany. Details and results are given in chapter 5.6.1.

### **5.5.5 Measurements of Methane at the Shang Zhuang Experimental Field Station**

As already mentioned above the experimental field station DBW was abandoned in October 2007 due to the spreading of Beijing county area. Shang Zhuang was the new experimental field station of the CAU. This station was located 15 km north-west of the CAU and about 9.5 km north-west of the Liulitun landfill (see Figure 5.15). Shang Zhuang was surrounded by

arable land as well as by small houses, respectively. A further test of ambient air methane concentration was done at Shang Zhuang from the 29<sup>th</sup> of September to the 2<sup>nd</sup> of October 2007 using the TDL-PA system without an ultrasonic anemometer. The device was in a house of the experimental station with a 20 m long Teflon tube led outside. The air was sucked at a height approximately 4 m above ground through the TDL-PA unit with a sampling rate of 2 Hz. Unfortunately due to problems with the headphone cable connecting the laptop and the electronic box the obtained methane concentrations were too low. Only after the exchange of the cable the data seemed to be correct. Then nearly all the time the concentration fluctuated about 2 ppm except a 3 ppm peak at 8 pm one evening.

The results showed no influence of the landfill or other methane emission sources but more research would be necessary to obtain reliable concentration data.

## 5.6 Methane Emissions from Cars

The hypothesis of methane being emitted by cars contributing to the elevated concentration levels in Beijing made necessary a study of scientific papers dealing with that topic. There were several researchers who conducted studies of the methane emissions from cars. The applied measurement techniques were diverse and contained:

- Chemical ionization mass spectrometry
- Tunable infrared laser differential absorption spectroscopy
- Fourier transform infrared spectroscopy
- Gas chromatography with flame ionization detection
- Diode laser photoacoustic detection
- Tunable diode laser absorption spectroscopy

Experiments were conducted on the one hand using only the engine in the laboratory while on the other hand tailpipe measurements with chassis dynamometer test benches or cars driving on the streets were done. Moreover due to the applied measurement technique the exhaust emissions were either collected in bags or analyzed directly. During all studies methane was detected but the amount of the emission fluctuated.

During the starting phase of a car high methane concentrations had been observed. These so called cold start emissions were the most important source for traffic-related hydrocarbon emissions [Heeb et al. 2003]. Heeb discovered that with the prolonged use of the motor of a vehicle its emissions of methane increased. By comparing cars without exhaust gas after-treatment (EURO-0, model year 1984 – 1986) with several catalyst vehicles (EURO-1 – 3, model year 1991 – 2001) clear improvements at cold start as well as hot engine conditions were observed. For cars without a catalyst about 80% of the methane cold start emissions were released in the first 76 seconds or 0.49 km of driving. For these cars the cold start duration corresponded to the time period in which the engine was operated under choke conditions. The cold start of catalyst vehicles was limited by the time needed for catalyst light-off [Heeb et al. 2003]. Due to the fact that methane was not present in gasoline it must be formed during the combustion process. Moreover it was expected that methane was stored in the thin gasoline film covering the cold walls of the combustion chamber or other parts of the engine and the tailpipe system. It was then released very fast from these cold engine walls [Heeb et al. 2003]. Cihelka used a car without catalytic converter (Tatra 613-3, manufactured

1989) and observed cold start methane concentrations of about 125 ppm but the concentration increased to about 800 ppm under warm motor conditions [Cihelka et al. 2005]. Gerard discovered an abrupt methane peak in the range of several hundred ppm while starting the engine fueled with unleaded gasoline with an octane rating of 95 [Gerard et al. 2007]. Due to the air-fuel mixture being rich in fuel and unburned hydrocarbons, methane was present in the exhaust. After a few seconds a rapid decrease in methane concentration was observed as the combustion was close to complete. During the experiment the air-fuel ratio was varied leading to an increase of methane as the ratio became richer. Unfortunately the methane concentration during decreasing as well as increasing of the throttle could not be detected due to the relatively high detection limit of 90 ppm [Gerard et al. 2007]. The same effect of increasing methane emissions due to richer air-fuel ratios was found out by Zervas. During operation of a diesel engine concentrations ranged from 2 to 4.6 ppm [Zervas et al. 2001]. The effect of operating age of a three-way catalytic converter on methane emissions was studied by Takigawa [Takigawa et al. 2005]. A maximum methane concentration of about 150 ppm was discovered in the exhaust using a converter with 78,000 km use. This was 1.5 times that for a new converter. In addition it was found out that the methane concentration to total hydrocarbon increased with increasing vehicle speed. While increasing the vehicle speed from 5 to 50 km h<sup>-1</sup> a reduction in methane concentration was observed for a new catalytic converter (70 ppm – 50 ppm) whereas the old converter released more methane (70 ppm – 100 ppm). Methane emission from the fuel of regular grade was 1.5 times higher than that of premium grade. [Takigawa et al. 2005]. In contrast to that no higher methane emissions were detected for diesel engines with increasing age of operation [Bikas et al. 2007]. By comparing cold start emissions at different ambient air temperatures Weilenmann observed that the ambient temperature had a significantly larger influence on cold start emissions than the driving style [Weilenmann et al. 2005].

The methane emissions of compressed natural gas (CNG) buses were studied by Herndon using a chase vehicle. It was shown that CNG powered buses emit considerable levels of methane per carbon dioxide as compared to diesel buses. Additionally events of elevated levels of methane without concomitant carbon dioxide were observed for 3 – 8 seconds. This was explained with the propensity for CNG buses to “backfire” [Herndon et al. 2005]. The total contribution of mobile source methane to the global burden was estimated by Nam to be 0.3 – 0.4%. Moreover Nam found out that CNG fueled vehicles had greater methane emissions than gasoline fueled vehicles [Nam et al. 2004].

Because of the huge differences of the amount of methane emissions studied by the above mentioned researches an own pilot study with the TDL-PA system and a passenger car was carried out in Germany. The aim was on the one hand to check whether the TDL-PA device was suitable for such measurements and on the other hand to detect methane emissions from that car while the engine was operated under different conditions (see chapter 5.6.1).

### 5.6.1 Measurements of Methane by the Tunable Diode Laser Photoacoustic Device

To check methane emissions from cars a pilot study with the TDL-PA system was carried out in Germany. For that purpose a 20 m long Teflon tube was connected to the tailpipe of a parked passenger car (Opel Corsa C, manufactured 2004, EURO-4) fueled with unleaded gasoline with an octane rate of 95. The exhaust gases were sucked through the TDL-PA unit with a flow rate of  $0.5 \text{ l min}^{-1}$ . The sampling rate was set to 2 Hz. Engine idle as well as 2000 rounds per minute were tested. The results are shown in Figure 5.21.

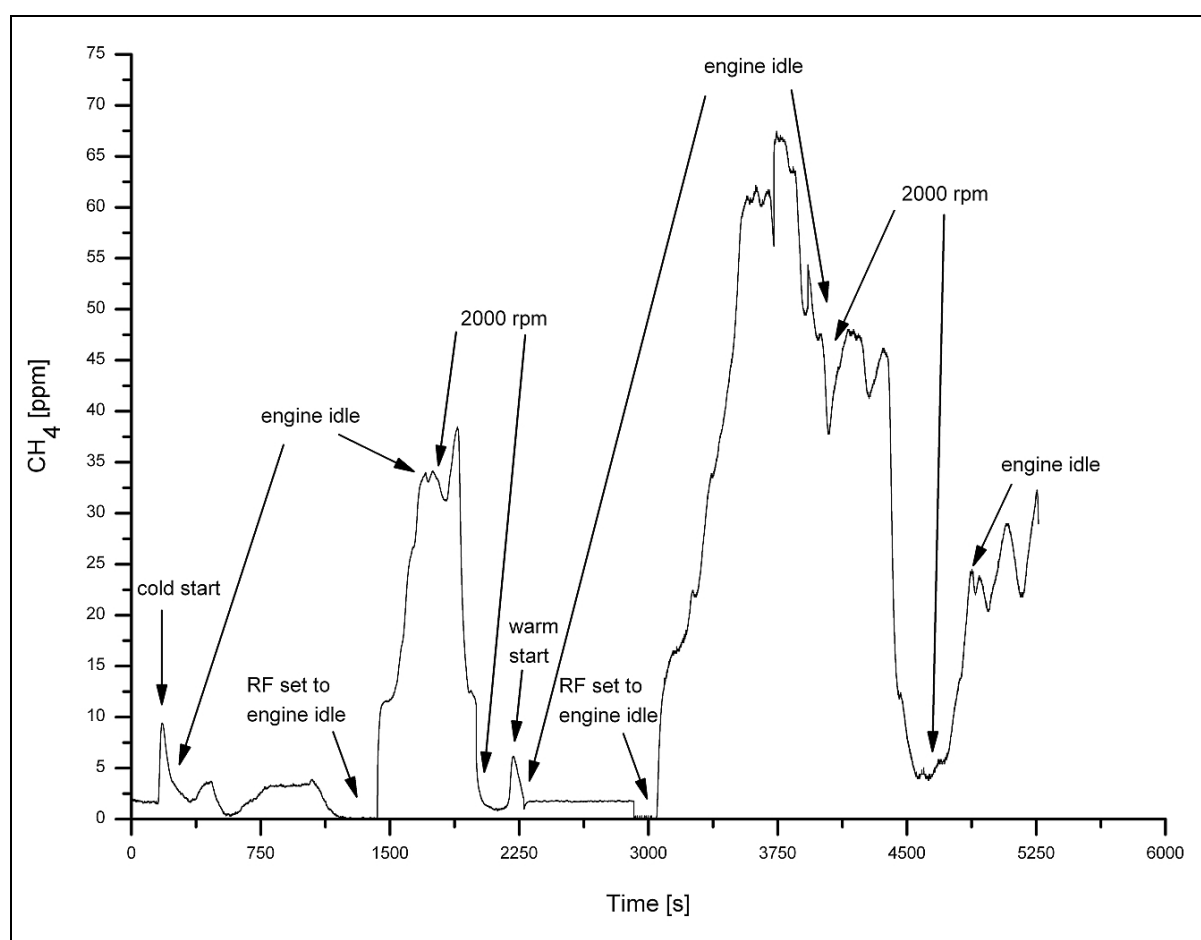


**Figure 5.21:** Methane emissions from a car measured with TDL-PA system. Resonance frequency (RF) was set according to engine idle condition. As noted the engine was rev up to 2000 rounds per minute (2000 rpm).

As described in chapter 4.2.5 the resonance frequency was dependent on temperature, humidity and atmospheric composition and must be checked before and during measurements. The TDL-PA measurement was started using the ambient air resonance frequency of about 6700 Hz. It can be seen in Figure 5.21 that directly after starting of the car the methane concentration sharply increased showing a cold start emission effect. Then the atmospheric composition of the sampling air changed and so did the resonance frequency leading to a decrease of the signal. After checking the resonance frequency again it was set to the new maximum of about 6600 Hz for the engine idle condition. Instantaneous the PA signal rose and methane concentration up to levels of about 35 ppm were detected. The engine was rev up to 2000 rounds per minute leading to an increase in methane concentration on the one hand as well as to a shift of the resonance frequency on the other hand. The new maximum frequency was about 6550 Hz for 2000 rounds per minute. The methane concentration was now at ambient levels while the engine was still at 2000 rounds per minute. The engine was turned off and started again showing a warm start methane peak. After idle operating of the engine and adaptation of the resonance frequency methane concentrations as high as 65 ppm were observed. Another rev up of the engine showed the same pattern as before.

It was assumed that the catalytic converter was fully functional only if the engine was operated under load due to increased temperature of the engine. If the engine was idle for some time high methane emissions occurred. Unfortunately it was not possible to follow the methane emissions with the TDL-PA system according to the shifted resonance frequency. Especially the cold start emissions were suspected to be a lot higher than measured in this study.

Taking into consideration that most of the cars, especially the freight vehicles, in Beijing were not equipped with a catalytic converter they could be considered as a strong methane emission source. This hypothesis correlated well with the lower methane concentration data obtained at the CAU during the traffic control campaign (see chapter 5.5.2 and Figure 5.12). To verify this hypothesis further research on this topic should be conducted.

## 5.7 Ammonia Emission Measurements

As already mentioned in chapter 4.5.1 there had been some problems using the TDL-PA detection system for ammonia emission measurements. The calibration of the device with certified gas mixtures and two-stage valves yielded a detection limit of 111 ppb (see Figure 4.9). It was necessary to purge the system several times with nitrogen to get rid of water vapor as well as of residual ammonia, respectively. By keeping the relative humidity of the gas as low as possible (usually 0.1%) after passing through the PA unit it was verified that the calibration was not biased by the adsorption of ammonia.

For application of the TDL-PA system in DBW an open dynamic chamber was designed and constructed by the Chinese counterparts. Unfortunately the Plexiglas available in China was of poor quality and durability. Its thickness was only 3 mm, compared to 8 mm of the hoods manufactured in Germany for the closed chambers. That was why the open dynamic chamber was mechanically instable and leaky. After some weeks the open dynamic chamber was broken due to flexing of the panels. Moreover there was no pump available in DBW with sufficient pumping capacity of about  $100 \text{ l min}^{-1}$  to guarantee that ammonia was not consumed inside of the chamber.

That was why the already existing as well as the newly built closed chambers, respectively, were used for ammonia measurements. During closure of the old chambers the relative humidity inside of them increased rapidly. Although the sampling air was passing two Nafion dryers before entering the PA unit the relative humidity at the gas outlet of the box was higher than 40%. This led to adsorption of emitted ammonia inside of the chambers on the one hand while on the other hand residual ammonia inside of the tubes and the TDL-PA system was released. A release of residual ammonia after checking the calibration with a certified gas mixture of 5 ppm  $\text{NH}_3$  in  $\text{N}_2$  is shown in Figure 5.22. The system was purged with nitrogen for more than one hour before closure of the chamber for 60 minutes and starting of the measurement. As can be seen there was still some ammonia available that was released by the humid sampling air.

All other ammonia data obtained by applying the closed chambers as well as measuring ambient air concentrations were below the detection limit of the TDL-PA system.

Hence no ammonia emissions could be verified during this work.

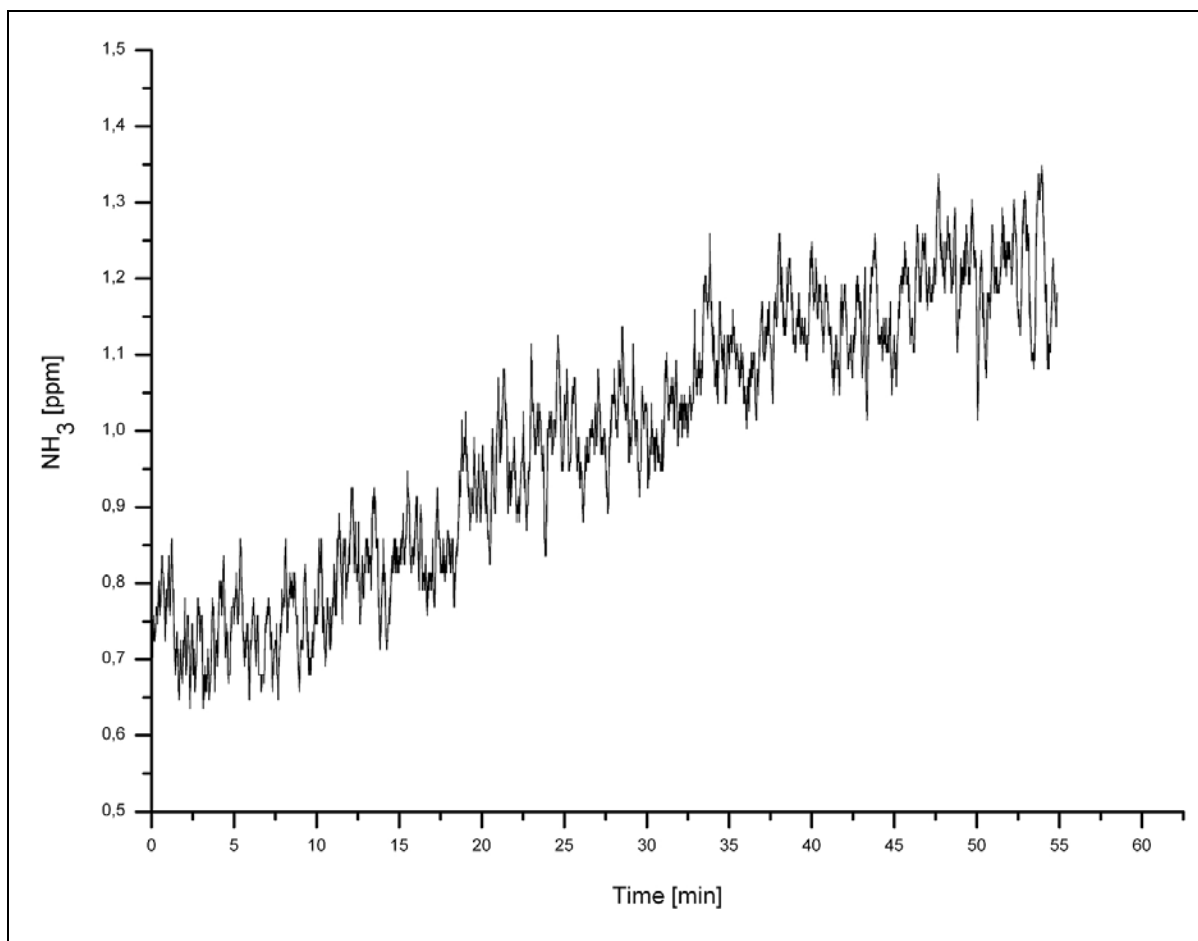


**Figure 5.22:** Release of residual ammonia inside of the tubes and TDL-PA system after applying 5 ppm NH<sub>3</sub> in N<sub>2</sub>. The system was purged with N<sub>2</sub> for about one hour and the chamber measurement started afterwards.

It is necessary to further improve the detection limit of the TDL-PA system to measure ambient air ammonia concentrations. This could be achieved by replacing the laser diode with a higher powered one or with a laser diode emitting at wavelengths with higher absorptivity of ammonia. At the time of construction of the TDL-PA system no such laser diodes were commercially available. Another improvement regarding the design as well as the construction of the open dynamic chambers would be the use of thicker and more durable Plexiglas. To remove the water vapor from the sampling air a drying agent that do not lead to adsorption of ammonia could be applied. By implementing all these suggestions a reliable system for ammonia measurements would be available.

## 6 Summary and Outlook

The present thesis was conducted at the Institute of Physics and Meteorology at the University of Hohenheim within the scope of the International Research Training Group “Modeling Material Flows and Production Systems for Sustainable Resource Use in Intensified Crop Production in the North China Plain”. The project is a cooperation between the University of Hohenheim and the China Agricultural University (CAU) in Beijing, China, financed by the German Research Foundation as well as the Chinese Ministry of Education, respectively. One aim of the project is to study the exchange of climate relevant trace gases between arable cultivated soils and the atmosphere in the North China Plain. For that purpose mobile, robust and sensitive measuring devices are needed.

Two devices that meet these demands are presented in this thesis. They are based on Tunable Diode Laser Photoacoustic Spectroscopy (TDL-PAS) and were developed in the working group “Spectroscopy”. These devices are capable of real-time in situ detection of trace gases. For methane a detection limit of 85 ppb and for ammonia of 111 ppb was achieved, respectively. For the field campaign at the experimental field Dongbeiwang (DBW) in Beijing it was necessary to optimize the instruments due to the harsh conditions in China, e.g. high variation in temperature, high humidity and particulate matter emissions. This included accurate thermally stabilization of the system as well as long-term stability of the laser diode and the possibility of unattended operation over a period of several days. These prerequisites were fulfilled and evaluated in Germany before the devices were brought to China for the field campaign in the years 2006 and 2007. Additionally, mobile closed chambers for the trace gas exchange measurements were designed in Germany. They consisted of two parts: One frame installed permanently in the soil, therein agricultural crops could be planted, and a hood placed on it during the measurement and removed afterwards again. Altogether seven frames made from stainless steel were constructed by a company located in Beijing. Three hoods of different heights (250, 500 and 1000 mm) were made from 8 mm colorless Plexiglas and were built by a German company. The innovation of this design was the possibility to insert up to eight cooling packs that cooled down the enclosed air in the chambers by mixing it via two fans. By comparing measurements with and without applying cooling packs it was shown that the temperature difference between both situations was increasing up to 10 K. According to ambient air temperature measurements the test also showed that by applying cooling packs the temperature of the enclosed air could be adapted close to ambient

conditions. After installation of the closed chambers in DBW a test checking the gas tightness had to be performed. With this test leakages of the frames, hoods and tubes should be discovered. This was done by injection of 2 ml ethane into the closed chambers and studying the concentration decrease within one hour of closure time. For this test the permanently installed gas chromatograph in the measurement container in DBW was used, connected by Teflon tubes to the closed chambers. All closed chambers showed leakages lower than 10% and therefore could be considered as tight.

The planting and irrigation scheme of the main field experiment was adopted to make a statement about the soil-atmosphere exchange of methane of the main field experiment. For that purpose winter wheat and summer maize were planted in October 2006 and June 2007, respectively. Due to the lack of adequate precipitation winter wheat had to be irrigated by flooding (border irrigation). Summer maize had to be irrigated only directly after fertilizing. Two fertilization schemes were applied which differed on the amount of N-fertilizer used. One scheme was the farmers practice applying  $100 \text{ kg N ha}^{-1}$  and the other scheme was a reduced input of  $50 \text{ kg N ha}^{-1}$ . Both schemes were used for the closed chamber measurements so that six of the frames were planted with winter wheat and summer maize, respectively, while one frame contained only bare soil as control plot.

For methane measurements the chambers were operated in the dynamic mode, so the air inside of the chamber was circulated through the TDL-PA system and pumped back into the chamber. The increase or decrease in methane concentration with time was determined and flux rates were calculated. The obtained data confirmed that the soil in DBW, a Calcic Cambisol according to FAO classification, could be considered as a methane sink. The exchange rate ranged from  $-0.17$  to  $-3.33 \text{ mg CH}_4\text{-C m}^{-2} \text{ d}^{-1}$  for winter wheat and from  $-0.68$  to  $-2.07 \text{ mg CH}_4\text{-C m}^{-2} \text{ d}^{-1}$  for bare soil. For summer maize the exchange rate was slightly lower and ranged from  $-0.51$  to  $-1.0 \text{ mg CH}_4\text{-C m}^{-2} \text{ d}^{-1}$  and from  $-0.53$  to  $-1.14 \text{ mg CH}_4\text{-C m}^{-2} \text{ d}^{-1}$  for the control plot.

Due to the fact that elevated methane concentrations at daybreak were detected during the exchange measurements at the plots planted with winter wheat as well as at the control plot a diurnal variation in methane concentration was assumed. To verify and quantify this diurnal variation in methane concentration at DBW, one plot was selected for a 24 hour measurement campaign. During this measurement campaign ambient air methane concentrations of up to 22 ppm were observed during nighttime, which was elevenfold the normal concentration.

Because the previous exchange measurements revealed that methane was not emitted by the soil it must have originated from somewhere else. After the 24-hour measurement campaign the ambient air methane concentrations in DBW as well as at other places in the vicinity of DBW were studied to detect the source of the methane emissions. For that purpose an ultrasonic anemometer for wind direction and wind speed measurement was combined with the TDL-PA system. A diurnal variation with maximum methane concentrations of about 40 ppm during nighttime and early morning and minimum concentrations of about 1.4 ppm during the afternoon were detected in DBW. Research conducted at the campus of the CAU, 3.2 km south of DBW, showed a similar pattern. These results confirmed the urban heat island effect where stable atmospheric layering dominates during the night and a mixing layer dominates during daytime. According to literature the height of this atmospheric boundary layer in Beijing in autumn was of 1 km thickness during daytime and of 200–400 m during nighttime [Zhang et al. 2006]. Moreover the high methane concentrations in the night verified the assumption of a methane emission source in the vicinity of DBW and the CAU. The search for a potential emission source revealed a landfill approximately 6 km north-west of the CAU as well as 5.5 km west of DBW. Measurements conducted at the landfill site itself showed a diurnal methane emission pattern as well, with maximum concentrations up to 450 ppm during nighttime and minimum concentrations of about 10 ppm during daytime.

The first day of a four-day traffic control campaign enacted by the Chinese government was by chance recorded during the CAU measurements of ambient methane concentrations. Each day of this control 1.3 million cars were taken off from the roads of Beijing, a procedure to test the improvement of the air quality towards the Beijing Olympic Games 2008. The methane concentration peak of 7 ppm was only half the amount of the former two days.

Several working groups showed that methane was emitted by cars but the amount depended on the type and age of the installed catalytic converter. To check methane emissions from cars a pilot study with the TDL-PA system was carried out in Germany. For that purpose a Teflon tube was connected to the tailpipe of a parked passenger car (Opel Corsa C, manufactured 2004, EURO-4) fueled with unleaded gasoline with an octane rate of 95. Methane emissions of about 65 ppm during engine idle operation were detected. Unfortunately it was not possible to continuously measure the concentration while revving the engine due to a shifted resonance frequency because of a change in the composition of the exhaust gas and hence of the resonance frequency of the TDL-PA system. It was assumed that the catalytic converter is

fully functional of oxidizing methane only if the engine is operated under load due to increased temperature of the engine and thus of the catalytic converter.

Taking into consideration that in China especially the freight vehicles were not equipped with a catalytic converter and were only allowed to drive through Beijing from midnight to 6 am they could be considered as a strong methane emission source. To verify this hypothesis further research on the methane emission by cars should be conducted.

For ammonia measurements with the TDL-PA system an open dynamic chamber was designed and constructed by the Chinese counterparts. Unfortunately the Plexiglas available in China was of poor quality and durability. That was why the open dynamic chamber was mechanically instable and leaky and could not be used for measurements. Therefore, ammonia emission measurements were conducted by using the closed dynamic chambers but the obtained data were below the detection limit of 111 ppb. Furthermore the humidity of the sampling air led to adsorption of ammonia inside of the tubes and the TDL-PA system although two Nafion dryers were interconnected. This residual ammonia was then sometimes released and biased the measurements.

The suitability of long-term real-time in situ measurements of methane was demonstrated in the present thesis. Moreover the range of application of this TDL-PA system was not only limited to soil-atmosphere exchange studies but also ambient methane concentrations as well as car exhaust measurements were realizable.

Other trace gases like nitrous oxide and carbon dioxide can be studied by using the same TDL-PA system if a suitable laser diode for the detection of the trace gas of interest are available.

For ammonia measurements with the TDL-PA system it would be necessary to further improve the detection limit. This could be achieved by replacing the laser diode with a higher powered one or with a laser diode emitting at wavelengths with higher absorptivity of ammonia. At the time of construction of the TDL-PA system no such laser diodes were commercially available. Another improvement regarding the design as well as the construction of the open dynamic chambers would be the use of thicker and more durable Plexiglas. To remove the water vapor from the sampling air a drying agent that do not lead to adsorption of ammonia could be applied. By implementing all these suggestions a reliable system for ammonia measurements would be available too.

## 7 Zusammenfassung und Ausblick

Die vorliegende Arbeit wurde am Institut für Physik und Meteorologie der Universität Hohenheim im Rahmen des Internationalen Graduiertenkollegs „Modellierung von Stoffflüssen und Produktionssystemen für eine nachhaltige Ressourcennutzung in intensiven Acker- und Gemüsebausystemen in der Nordchinesischen Tiefebene“ erstellt. Das Projekt ist eine Kooperation zwischen der Universität Hohenheim und der Chinesischen Agraruniversität (China Agricultural University, CAU) in Peking, China. Das Graduiertenkolleg wurde bilateral von der Deutschen Forschungsgemeinschaft sowie dem Chinesischen Bildungsministerium (Chinese Ministry of Education) finanziert. Ein Projektziel war die Untersuchung des klimarelevanten Treibhausgas austauschs zwischen landwirtschaftlich genutzten Böden und der Atmosphäre in der Nordchinesischen Tiefebene. Zu diesem Zweck wurden mobile, robuste und empfindliche Messgeräte benötigt.

Zwei Messgeräte, die diese Anforderungen erfüllen, werden in dieser Arbeit präsentiert. Sie basieren auf dem Prinzip der photoakustischen Spektroskopie mithilfe von Diodenlasern (Tunable Diode Laser Photoacoustic Spectroscopy, TDL-PAS) und wurden in der Arbeitsgruppe „Spektroskopie“ entwickelt. Die Geräte sind für in situ Echtzeitmessungen von Spurengasen geeignet. Nachweisgrenzen bei Methan von 85 ppb und bei Ammoniak von 111 ppb wurden erzielt. Für die Messkampagne auf dem Versuchsfeld Dongbeiwang (DBW) in Peking war es notwendig die Instrumente an die rauen Umweltbedingungen in China, wie zum Beispiel starke Temperaturschwankungen, hohe Luftfeuchtigkeit sowie große Feinstaubemissionen anzupassen. Dafür waren eine präzise Temperaturstabilisierung des Systems sowie eine Langzeitstabilität der verwendeten Laserdiode nötig. Ferner sollte die Möglichkeit eines mehrtägigen unbeaufsichtigten Betriebs gegeben sein. Nachdem diese Voraussetzungen in Deutschland erfüllt und verifiziert wurden, erfolgte der Transport der Geräte nach China. Im Rahmen einer Messkampagne in den Jahren 2006 und 2007 wurden in Peking Daten über den Spurengasaustausch erhoben. Des Weiteren sind in Deutschland mobile, geschlossene Kammern für die Spurengasmessungen entwickelt worden. Sie bestanden aus zwei Teilen: einem im Boden installierten Rahmen aus rostfreiem Edelstahl, in den verschiedene Ackerfrüchte gepflanzt werden konnten, sowie einer Plexiglashaube, die für einen definierten Zeitraum, gewöhnlich für 60 Minuten, auf dem Rahmen mittels Kistenschlössern befestigt und anschließend wieder entfernt wurde. Insgesamt wurden sieben Rahmen in China gebaut und in DBW installiert. Drei Hauben unterschiedlicher Höhe (250,

500 und 1000 mm) wurden aus 8 mm dickem, farblosem Plexiglas in Deutschland gebaut und ebenfalls nach China transportiert.

Die Innovation dieser Messkammern bestand aus der Möglichkeit, bis zu acht Kühllakkus im Rahmen zu befestigen, um den Temperaturanstieg der eingeschlossenen Luft zu minimieren. Zu diesem Zweck wurden zwei Ventilatoren verwendet, die für eine gleichmäßige Durchmischung der eingeschlossenen Luft sorgten. Vergleichsmessungen ergaben eine Reduktion des Temperaturanstiegs um bis zu 10 K bei Einsatz der Kühllakkus. Außerdem konnte die Temperatur der eingeschlossenen Luft mit Hilfe der Kühllakkus auf nahezu Umgebungstemperatur stabilisiert werden.

Nach der Installation der geschlossenen Kammern in DBW musste die Dichtigkeit überprüft werden. Mit Hilfe dieses Tests sollten Undichtigkeiten der Rahmen, Hauben und Schlauchleitungen aufgespürt werden. Zu diesem Zweck wurden in die geschlossenen Kammern 2 ml Ethan injiziert und die Konzentrationsabnahme innerhalb von 60 Minuten gemessen. Dazu wurde ein im Messcontainer in DBW stationär installierter Gas-Chromatograph genutzt, der mit Teflonschläuchen mit den geschlossenen Kammern verbunden wurde. Alle geschlossenen Kammern zeigten eine Ethanabnahme geringer als 10% und galten somit als dicht.

Bepflanzung, Düngung und Bewässerung der Rahmen wurden vom Hauptfeldversuch übernommen, um Aussagen über den Spurengasaustausch von Methan machen zu können. Dazu wurden sechs Rahmen im Oktober 2006 mit Winterweizen und im Juni 2007 mit Sommermais bepflanzt. Der siebte Rahmen diente als Kontrollfläche und blieb unbepflanzt. Aufgrund unzureichender Niederschläge musste der Winterweizen bewässert werden. Der Sommermais wurde nur direkt nach der Düngung bewässert. Diese unterschied sich in der Menge des ausgebrachten Stickstoffdüngers. Einerseits wurde „farmers practice“ mit  $100 \text{ kg N ha}^{-1}$ , andererseits „reduced input“ mit  $50 \text{ kg N ha}^{-1}$  angewandt.

Für die Methanmessungen wurde die dynamische Kammermethode angewandt, wobei die Methankonzentration in der geschlossenen Kammer kontinuierlich bestimmt wurde, indem das Gas mittels einer Pumpe aus der Haube heraus und durch das Messsystem im Umluftverfahren gepumpt wurde. Aus der Zu- oder Abnahme der Methankonzentration während der Kammerschließzeit konnten Austauschraten berechnet werden. Die ermittelten Daten ergaben, dass es sich bei dem Boden in DBW, einem „Calcaric Cambisol“ nach FAO Klassifikation, um eine Methansenke handelte. Die Austauschraten lagen zwischen  $-0,17$  und

$-3,33 \text{ mg CH}_4\text{-C m}^{-2} \text{ d}^{-1}$  bei Winterweizen und zwischen  $-0,68$  und  $-2,07 \text{ mg CH}_4\text{-C m}^{-2} \text{ d}^{-1}$  bei unbedecktem Boden. Die Austauschraten bei Sommermais waren etwas geringer und lagen zwischen  $-0,51$  und  $-1,0 \text{ mg CH}_4\text{-C m}^{-2} \text{ d}^{-1}$  sowie zwischen  $-0,53$  und  $-1,14 \text{ mg CH}_4\text{-C m}^{-2} \text{ d}^{-1}$  für die Kontrollfläche.

Während der Austauschmessungen wurden sowohl bei Winterweizen als auch bei der Kontrollfläche morgens erhöhte Methankonzentrationen gemessen. Deshalb wurde von einem Tagesgang der Methankonzentration ausgegangen, der während einer 24-Stunden-Messung in DBW untersucht wurde. Im Verlauf dieser Messung konnten nachts Methankonzentrationen in der Umgebungsluft von bis zu 22 ppm, dem elffachen der normalen Konzentration, nachgewiesen werden. Da während der vorangegangenen Messungen in DBW keine Methanemissionen aus dem Boden auftraten, wurde angenommen, dass das Methan aus einer anderen Quelle stammte. Nach diesem Ergebnis wurden Messungen der Umgebungskonzentration von Methan an anderen Orten in der Nähe von DBW durchgeführt, um die Methanquelle zu identifizieren. Zu diesem Zweck wurde ein Ultraschallanemometer zur Windrichtungs- und Windgeschwindigkeitsmessung mit dem TDL-PA System gekoppelt. So konnte während einer mehrtägigen Messung in DBW ein Methantagesgang mit nächtlichen Maximumkonzentrationen von bis zu 40 ppm und nachmittäglichen Minimumkonzentrationen von 1,4 ppm verifiziert werden. Eine Mehrtagesmessung auf dem Campus der CAU, 3,2 km südlich von DBW, lieferte ein ähnliches Resultat. Dies deutete auf einen Tagesgang der atmosphärischen Grenzschicht durch den Einfluss der städtischen Wärmeinsel hin. Nachts entsteht durch Temperaturinversion eine statisch stabile Luftschicht, die sich nach Sonnenaufgang durch turbulente Wärmetransporte von der Unterlage erwärmt und anschließend auflöst. Tagsüber entsteht eine Schicht mit guter Durchmischung, die sogenannte Mischungsschicht. Die Höhe dieser atmosphärischen Grenzschicht wurde für den Herbst in Peking von Zhang berechnet. Es zeigten sich Höhen von 1 km tagsüber und 200 – 400 m nachts [Zhang et al. 2006]. Durch die erhöhten nächtlichen Methankonzentrationen sowohl in DBW als auch an der CAU konnte belegt werden, dass sich eine Methanquelle in der näheren Umgebung der Messorte befinden musste. Eine Mülldeponie etwa 5,5 km westlich von DBW und 6 km nordwestlich der CAU konnte als Methanquelle identifiziert werden. Messungen auf der Deponie ergaben ebenfalls einen Tagesgang der Methankonzentrationen mit maximalen Emissionen von bis zu 450 ppm während der Nacht und Minimumkonzentration von 10 ppm tagsüber.

Während der Messkampagne an der CAU wurde zufällig der erste Tag einer viertägigen Verkehrsregulierung, veranlasst durch die Chinesische Regierung, aufgezeichnet. Während der Regulierung wurden täglich 1,3 Millionen Autos von den Straßen Pekings verbannt, um die Verbesserungen der Luftqualität im Hinblick auf die Olympischen Sommerspiele 2008 zu untersuchen. Mit einem Maximum von 7 ppm war die Methankonzentration an der CAU nur halb so hoch wie die beiden Tage zuvor.

Die Methanemissionen von Autos wurden von verschiedenen Wissenschaftlern untersucht und in mehreren Studien beschrieben. Die dabei ermittelten Konzentrationen hingen vom Alter der Katalysatoren sowie der Fahrgeschwindigkeit ab.

Eine eigene Untersuchung in Deutschland, wobei die Abgase vom Auspuff eines geparkten Autos (Opel Corsa C, Baujahr 2004, EURO-4) mit Hilfe eines Teflonschlauchs zum TDL-PA System geleitet wurden, ergaben Methanemissionen von bis zu 65 ppm im Leerlaufbetrieb. Kaltstartemissionen konnten zwar nachgewiesen aber nicht quantifiziert werden, da sich aufgrund einer Änderung der Zusammensetzung der Autoabgase im Laufe der Untersuchung die Resonanzfrequenz um mehrere hundert Hz änderte und so zu einer Verminderung des TDL-PA Signals führte. Dementsprechend konnte die Methankonzentration nicht kontinuierlich verfolgt werden. Bei Erhöhung der Drehzahl auf 2000 Umdrehungen pro Minute sanken die Emissionen auf nahezu 0 ppm ab, stiegen aber im anschließenden Leerlaufbetrieb wieder auf Werte um 65 ppm. Es wird vermutet, dass der Katalysator erst bei erhöhter Drehzahl des Motors eine ausreichend hohe Temperatur erreicht, um Methan zu oxidieren.

Unter der Annahme, dass die meisten Lastkraftwagen in Peking nicht mit einem Katalysator ausgestattet sind und nur zwischen Mitternacht und 6 Uhr morgens durch Peking fahren dürfen, könnten sie ebenfalls als Methanquelle in Betracht kommen. Um diese Hypothese zu verifizieren, sind allerdings weitere Untersuchungen notwendig.

Für Ammoniakmessungen mit dem TDL-PA System wurde von den Chinesischen Kollegen eine offene, dynamische Kammer entwickelt und gebaut. Leider war das in China verfügbare Plexiglas von minderer Qualität und Haltbarkeit, was zu mechanischer Instabilität und Undichtigkeit der dynamischen Kammer führte. Daher wurden Ammoniakmessungen mit den geschlossenen Kammern durchgeführt, doch die gemessenen Werte lagen nahezu ausschließlich unterhalb der Nachweisgrenze des TDL-PA Systems von 111 ppb. Darüber hinaus führte die hohe Feuchtigkeit der Probenluft zu Kondensation und somit zu Adsorption von Ammoniak in den Schläuchen und dem TDL-PA System. Selbst der Einsatz zweier

Nafion Messgastrockner brachte keine Besserung. Das im System verbliebene Ammoniak wurde zeitweise wieder gelöst und führte dadurch zu erhöhten Messwerten.

Die Tauglichkeit des TDL-PA Systems für längerfristige Echtzeitmessungen von Methan konnte in der vorliegenden Arbeit gezeigt werden. Außerdem zeigte sich, dass der Einsatzbereich des Systems nicht nur auf Austauschmessungen beschränkt ist, sondern sich auch Umgebungsmethankonzentrationsmessungen sowie Messungen von Autoabgasen realisieren lassen.

Mit demselben System könnten problemlos auch andere Spurengase, wie zum Beispiel Lachgas oder Kohlendioxid nachgewiesen werden, vorausgesetzt, passende Laserdioden sind verfügbar.

Für verlässliche Ammoniakmessungen mit Hilfe des TDL-PA Systems ist eine Verbesserung der Nachweisgrenze notwendig. Dies könnte einerseits durch den Einsatz leistungsstärkerer Laserdioden oder andererseits durch die Wahl einer anderen Ammoniakabsorptionslinie erreicht werden. Allerdings waren zu der Zeit der Konstruktion des TDL-PA Systems keine anderen Laserdioden kommerziell verfügbar. Eine weitere Verbesserung betrifft die offene, dynamische Kammer. Hier wäre der Einsatz von stabilerem, höherwertigem Plexiglas sinnvoll. Um Wasserdampf aus der Probenluft zu entfernen sollte ein Trockenmittel, welches die Probenluft trocknet und gleichzeitig die Adsorption von Ammoniak verhindert, angewandt werden. Nach Umsetzung all dieser Vorschläge stünde ein mobiles und verlässliches System für Ammoniakmessungen zur Verfügung.



## 8 References

- Adams, K. M. (1988).** "Real time in situ measurements of atmospheric optical absorption in the visible via photoacoustic spectroscopy. 1. Evaluation of photoacoustic cells." *Appl. Opt.* **27**(19): 4052.
- Asman, W. A. H., M. A. Sutton, et al. (1998).** "Ammonia: Emission, atmospheric transport and deposition." *New Phytologist* **139**(1): 27.
- Avramides, E. and T. F. Hunter (1981).** "Vibrational-translational/rotational and vibrational-vibrational processes in methane: photoacoustic measurements." *Chem. Phys.* **57**: 441.
- Beerling, D. J., Tom Gardiner, et al. (2008).** "Missing methane emissions from leaves of terrestrial plants." *Global Change Biology* **14**(8): 1821-1826.
- Bell, A. G. (1880).** "On The Production And Reproduction Of Sound." *American Journal of Science-Third Series* **XX**(118): 305-324.
- Bell, A. G. (1881).** "Upon the production of sound by radiant energy." *Phil. Mag. J. Sci.* **11**(5): 510-528.
- Bergamaschi, P., M. Schupp, et al. (1994).** "High-precision direct measurements of  $^{13}\text{CH}_4/^{12}\text{CH}_4$  and  $^{12}\text{CH}_3\text{D}/^{12}\text{CH}_4$  ratios in atmospheric methane sources by means of a long-path tunable diode laser absorption spectrometer." *Applied Optics* **33**(33): 7704.
- Besson, J. P., S. Schilt, et al. (2006a).** "Ammonia trace measurements at ppb level based on near-IR photoacoustic spectroscopy." *Applied Physics B: Lasers and Optics* **85**(2-3): 323.
- Besson, J. P., S. Schilt, et al. (2006b).** "Sub-ppm multi-gas photoacoustic sensor." *Spectrochimica Acta - Part A: Molecular and Biomolecular Spectroscopy* **63**(5): 899.
- Bijnen, F. G. C., F. J. M. Harren, et al. (1996).** "Intracavity CO laser photoacoustic trace gas detection: Cyclic CH<sub>4</sub>, H<sub>2</sub>O and CO<sub>2</sub> emission by cockroaches and scarab beetles." *APPLIED OPTICS* **35**(27): 5357-5368.
- Bikas, G. and E. Zervas (2007).** "Nonregulated pollutants emitted from Euro 3 diesel vehicles as a function of their mileage." *Energy and Fuels* **21**(5): 2731.
- Böning-Zilkens, M. I. (2004).** *Comparative Appraisal of Different Agronomic Strategies in a Winter Wheat - Summer Maize Double Cropping System in the North China Plain with Regard to Their Contribution to Sustainability.* Aachen, Shaker Verlag.
- Boreal-laser. (2007).** from <http://boreal-laser.com/products/gfspecs.htm>.
- Breuer, L., H. Papen, et al. (2000).** "N<sub>2</sub>O emission from tropical forest soils of Australia." *Journal of Geophysical Research D: Atmospheres* **105**(D21): 26353.
- China.org. (2007).** "<http://www.china.org.cn/english/China/221355.htm>." 2008.
- Chow, W. W., S. W. Koch, et al. (1997).** *Semiconductor-Laser Physics.* Berlin, Springer.

- Cihelka, J., V. Horka, et al. (2005).** *Diode laser photoacoustic detection of automobile exhaust emissions.* Proceedings of 2005 7th International Conference on Transparent Optical Networks, ICTON 2005.
- Civis, S., V. Horká, et al. (2005).** "Room-temperature diode laser photoacoustic spectroscopy near 2.3  $\mu\text{m}$ ." *Applied Physics B: Lasers and Optics* **81**(6): 857.
- Claps, R., F. V. Englich, et al. (2001).** "Ammonia detection by use of near-infrared diode-laser-based overtone spectroscopy." *Applied Optics* **40**(24): 4387.
- Conrad, R. (1996).** "Soil microorganisms as controllers of atmospheric trace gases ( $\text{H}_2$ ,  $\text{CO}$ ,  $\text{CH}_4$ ,  $\text{OCS}$ ,  $\text{N}_2\text{O}$ , and  $\text{NO}$ )." *Microbiological Reviews* **60**(4): 609.
- Cottrell, T. L. and M. A. Day (1965).** "Effect of oxygen on vibrational relaxation in methane." *The Journal of Chemical Physics* **43**(4): 1433.
- Davidson, E. A. and J. P. Schimel (1995).** *Microbial processes of production and consumption of nitric oxide, nitrous oxide and methane.*, Blackwell Science.
- De Tommasi, E., G. Casa, et al. (2006).** "High precision determinations of  $\text{NH}_3$  concentration by means of diode laser spectrometry at 2.005  $\mu\text{m}$ ." *Applied Physics B: Lasers and Optics* **85**(2-3): 257.
- Denman, K. L., G. Brasseur, et al. (2007).** *Couplings Between Changes in the Climate System and Biogeochemistry.* Climate Change 2007: The Physical Science Basis. Contribution of Working Group I to the Fourth Assessment Report of the Intergovernmental Panel on Climate Change. S. Solomon, D. Qin, M. R. Manning et al. Cambridge, United Kingdom and New York, NY, USA, Cambridge University Press.
- Denmead, O. T., J. R. Simpson, et al. (1977).** "Direct Field Measurement of Ammonia Emission After Injection of Anhydrous Ammonia." *Soil Science Society of America Journal* **41**(5): 1001.
- Diehl, R. (2000).** *High-Power Diode Lasers: Fundamentals, Technology, Applications.* Berlin, Springer.
- DIN-32645 (1994).** *Nachweis-, Erfassungs- und Bestimmungsgrenze; Ermittlung unter Wiederholbedingungen; Begriffe, Verfahren, Auswertung.* Berlin, Beuth-Verlag.
- Dlugokencky, E. J., K. A. Masarie'T, et al. (1998).** "Continuing decline in the growth rate of the atmospheric methane burden." *Nature* **393**(6684): 447.
- Drägerwerk, A. (1994).** *Dräger Tube Handbook: Soil, Water and Air Investigations as well as Technical Gas Analysis.* Lübeck, Drägerwerk Aktiengesellschaft.
- Dueck, T. and A. Van Der Werf (2008).** "Are plants precursors for methane?" *New Phytologist* **178**(4): 693.
- Dueck, T. A., R. De Visser, et al. (2007).** "No evidence for substantial aerobic methane emission by terrestrial plants: A  $^{13}\text{C}$ -labelling approach." *New Phytologist* **175**(1): 29.
- Erisman, J. W., A. Bleeker, et al. (2007).** "Reduced nitrogen in ecology and the environment." *Environmental Pollution* **150**(1): 140.

- Erisman, J. W., A. Hensen, et al. (2002).** "NitroGenius: A nitrogen decision support system: A game to develop the optimal policy to solve the Dutch nitrogen pollution problem." *Ambio* **31**(2): 190.
- Erisman, J. W., A. W. M. Vermetten, et al. (1988).** "Vertical distribution of gases and aerosols: The behaviour of ammonia and related components in the lower atmosphere." *Atmospheric Environment* **22**(6): 1153.
- Etheridge, D. M., L. P. Steele, et al. (1998).** "Atmospheric methane between 1000 A.D. and present: Evidence of anthropogenic emissions and climatic variability." *Journal of Geophysical Research D: Atmospheres* **103**(D13): 15979.
- Fangmeier, A., A. Hadwiger-Fangmeier, et al. (1994).** "Effects of atmospheric ammonia on vegetation - A review." *Environmental Pollution* **86**(1): 43.
- FAO (1998).** *World Reference Base for Soil Resources*. Rome, Food and Agriculture Organization of the United Nations.
- Fenn, M. E., M. A. Poth, et al. (1998).** "Nitrogen excess in North American ecosystems: Predisposing factors, ecosystem responses, and management strategies." *Ecological Applications* **8**(3): 706.
- Filho, M. B., M. G. Da Silva, et al. (2006).** "Ammonia detection by using quantum-cascade laser photoacoustic spectroscopy." *Applied Optics* **45**(20): 4966.
- Finlayson-Pitts, B. J. and J. N. Pitts Jr (1999).** *Chemistry of the upper and lower atmosphere*. New York, Academic Press.
- Foken, T. (2003).** *Angewandte Meteorologie Mikrometeorologische Methoden*. Berlin, Springer.
- Francey, R. J., M. R. Manning, et al. (1999).** "A history of  $\delta^{13}C$  in atmospheric  $CH_4$  from the Cape Grim Air Archive and Antarctic firn air." *Journal of Geophysical Research D: Atmospheres* **104**(D19): 23631.
- Galbally, I. E. and C. R. Roy (1983).** "The fate of nitrogen compounds in the atmosphere." *Developments in Plant & Soil Science* **9**: 265.
- Galloway, J. N., J. D. Aber, et al. (2003).** "The nitrogen cascade." *BioScience* **53**(4): 341.
- Gerard, Y., R. J. Holdsworth, et al. (2007).** "Multispecies in situ monitoring of a static internal combustion engine by near-infrared diode laser sensors." *Applied Optics* **46**(19): 3937.
- Grossel, A., V. Zeninari, et al. (2007).** "Optimization of a compact photoacoustic quantum cascade laser spectrometer for atmospheric flux measurements: Application to the detection of methane and nitrous oxide." *Applied Physics B: Lasers and Optics* **88**(3): 483.
- Hall, R. N., G. E. Fenner, et al. (1962).** "Coherent light emission from GaAs junctions." *Physical Review Letters* **9**(9): 366.
- Hammerich, M., A. Olafsson, et al. (1992).** "Photoacoustic study of kinetic cooling." *Chemical Physics* **163**: 173.

**Hansen, J., M. Sato, et al. (2000).** "Global warming in the twenty-first century: An alternative scenario." Proceedings of the National Academy of Sciences of the United States of America **97**(18): 9875.

**Harren, F. J. M., G. Cotti, et al. (2000).** "Photoacoustic Spectroscopy in Trace Gas Monitoring." Encyclopedia of Analytical Chemistry: 2203-2226.

**Heeb, N. V., A. M. Forss, et al. (2003).** "Methane, benzene and alkyl benzene cold start emission data of gasoline-driven passenger cars representing the vehicle technology of the last two decades." Atmospheric Environment **37**(37): 5185.

**Herndon, S. C., J. H. Shorter, et al. (2005).** "Real-time measurements of SO<sub>2</sub>, H<sub>2</sub>CO, and CH<sub>4</sub> emissions from in-use curbside passenger buses in New York City using a chase vehicle." Environmental Science and Technology **39**(20): 7984.

**Hess, P. (1992).** *Principles of photoacoustic and photothermal detection in gases.* New York, Elsevier.

**Houghton, J. (2004).** *Global warming: the complete briefing.* Cambridge, UK; New York, Cambridge University.

**Houweling, S., T. Roeckmann, et al. (2006).** "Atmospheric constraints on global emissions of methane from plants." Geophysical Research Letters **33**(15).

**Hseung, Y. (1986).** *The Soil Atlas of China.* Beijing, Cartographic Publishing House.

**Hu, X., S. Liu, et al. (2005).** "Numerical simulation of wind and temperature fields over Beijing area in summer." Acta Meteorologica Sinica **19**(1): 120.

**Hutchinson, G. L. and E. A. Brams (1992).** "NO versus N<sub>2</sub>O emissions from an NH<sub>4</sub><sup>+</sup>-amended Bermuda grass pasture." Journal of Geophysical Research **97**(D9): 9889.

**Hutchinson, G. L. and A. R. Mosier (1981).** "Improved soil cover method for field measurement of nitrous oxide fluxes." Soil Sci. Soc. Am. J. **45**: 311.

**Innova. (2007).** from [http://www.innova.dk/INNOVA-1412.gas\\_monitoring4.0.html](http://www.innova.dk/INNOVA-1412.gas_monitoring4.0.html).

**IPCC (1990).** *Climate Change: The Intergovernmental Panel on Climate Change Scientific Assessment.* Cambridge, United Kingdom and New York, NY, USA, Cambridge University Press.

**IPCC (2007).** *Climate Change 2007: The Physical Science Basis. Contribution of Working Group I to the Fourth Assessment Report of the Intergovernmental Panel on Climate Change.* Cambridge, United Kingdom and New York, NY, USA, Cambridge University Press.

**Iseki, T. (2004).** "A portable remote methane detector using an InGaAsP DFB laser." Environmental Geology (Berlin, Germany) **46**(8): 1064-1069.

**Johnson, R. H., R. Gerlach, et al. (1982).** "Loss Mechanisms in Resonant Spectrophones." Applied Optics **21**(1): 81.

- Jungkunst, H. F., R. Sauter, et al. (2006).** "Verifying three types of methane fluxes from soils by testing the performance of a novel mobile photoacoustic method versus a well-established gas chromatographic one." *Environmental Science and Technology* **40**(20): 6425.
- Kapitanov, V. A., V. Zeninari, et al. (2002).** "Optimisation of photoacoustic resonant cells with commercial microphones for diode laser gas detection." *Spectrochimica acta. Part A, Molecular and biomolecular spectroscopy* **58**(11): 2397.
- Keppler, F., J. T. G. Hamilton, et al. (2006).** "Methane emissions from terrestrial plants under aerobic conditions." *Nature (London, United Kingdom)* **439**(7073): 187-191.
- Keppler, F., J. T. G. Hamilton, et al. (2008).** "Methoxyl groups of plant pectin as a precursor of atmospheric methane: Evidence from deuterium labelling studies." *New Phytologist* **178**(4): 808.
- Kerr, E. L. and J. G. Atwood (1968).** "The laser illuminated absorptivity spectrophone: a method for measurement of weak absorptivity in gases at laser wavelengths." *Appl. Opt.* **7**: 915.
- Kirschbaum, M. U. F., D. Bruhn, et al. (2006).** "A comment on the quantitative significance of aerobic methane release by plants." *Functional Plant Biology* **33**(6): 521.
- Kleine, D., M. Mürtz, et al. (2001).** "Atmospheric trace gas analysis with cavity ring-down spectroscopy." *Israel Journal of Chemistry* **41**(2): 111.
- Kneubühl, F. K. and M. W. Sigrist (2005).** *Laser*. Stuttgart; Leipzig, Teubner.
- Kogge, M. (2002).** "Subproject B2: Management and Fate of Nitrogen Fertilizer and its N losses into the Environment in Wheat/Maize Cropping System." 2007, from [https://www.uni-hohenheim.de/chinaproject/publ/B2\\_Report\\_final/B2\\_Final\\_Report\\_Kogge.pdf](https://www.uni-hohenheim.de/chinaproject/publ/B2_Report_final/B2_Final_Report_Kogge.pdf).
- Köppen, W. (1918).** "Klassifikation der Klimate nach Temperatur, Niederschlag und Jahreslauf." *Petermanns Geographische Mitteilungen* **64**: 193.
- Koskinen, V., J. Fonsen, et al. (2006).** "Extremely sensitive trace gas analysis with modern photoacoustic spectroscopy." *Vibrational Spectroscopy* **42**(2): 239.
- Kosterev, A. A. and F. K. Tittel (2004).** "Ammonia detection by use of quartz-enhanced photoacoustic spectroscopy with a near-IR telecommunication diode laser." *APPLIED OPTICS* **43**(33): 6213-6217.
- Kreuzer, L. B. (1971).** "Ultralow gas concentration infrared absorption spectroscopy." *Journal of Applied Physics* **42**(7): 2934.
- Krupa, S. V. (2003).** "Effects of atmospheric ammonia (NH<sub>3</sub>) on terrestrial vegetation: A review." *Environmental Pollution* **124**(2): 179.
- Länderbericht-China (2007).** *Geschichte - Politik - Wirtschaft - Gesellschaft*. Bonn, Bundeszentrale für politische Bildung.
- Langford, A. O. and F. C. Fehsenfeld (1992).** "Natural vegetation as a source or sink for atmospheric ammonia: A case study." *Science* **255**(5044): 581.

- Le Treut, H., R. Somerville, et al. (2007).** *Historical Overview of Climate Change*. Climate Change 2007: The Physical Science Basis. Contribution of Working Group I to the Fourth Assessment Report of the Intergovernmental Panel on Climate Change. S. Solomon, D. Qin, M. R. Manning et al. Cambridge, United Kingdom and New York, NY, USA, Cambridge University Press.
- Lelieveld, J., P. J. Crutzen, et al. (1998).** "Changing concentration, lifetime and climate forcing of atmospheric methane." *Tellus, Series B: Chemical and Physical Meteorology* **50**(2): 128.
- Lenhard, U. and G. Gravenhorst (1980).** "Evaluation of ammonia fluxes into the free atmosphere over Western Germany." *Tellus* **32**(1): 48.
- Lewicki, R., G. Wysocki, et al. (2007).** "Carbon dioxide and ammonia detection using 2  $\mu\text{m}$  diode laser based quartz-enhanced photoacoustic spectroscopy." *Applied Physics B: Lasers and Optics* **87**(1): 157.
- Li, C. P., G. X. Li, et al. (2007).** "Ambient air monitoring of Beijing MSW logistics facilities in 2006." *Environmental Monitoring and Assessment*: 1.
- Link, A. (2005).** *Optimierung und Evaluierung unterschiedlicher empfindlicher spektroskopischer Messverfahren für klimarelevante Gase*. Berlin, WVB Wissenschaftl. Verl. Berlin. ISBN 3-86573-121-X
- Liu, X. M., F. Hu, et al. (2006).** "Summer urban climate trends and environmental effect in the Beijing area." *Chinese Journal of Geophysics (Acta Geophysica Sinica)* **49**(3): 689.
- Lowe, D. C. (2006).** "Global change: A green source of surprise." *Nature* **439**(7073): 148.
- Luft, K. F. (1943).** "Über eine neue Methode der registrierenden Gasanalyse mit Hilfe der Absorption ultraroter Strahlen ohne spektrale Zerlegung." *Zeitschrift für Technische Physik* **24**: 97.
- Lundsberg-Nielsen, L., F. Hegelund, et al. (1993).** "Analysis of the high-resolution spectrum of ammonia ( $14\text{NH}_3$ ) in the near-infrared region, 6400-6900  $\text{cm}^{-1}$ ." *Journal of Molecular Spectroscopy* **162**(1): 230-245.
- Mack, U. D. (2005).** *Bodenwasserhaushalt und Nitratauswaschung unter bewässertem Getreide- und Gemüseanbau in der Nordchinesischen Tiefebene*. Stuttgart, Inst. für Bodenkunde und Standortslehre.
- Maddaloni, P., P. Malara, et al. (2006).** "Two-tone frequency modulation spectroscopy for ambient-air trace gas detection using a portable difference-frequency source around 3  $\mu\text{m}$ ." *Applied Physics B: Lasers and Optics* **85**(2-3): 219.
- Matson, P. A. and R. C. Harriss (1995).** "Trace gas exchange in an ecosystem context: multiple approaches to measurement and analysis." *Biogenic Trace Gases: Measuring Emissions from Soil and Water*: 1-13.
- Matthias, A. D., A. M. Blacker, et al. (1980).** "A simple chamber technique for field measurement of emissions of nitrous oxide from soils." *Journal of Environmental Quality* **9**(2): 251.

- Miklos, A., P. Hess, et al. (2001).** "*Application of acoustic resonators in photoacoustic trace gas analysis and metrology.*" REVIEW OF SCIENTIFIC INSTRUMENTS **72**(4): 1937-1955.
- Morse, P. M. and K. U. Ingard (1986).** *Theoretical Acoustics*. Princeton, NJ, Princeton University Press.
- Nadezhdinskii, A., A. Berezin, et al. (1999).** "*High sensitivity methane analyzer based on tuned near infrared diode laser.*" Spectrochimica Acta - Part A: Molecular and Biomolecular Spectroscopy **55**(10): 2083.
- Nam, E. K., T. E. Jensen, et al. (2004).** "*Methane Emissions from Vehicles.*" Environmental Science and Technology **38**(7): 2005.
- Nelson, D. D., B. McManus, et al. (2004).** "*High precision measurements of atmospheric nitrous oxide and methane using thermoelectrically cooled mid-infrared quantum cascade lasers and detectors.*" Spectrochimica Acta Part A-Molecular and Biomolecular Spectroscopy **60**(14): 3325-3335.
- Nelson, D. W. (1982).** *Gaseous losses of nitrogen other than through denitrification*. Madison, WI, American Society of Agronomy.
- Ngai, A. K. Y., S. T. Persijn, et al. (2006).** "*Automatically tunable continuous-wave optical parametric oscillator for high-resolution spectroscopy and sensitive trace-gas detection.*" Applied Physics B: Lasers and Optics **85**(2-3): 173.
- Olivier, J. G. J., A. F. Bouwman, et al. (1998).** "*Global air emission inventories for anthropogenic sources of NO(x), NH<sub>3</sub> and N<sub>2</sub>O in 1990.*" Environmental Pollution **102**(SUPPL. 1): 135.
- Omnisens. (2007).** from [http://www.omnisens.ch/products/products\\_gas\\_tga.htm](http://www.omnisens.ch/products/products_gas_tga.htm).
- Owens, M. A., C. C. Davis, et al. (1999).** "*A photothermal interferometer for gas-phase ammonia detection.*" Analytical Chemistry **71**(7): 1391.
- Pao, Y.-H. (1977).** *Optoacoustic Spectroscopy and Detection*. New York, Academic Press.
- Peeters, R., G. Berden, et al. (2000).** "*Open-path trace gas detection of ammonia based on cavity-enhanced absorption spectroscopy.*" Applied Physics B: Lasers and Optics **71**(2): 231-236.
- Pokhrel, D. and T. Viraraghavan (2005).** "*Municipal solid waste management in Nepal: Practices and challenges.*" Waste Management **25**(5): 555.
- Pushkarsky, M. B., M. E. Webber, et al. (2003).** "*Ultra-sensitive ambient ammonia detection using CO<sub>2</sub>-laser-based photoacoustic spectroscopy.*" Applied Physics B: Lasers and Optics **77**(4): 381.
- Reinhardt, T. (2002).** *Photoakustischer Nachweis von Ammoniak mit Diodenlasern im Spektralbereich des Nahen Infrarot*. Institut für Physik Fakultät I Allgemeine und Angewandte Naturwissenschaften. Stuttgart, Universität Hohenheim. **Dissertation:** 91.
- Römpp, H. (1995).** *Römpp Chemie Lexikon*. Stuttgart, Thieme.

- Rooth, R. A., A. J. L. Verhage, et al. (1990).** "Photoacoustic measurement of ammonia in the atmosphere: Influence of water vapor and carbon dioxide." *Appl. Opt.* **29**(25): 3643.
- Rosencwaig, A. (1980).** *Photoacoustics and Photoacoustic Spectroscopy*. New York, Wiley.
- Rothman, L. S., A. Barbe, et al. (2003).** "The HITRAN molecular spectroscopic database: Edition of 2000 including updates through 2001." *Journal of Quantitative Spectroscopy and Radiative Transfer* **82**(1-4): 5.
- Rothman, L. S., D. Jacquemart, et al. (2005).** "The HITRAN 2004 molecular spectroscopic database." *Journal of Quantitative Spectroscopy and Radiative Transfer* **96**(2 SPEC. ISS.): 139.
- Sauter, R. (2004).** *Photoakustischer Nachweis von Methan mit Diodenlasern im Spektralbereich des Nahen Infrarot*. Aachen, Shaker Verlag. ISBN 3-8322-3388-1
- Schendel, J. S., R. E. Stickel, et al. (1990).** "Atmospheric ammonia measurement using a VUV/photofragmentation laser-induced fluorescence technique." *Appl. Opt.* **29**: 4924.
- Schilt, S., J. P. Besson, et al. (2005).** *Methane monitoring by near infrared photoacoustic spectroscopy: The importance of relaxation phenomena*. *Journal De Physique*. IV: JP.
- Schilt, S., J. P. Besson, et al. (2006).** "Near-infrared laser photoacoustic detection of methane: The impact of molecular relaxation." *Applied Physics B: Lasers and Optics* **82**(2 SPEC. ISS.): 319.
- Schmidt, W. (2005).** *Optical Spectroscopy in Chemistry and Life Sciences. An Introduction.*, Wiley-VCH.
- Schmohl, A., A. Miklós, et al. (2002).** "Detection of ammonia by photoacoustic spectroscopy with semiconductor lasers." *Applied Optics* **41**(9): 1815.
- Scotoni, M., A. Rossi, et al. (2006).** "Simultaneous detection of ammonia, methane and ethylene at 1.63  $\mu\text{m}$  with diode laser photoacoustic spectroscopy." *Applied Physics B: Lasers and Optics* **82**(3): 495-500.
- Seibert, P., F. Beyrich, et al. (2000).** "Review and intercomparison of operational methods for the determination of the mixing height." *Atmospheric Environment* **34**(7): 1001.
- Siegmann, A. E. (1986).** *Lasers*. California, University Science Books.
- Simpson, I. J., T. Y. Chen, et al. (2002).** "Implications of the recent fluctuations in the growth rate of tropospheric methane." *Geophysical Research Letters* **29**(10).
- Sinofile. (2007).** "[http://www.sinofile.net/saiweng/sip\\_blog.nsf/d6plinks/YZHI-72F5KX](http://www.sinofile.net/saiweng/sip_blog.nsf/d6plinks/YZHI-72F5KX)." 2008.
- Smith, K. A. and F. Conen (2004).** "Measurement of trace gases. Part 1. Gas analysis, chamber methods, and related procedures." *Soil and Environmental Analysis* (3rd Edition): 433-476.

- So, S., F. Koushanfar, et al. (2007).** *LaserSPECKs: Laser SPECTroscopic trace-gas sensor networks - Sensor integration and applications.* IPSN 2007: Proceedings of the Sixth International Symposium on Information Processing in Sensor Networks.
- Socolow, R. H. (1999).** "Nitrogen management and the future of food: Lessons from the management of energy and carbon." *Proceedings of the National Academy of Sciences of the United States of America* **96**(11): 6001.
- Spahni, R., J. Chappellaz, et al. (2005).** "Atmospheric methane and nitrous oxide of the late pleistocene from Antarctic Ice Cores." *Science* **310**(5752): 1317.
- Stull, R. B. (1988).** *An introduction to boundary layer meteorology.* Dordrecht, Boston, London, Kluwer Academic Publishers.
- Su, F., M. Shao, et al. (2002).** "Estimates of methane emissions in Beijing using a backward trajectory inversion model." *Chemical Speciation and Bioavailability* **14**(1-2): 43-48.
- Sutton, M. A., C. Milford, et al. (2001).** "Biosphere-atmosphere interactions of ammonia with grasslands: Experimental strategy and results from a new European initiative." *Plant and Soil* **228**(1): 131.
- Takigawa, A., A. Matsunami, et al. (2005).** "Methane emission from automobile equipped with three-way catalytic converter while driving." *Energy* **30**(2-4 SPEC. ISS.): 461.
- Tisdale, S. L., W. L. Nelson, et al. (1993).** *Soil Fertility and Fertilizers.* New York, Macmillan Publishing Company.
- Töpfer, T., K. P. Petrov, et al. (1997).** "Room-temperature mid-infrared laser sensor for trace gas detection." *Applied Optics* **36**(30): 8042-8049.
- Uhl, R. (2001).** *Spektrometrische Elementbestimmung mit Diodenlasern in Gleichspannungs- und Hochfrequenzplasmen.* Stuttgart, Hohenheim 2001.
- Viengerov, M. (1938).** "A method for gas analysis, based on the Tyndall-Röntgen optical-acoustical phenomenon." *Doklady Akademii Nauk SSSR, Seriya A* **19**: 687-688.
- Wang, Z. P., X. G. Han, et al. (2008).** "Aerobic methane emission from plants in the Inner Mongolia steppe." *Environmental Science and Technology* **42**(1): 62.
- Webber, M. E., T. MacDonald, et al. (2005).** "Agricultural ammonia sensor using diode lasers and photoacoustic spectroscopy." *Measurement Science and Technology* **16**(8): 1547.
- Weilenmann, M., P. Soltic, et al. (2005).** "Regulated and nonregulated diesel and gasoline cold start emissions at different temperatures." *Atmospheric Environment* **39**(13): 2433.
- Werle, P., K. Maurer, et al. (2002).** "Spectroscopic gas analyzers based on indium-phosphide, antimonide and lead-salt diode-lasers." *Spectrochimica Acta - Part A Molecular and Biomolecular Spectroscopy* **58**(11): 2361.
- White, J. U. (1942).** "Long Optical Paths of Large Aperture." *J. Opt. Soc. Am.* **32**: 285-288.
- Williams, E. J. (1992).** "An intercomparison of five ammonia measurement techniques." *Journal of Geophysical Research* **97**(D11).

**Xiao, Y., X. Bai, et al. (2007).** "*The composition, trend and impact of urban solid waste in Beijing.*" *Environmental Monitoring and Assessment* **135**(1-3): 21.

**Zeninari, V., B. Parvitte, et al. (2003).** "*Methane detection on the sub-ppm level with a near-infrared diode laser photoacoustic sensor.*" *Infrared Physics and Technology* **44**(4): 253.

**Zervas, E., X. Montagne, et al. (2001).** "*Emission of specific pollutants from a compression ignition engine. Influence of fuel hydrotreatment and fuel/air equivalence ratio.*" *Atmospheric Environment* **35**(7): 1301.

**Zhang, X., X. Cai, et al. (2006).** "*Structures and characteristics of the atmospheric boundary layer over Beijing area in autumn.*" *Beijing Daxue Xuebao (Ziran Kexue Ban)/Acta Scientiarum Naturalium Universitatis Pekinensis* **42**(2): 220.

**Zharov, V. P. and V. S. Letokhov (1986).** *Laser Optoacoustic Spectroscopy.* Berlin, Springer.

## 9 Appendix

### 9.1 List of Tables

<b>Table 3.1:</b> Sources, sinks and atmospheric budgets of CH <sub>4</sub> (Tg yr <sup>-1</sup> ) according to IPCC [Lowe 2006].	15
<b>Table 3.2:</b> Global sources (TgN yr <sup>-1</sup> ) of NH <sub>3</sub> for the 1990s [Asman et al. 1998; IPCC 2007].	17
<b>Table 3.3:</b> Different ambient air methane and ammonia measuring devices. N/A = not applicable.	28
<b>Table 4.1:</b> Soil properties of the experimental field DBW [Mack 2005].	35
<b>Table 4.2:</b> Overview of the used devices and components for CH <sub>4</sub> and NH <sub>3</sub> measurements.	37
<b>Table 4.3:</b> Overview of the certified gases used for calibration.	47

## 9.2 List of Figures

- Figure 2.1:** Geographical location and administrative units of the NCP. Map provided by G. Bareth. .... 3
- Figure 2.2:** Detailed map of the NCP. Map provided by C. Rumbaer..... 4
- Figure 3.1:** Global average RF estimates and ranges in 2005 for anthropogenic carbon dioxide (CO<sub>2</sub>), methane (CH<sub>4</sub>), nitrous oxide (N<sub>2</sub>O) and other important agents and mechanisms, together with the typical geographical extent (spatial scale) of the forcing and the assessed level of scientific understanding (LOSU) [IPCC 2007]. .... 10
- Figure 3.2:** Atmospheric concentrations of carbon dioxide, methane and nitrous oxide over the last 10,000 years (large panels) and since 1750 (inset panels). Data shown are from ice cores (symbols with different colors for different studies) and from atmospheric samples (red lines). The corresponding RF is shown on the right hand axes of the large panels [IPCC 2007]. .... 11
- Figure 3.3:** Recent CH<sub>4</sub> concentrations and trends. (a) Time series of global CH<sub>4</sub> abundance mole fraction (in ppb) derived from surface sites operated by NOAA/GMD (blue lines) and AGAGE (red lines). The thinner lines show the CH<sub>4</sub> global averages and the thicker lines are the de-seasonalized global average trends from both networks. (b) Annual growth rate (ppb yr<sup>-1</sup>) in global atmospheric CH<sub>4</sub> abundance from 1984 through the end of 2005 (NOAA/GMD, blue), and from 1988 to the end of 2005 (AGAGE, red). The vertical lines indicate ±2 standard deviation uncertainties (95% confidence interval), and 1 standard deviation uncertainties are between 0.1 and 1.4 ppb yr<sup>-1</sup> for both AGAGE and NOAA/GMD. Note that the differences between AGAGE and NOAA/GMD calibration scales are determined through occasional intercomparisons [IPCC 2007]. .... 14
- Figure 3.4:** Sunlight is intercepted and aligned with a steering mirror (C, D), modulated with a chopper (B) and focused onto a glass bulb (A) [Bell 1881]. .... 20

<b>Figure 3.5:</b> Scheme of the physical processes occurring after optical excitation of molecules. Modulated or pulsed laser radiation leads to the population of rotational, vibrational, and electronic states. Collisional radiationless deactivation leads to localized transient heating. The resulting expansion launches standing or pulsed acoustic waves, which are detected with a microphone. ....	21
<b>Figure 3.6:</b> Resonant acoustic modes of a cylindrical closed chamber; the fundamental longitudinal, azimuthal and radial modes [Harren et al. 2000]. ....	23
<b>Figure 3.7:</b> Resonant acoustic cell designs. a) Simple pipe (tube) for excitation of longitudinal modes, b) pipe with two buffer volumes, c) Helmholtz resonator with separate sample and detection chambers for solid samples, d) coaxial excitation (e.g., of radial modes) in a cylinder, e) asymmetric multipass arrangement for excitation of azimuthal modes in a cylinder, and f) cylindrical cell suitable for excitation of the first radial mode with suppression of the window noise [Miklos et al. 2001]. ....	24
<b>Figure 3.8:</b> Acoustic spectrum of the PA cell for $T = 294,5$ K and 100 ppm $\text{NH}_3$ . Excited by speaker (top) and laser (bottom). The numbers represent the azimuthal ( $m$ ), radial ( $n$ ) and longitudinal ( $k$ ) acoustic modes. ....	25
<b>Figure 3.9:</b> Excitation by the laser diode of the second azimuthal mode of a resonant cell filled with 100 ppm $\text{NH}_3$ depending of modulation frequency. The Q-factor is determined to $Q = 185.04$ . ....	26
<b>Figure 3.10:</b> Schematic experimental setup of the TDL-PA device. ....	27
<b>Figure 4.1:</b> Satellite image of Beijing, including Dongbeiwang and China Agricultural University. Image provided by Google Earth. ....	34
<b>Figure 4.2:</b> Scheme of the White-type multipass arrangement including beam numbers. ....	38
<b>Figure 4.3:</b> View into the open PA detection unit. ....	39
<b>Figure 4.4:</b> Screenshot of the LabView user interface controlling the frequency. ....	42
<b>Figure 4.5:</b> Screenshot of the LabView user interface for measurement and data storage. ....	42

<b>Figure 4.6:</b> Absorption profile of methane at about 1650 nm (peak maximum at 1650.957 nm) and of carbon dioxide and water vapor, respectively, taken from the HITRAN database. ....	45
<b>Figure 4.7:</b> Absorption peak of water vapor near the two absorption lines of ammonia at 1512.2126 nm and 1512.2377 nm, respectively [Lundsberg-Nielsen et al. 1993]. Water vapor data were taken from the HITRAN database. ....	45
<b>Figure 4.8:</b> Calibration of the methane PA system. The calculated $3\sigma$ detection limit is 85 ppb. ....	49
<b>Figure 4.9:</b> Calibration of the ammonia PA system. The calculated $3\sigma$ detection limit is 111 ppb. ....	49
<b>Figure 4.10:</b> Schematic diagram of the support socket. ....	54
<b>Figure 4.11:</b> Cross section of support socket, support plate and hood (all values in mm). ....	55
<b>Figure 4.12:</b> Picture of an installed frame at the experimental field Dongbeiwang. ....	55
<b>Figure 4.13:</b> Gas tightness test result from the 25 <sup>th</sup> – 26 <sup>th</sup> of October 2006. ....	57
<b>Figure 4.14:</b> Temperature profile inside of the closed chamber with and without applying cooling packs. As a control mean ambient air temperature 3 cm above soil was measured close to the climate station in Dongbeiwang. Ambient air temperature at beginning of this study 31°C and at the end of this study 30.5°C. ....	58
<b>Figure 4.15:</b> Temperature difference between the situation without cooling packs and the situation with cooling packs. ....	59
<b>Figure 5.1:</b> Correlation coefficient of the same dataset. Raw data (top) and 12 minutes data points (bottom). ....	63
<b>Figure 5.2:</b> Daily sums of measured methane fluxes, precipitation and irrigation during winter wheat growing season from 24 <sup>th</sup> of April to the 16 <sup>th</sup> of June 2007. ....	64

- Figure 5.3:** 2<sup>nd</sup> of May 2007 methane concentration pattern inside of the closed chamber planted with winter wheat (I – IV) as well as bare soil (V) at different closure times. Ambient temperature measured 3 cm above soil. .... 65
- Figure 5.4:** 21<sup>st</sup> of May 2007 methane concentration pattern inside of the closed chamber planted with winter wheat (II – IV) as well as bare soil (I and V) at different closure times. Ambient temperature measured 3 cm above soil. All plots were irrigated with an amount of water of 13 mm at 8 am. .... 67
- Figure 5.5:** Daily sums of measured methane fluxes, precipitation and irrigation during summer maize growing season from the 26<sup>th</sup> of June to the 24<sup>th</sup> of July 2007. .... 68
- Figure 5.6:** Measurement of methane concentration inside of the closed chamber (I – IX), ambient air methane concentration, temperature and hourly exchange rate from the 23<sup>rd</sup> – 24<sup>th</sup> of July 2007. .... 70
- Figure 5.7:** Measurement of methane concentration (black) and wind direction (gray) on top of the container in Dongbeiwang from the 6<sup>th</sup> – 9<sup>th</sup> of August 2007. .... 73
- Figure 5.8:** Measurement of methane concentration (black) and wind speed (gray) on top of the container in Dongbeiwang from the 6<sup>th</sup> – 9<sup>th</sup> of August 2007. .... 74
- Figure 5.9:** Correlation between methane concentration and wind direction measured on top of the container in Dongbeiwang from the 6<sup>th</sup> – 9<sup>th</sup> of August 2007. All data with a wind speed below 0.3 m s<sup>-1</sup> were omitted. .... 75
- Figure 5.10:** Correlation between methane concentration and wind speed measured on top of the container in Dongbeiwang from the 6<sup>th</sup> – 9<sup>th</sup> of August 2007. All data below 0.3 m s<sup>-1</sup> were omitted. .... 76
- Figure 5.11:** Correlation between wind speed and wind direction measured on top of the container in Dongbeiwang from the 6<sup>th</sup> – 9<sup>th</sup> of August 2007. All data below 0.3 m s<sup>-1</sup> were omitted. .... 76
- Figure 5.12:** Measurement of methane concentration (black) and wind direction (gray) on the top of the China Agricultural University from the 14<sup>th</sup> – 17<sup>th</sup> of August 2007. .... 77

<b>Figure 5.13:</b> Measurement of methane concentration (black) and wind speed (gray) on the top of the China Agricultural University from the 14 <sup>th</sup> – 17 <sup>th</sup> of August 2007.....	78
<b>Figure 5.14:</b> Correlation between methane concentration and wind direction measured on top of the China Agricultural University from the 14 <sup>th</sup> – 17 <sup>th</sup> of August 2007. All data with a wind speed below 0.3 m s <sup>-1</sup> were omitted. ....	79
<b>Figure 5.15:</b> Overview of the measuring sites DBW, CAU, Liulitun landfill, Beijing University and Shang Zhuang for ambient air methane measurements. Image provided by Google Earth. ....	80
<b>Figure 5.16:</b> Overview of the Liulitun landfill and the position of the TDL-PA system. Image provided by Google Earth. ....	82
<b>Figure 5.17:</b> Measurement of methane concentration (black) and wind direction (gray) at the Liulitun landfill from the 3 <sup>rd</sup> – 5 <sup>th</sup> of September 2007. ....	83
<b>Figure 5.18:</b> Correlation between methane concentration detected by the TDL-PA system and wind direction measured at the Liulitun landfill from the 3 <sup>rd</sup> – 5 <sup>th</sup> of September 2007. All data with a wind speed below 0.3 m s <sup>-1</sup> were omitted. ....	84
<b>Figure 5.19:</b> Comparison of methane concentration measured with TDL-PA and wind speed at Liulitun landfill and methane concentration measured with GC at Dongbeiwang from the 3 <sup>rd</sup> – 5 <sup>th</sup> of September 2007. ....	85
<b>Figure 5.20:</b> Comparison of methane concentration measured with TDL-PA at Beijing University (black) and methane concentration measured with GC at Dongbeiwang (gray) from the 5 <sup>th</sup> – 8 <sup>th</sup> of September 2007. ....	86
<b>Figure 5.21:</b> Methane emissions from a car measured with TDL-PA system. Resonance frequency (RF) was set according to engine idle condition. As noted the engine was rev up to 2000 rounds per minute (2000 rpm). ....	91
<b>Figure 5.22:</b> Release of residual ammonia inside of the tubes and TDL-PA system after applying 5 ppm NH <sub>3</sub> in N <sub>2</sub> . The system was purged with N <sub>2</sub> for about one hour and the chamber measurement started afterwards. ....	94

---

## Acknowledgements

I would like to thank everybody who contributed to the success of this work.

Special thanks go to Prof. Dr. U. Haas for putting me in charge of the execution of the subproject 1.4 and for his support both in Germany and China. I am thankful for the convenient working atmosphere and his critical comments.

Many thanks to Prof. Dr. A. Fangmeier for his interest in my work and the co-correction of my thesis.

Many thanks to Dr. H.-D- Wizemann for fruitful discussions and his interest in my work.

Thanks to Mr. O. Eberwein for construction and fabrication of many mechanical components and for his professional support during the design of required parts.

I am also grateful for collaborative help from scientists of the IRTG.

From the German side I would like to thank all of my research fellows, especially Jenny Kopsch, Roland Kröbel, Christian Rumbaur and Ulrich Schwarz for their extensive help, friendship and support during my time in China.

Regarding the Chinese side special thanks go to Prof. Dr. Jiang Rongfeng, Dr. Su Fang, Huang Binxiang and Hu Xiaokang for their help with the experiments and their permanent willingness to discuss my work.

For reading the manuscript and general support I would like to thank Dr. Merle Hillebrand.

Thanks to the German Research Foundation (DFG) and the Chinese Ministry of Education for funding this project and to the University of Hohenheim for the Landesgraduiertenförderung.

My thanks go to everybody at the Institute of Physics and Meteorology who contributed to the success of this work.

Finally, my special thanks go to my parents for their constant support.

---

# Curriculum Vitae

**Malte Hillebrand**

**21.06.1976 in Essen**

## Career History

- 9/04 – present      **University of Hohenheim, Stuttgart, Germany**  
PhD student at the Institute of Physics and Meteorology  
Member of the International Research Training Group “Sustainable Resource Use in the North China Plain”
- 10/97 – 12/03      **Ruhr-University Bochum, Bochum, Germany**  
German Diplom (Graduate Diploma) in Geography  
Major in Climatology with minors in geology, cartography and botany  
Thesis: “3-dimensional visualization of ENVI-met modeling results with ArcGIS”
- 9/96 – 10/97      **Kolping-Berufsbildungswerk Essen, Essen, Germany**  
Alternative civilian servant
- 1986 – 1996      **Burggymnasium Essen, Essen, Germany**  
Abitur (High School Diploma)

---

## **Erklärung**

Hiermit erkläre ich, dass ich die vorliegende Arbeit selbständig gefertigt, keine anderen als die angegebenen Quellen und Hilfsmittel benutzt und wörtlich oder inhaltlich übernommene Stellen als solche kenntlich gemacht habe.